Developmental and Neuromodulatory Influences on Cortical Population Activity and Perceptual Behavior

by

Katerina Acar

BS, University of Pittsburgh, 2015

Submitted to the Graduate Faculty of the

Dietrich School of Arts and Sciences in partial fulfillment

of the requirements for the degree of

Doctor of Philosophy

University of Pittsburgh

2022

UNIVERSITY OF PITTSBURGH

DIETRICH SCHOOL OF ARTS AND SCIENCES

This dissertation was presented

by

Katerina Acar

It was defended on

July 14, 2022

and approved by

Caroline Runyan, Assistant Professor, Department of Neuroscience

Marlene Cohen, Professor, Department of Neuroscience

Neeraj Gandhi, Professor, Department of Bioengineering

William Stauffer, Assistant Professor, Department of Neurobiology

Joshua Gold, Professor, Department of Neuroscience, University of Pennsylvania

Dissertation Director: Matthew Smith, Associate Professor, Biomedical Engineering and Neuroscience, Carnegie Mellon University

Developmental and Neuromodulatory Influences on Cortical Population Activity and Perceptual Behavior

Katerina Acar, PhD

University of Pittsburgh, 2022

All organisms, including human beings, rely on the ability to perceive and respond to sensory stimuli in order to thrive in any environment, whether natural or man-made. The accuracy of our perceptual decisions and actions, or the choices we make based on the available sensory information, depends on the activity of neurons throughout a network of brain regions with diverse functions such as sensory information processing, motor output preparation, and even internal behavioral state regulation. The purpose of this dissertation was to better understand the neural basis for variability in visual perception. We studied 1) how abnormal early visual experiences may influence sensory information processing by populations of primary visual cortex (V1) neurons and 2) how activation of the locus coeruleus (LC), the primary source of noradrenergic neuromodulation in the central nervous system, may influence cortical population activity patterns and perceptual behavior.

We first recorded and analyzed the visually evoked activity of V1 neuronal populations in rhesus macaques with strabismic amblyopia. Amblyopia is a disorder of the visual system that can arise when visual input through the two eyes is imbalanced during a critical window in development. We found evidence that changes in the strength and pattern of coordinated activity across populations of V1 neurons may contribute to degraded visual representations in amblyopia, potentially making it more difficult to read out evoked activity to support perceptual decisions.

In a separate set of experiments, we simultaneously recorded from single LC units and a population of neurons in prefrontal cortex (PFC), a region known to contribute to goal-directed behavior during cognition. We recorded these neural signals while rhesus macaques engaged in a task that required them to detect changes in visual stimuli and report their decisions by making saccadic eye movements. We first sought to understand how transient, burst-like changes in LC activation within trials of the task relate to sensory and motor aspects of perceptual decision making. Subsequently, we investigated whether over-time changes in baseline LC activity may track variability in coordinated PFC population activity and perceptual behavior.

Table of Contents

Preface xii

1.0 General Introduction 1

1.1 Pathways for Visual Perception and Visually Guided Eye Movements in Primates 1

1.2 What Determines the Reliability of Visual Perception? 3

1.3 The Locus Coeruleus – Norepinephrine Neuromodulatory System 5

1.3.1 Anatomical Organization of the LC-NE System 6

1.3.2 Noradrenergic Modulation of Target Neuron Responses 10

1.3.3 Existing Theories of LC function 11

1.4 Perceptual Decision Making 14

1.5 Behaviorally Relevant Signals Encoded by Populations of Neurons 16

2.0 Altered Functional Interactions between Neurons in Primary Visual Cortex of Macaque Monkeys with Experimental Amblyopia 19

2.1 Introduction 19

2.2 Methods 22

2.3 Results 30

2.3.1 Behavioral Deficits in Amblyopic Monkeys 31

2.3.2 Amblyopia Affects Individual Neuronal Responsivity 33

2.3.3 Amblyopia Alters Both Response Variability and Coordinated Population Activity in V1 35

2.3.4 Stimulus-dependent Correlation Structure is Modified in Amblyopic V1 39

2.3.5 Increased Correlations Predominate among Amblyopic V1 Neurons that Preferentially Respond to Fellow Eye 43

2.3.6 Decoding Stimulus Orientation from Amblyopic V1 Population Activity ...47

2.3.7 Effect of Stimulus Contrast on Correlated Variability in Amblyopic V1 49

2.4 Discussion 54

2.4.1 Altered Circuitry in V1 of Amblyopes 54

2.4.2 Decoding Information from V1 Populations 57

2.4.3 Theories for the Neural Basis of Amblyopia....59

3.0 Phasic Activation of Locus Coeruleus Neurons During Perceptual Decision Making 60

3.1 Introduction 60

3.2 Methods 62

3.2.1 Subjects 62

3.2.2 Electrophysiology 62

3.2.3 Behavior 65

3.2.4 Data Analysis 67

3.3 Results.... 69

3.3.1 Identification of LC Units....69

3.3.2 Task Performance 72

3.3.3 Task-related LC Phasic Activation....75

3.3.4 Impact of LC Phasic Responses on Perceptual Behavior....78

3.3.4.1 LC Phasic Responses Are Not Modulated by Behavioral Outcome . 79

3.3.4.2 Relating LC Phasic Responses to Behavioral Sensitivity and Criterion 82

3.3.4.3 LC Phasic Responses Do Not Predict Behavioral Response Times .. 86

3.3.5 Function of LC Phasic Responses during Choice Period 89

3.4 Discussion 94

3.4.1 Significance of LC Phasic Activation for Sensory Perception and Decision Making 94

3.4.2 LC Phasic Activation Prepares an Animal for Important Behavioral Responses 98

4.0 Fluctuations in Baseline Activity of Locus Coeruleus Neurons Track Changes in Pupil Diameter and Cortical Population Activity Over Time 104

4.1 Introduction 104

4.2 Methods 108

4.2.1 Subjects and Surgical Preparation 108

4.2.2 Data Collection 109

4.2.3 Data Analysis 111

4.2.3.1 Time Windows 111

4.2.3.2 Estimating Changes in PFC Population Activity on Different Timescales..... 112

4.2.3.3 Quantification and Statistics..... 115

4.3 Results..... 116

4.3.1 Relationship between Pupil Diameter and LC Spiking Activity Across Trials of a Perceptual Decision Making Task.....116

4.3.2 Relationship between Spiking Activity of Simultaneously Recorded Individual LC and PFC Neurons.....121

4.3.3 Relationships Between Pupil Diameter, LC Single Unit Activity, and PFC Population Activity Over Multiple Timescales.....124

4.3.3.1 Relationships Between Pupil Diameter, LC Single Unit Activity and PFC Population Activity over Fast, Trial-to-trial Timescale (seconds)..... 127

4.3.3.2 Relationships Between Pupil Diameter, LC Single Unit Activity and PFC Population Activity over Slow Timescale (minutes) 131

4.4 Discussion 133

4.4.1 Relationship Between Pupil Diameter and LC Activity 133

4.4.2 Relationships Between Simultaneous Changes in PFC Activity, LC Activity and Pupil Diameter 135

5.0 General Discussion..... 143

5.1 Recent Advances in Understanding the Neural Basis of Visual Perception 143

5.2 How Well Do We Understand the Neural and Behavioral Effects of Neuromodulation by the LC-NE System?..... 146

Bibliography 149

List of Figures

Figure 1. Behavioral assessment of strabismic amblyopes and visually normal animals. ... 32

Figure 2. Comparison of neuronal firing rates in response to normal and amblyopic eye stimulation. ... 34

Figure 3. Effect of amblyopia on individual and shared variability of responses to full contrast stimuli in a population of V1 neurons. ... 38

Figure 4. Dependence of r_{sc} on distance and tuning similarity in amblyopic V1. ... 42

Figure 5. Relationship between ocular dominance changes and increased correlations in amblyopic V1. ... 46

Figure 6. Decoding grating orientation from fellow or amblyopic eye stimulation. ... 48

Figure 7. ... 52

Figure 8. Dependence of spike count correlation on stimulus contrast. ... 53

Figure 9. Confirming Locus Coeruleus (LC) location. ... 71

Figure 10. Behavioral task and performance. ... 74

Figure 11. Task-related LC phasic activation. ... 77

Figure 12. LC phasic activation across different behavioral outcomes. ... 81

Figure 13. LC population average responses to different amplitudes of orientation changes. ... 84

Figure 14. Comparing LC phasic activation between periods of high and low perceptual sensitivity or criterion. ... 85

Figure 15. Comparing LC phasic activation between long and short behavioral response times. ... 88

Figure 16. LC phasic activation during the choice period in version 2 of the perceptual decision making task. 91

Figure 17. Microsaccade-related phasic activation of LC neurons. 93

Figure 18. Trial-to-trial relationships between mean pupil diameter and LC spike rate in 2 monkeys. 119

Figure 19. Trial-to-trial relationships between mean visual stimulus-evoked pupil diameter and LC spike rate in 2 monkeys. 120

Figure 20. Trial-to-trial relationship between spiking activity of simultaneously recorded individual LC and PFC neurons. 123

Figure 21. Drift in PFC population activity over the course of an example session. 126

Figure 22. Relationship between *trial-to-trial fluctuations* in LC activity, pupil diameter and co-variability in PFC population activity. 128

Figure 23. Relationship between trial-to-trial fluctuations in pupil diameter, changes in PFC population activity along trial-to-trial axis, and *30-second estimates of baseline LC activity*. 130

Figure 24. Relationships between *slow timescale fluctuations* in LC activity, pupil diameter and co-variability in PFC population activity. 132

Figure 25. Fluctuations in simultaneously monitored pupil diameter, LC baseline activity, PFC population activity and behavioral performance over the course of time in an example experimental session from Monkey Wa. 141

Figure 26. Fluctuations in simultaneously monitored pupil diameter, LC activity, PFC population activity and behavioral performance over the course of time in an example experimental session from Monkey Do. 142

Preface

Acknowledgements:

I would like to express my gratitude to several people who have supported me in various ways as I worked towards completing my PhD degree. First of all, I thank my advisor, Matthew Smith for being an amazing mentor. Matt, I learned so much from you, and I am deeply grateful for your guidance and encouragement over the course of my PhD work. I would also like to thank my committee members Marlene Cohen, Caroline Runyan, Raj Gandhi, Bill Stauffer, and Josh Gold. I've truly enjoyed our scientific discussions, and I really appreciate all of the feedback you've given me. Additionally, I would like to thank past and present members of the Smith lab for being good company and creating a wonderful work environment.

I would like to dedicate this work to my husband Umut, my mom Eleonora, and my grandparents Ludmila and Nikolai. I am deeply grateful for the unconditional love, encouragement, and positive energy that you have surrounded me with.

Chapter 2 has been previously published:

Acar, K., Kiorpes, L., Movshon, J. A., & Smith, M. A. (2019). Altered functional interactions between neurons in primary visual cortex of macaque monkeys with experimental amblyopia. Journal of Neurophysiology, 122(6), 2243-2258.

1.0 General Introduction

This introductory chapter provides a brief review of what is currently known about the neural processes underlying visual perception, with a focus on the primate visual system. The subsequent chapters present and discuss the results of research work aimed at improving our understanding of the neural basis for variability in perceptual behavior.

1.1 Pathways for Visual Perception and Visually Guided Eye Movements in Primates

The first step in visual processing occurs when a sharp image of the external world is projected onto the retina of the eye. Light-sensitive photoreceptors in the retina convert the light information to neural signals (electrical impulses), which are transmitted down the optic nerve fibers to the lateral geniculate nucleus (LGN) of the thalamus (Hubel & Wiesel, 1977). Geniculocortical axonal projections comprise a prominent visual pathway that carries the visual information from the LGN to the primary visual cortex (V1, or striate cortex), the first stage of cortical processing in the visual system (Hubel & Wiesel, 1977; Wilson et al., 1967). V1 is the first site at which information from both eyes fuses to be represented by single cells (Hubel & Wiesel, 1962). V1 neurons selectively respond to the orientation of edges or contours of visual stimuli (Hubel & Wiesel, 1959, 1977). From V1, visual information is transmitted among higher visual and temporal cortical areas which represent more complex stimulus features such as motion direction (middle temporal area, MT), shape (V4), color (V2, V4), and whole objects (inferotemporal cortex, IT). Although the processing of visually-evoked neural signals begins at

the retinal photoreceptors, visual perception of whole scenes and details (i.e., color, objects, motion, depth) is a final product of neural processing across a distributed network of cortical and subcortical regions with visual, visuomotor, and motor functions (Felleman & van Essen, 1991; Macko et al., 1982; van Essen, 2003). Information processing in V1 and subsequent regions along the visual pathway serves to help interpret the newly received visual information, integrate it with prior knowledge, and guide any motor responses deemed necessary upon perception.

Saccades are rapid, voluntary eye movements that allow animals to foveate different parts of visual scenes, and thus sample and integrate the available information from the visual surroundings. Several regions of the visual system (e.g., V4, MT, IT) supply information for guiding saccades via anatomical connections with parietal, frontal and subcortical areas that control saccade planning and execution (Gattass et al., 2014; Mohler & Wurtz, 1977; Schall, 2015; Schall et al., 1995; Schiller & Tehovnik, 2005; Schmolesky et al., 1998). The lateral intraparietal area (LIP), the dorsolateral prefrontal cortex (dlPFC), the frontal eye fields (FEF), and the superior colliculus (SC) are some of the major brain regions involved in integrating visual information for guiding subsequent eye movements (Basso et al., 2021; Colby et al., 1996; Funahashi, 2014; T. Moore & Armstrong, 2003; Noudoost et al., 2014; Schall, 2015; Schiller & Tehovnik, 2005; Sparks, 1986; Wurtz et al., 2001). Neurons in these brain regions have been shown to have distinct visual stimulus-evoked and saccade-related responses (Bruce & Goldberg, 1985; Bullock et al., 2017; Colby et al., 1996; Funahashi et al., 1991; Robinson, 1972; Schiller & Koerner, 1971; Schiller & Stryker, 1972; Sparks, 1978, 1986). Substantial evidence from previous studies indicates that these sensorimotor regions also play an important role in cognitive processes such as attention and perceptual decision making (Basso et al., 2021; Bisley & Goldberg, 2003; Colby

et al., 1996; Ding & Gold, 2012; Gold & Shadlen, 2003; Huk et al., 2017; Jun et al., 2021; Kim & Shadlen, 1999; Krauzlis et al., 2013; T. Moore, 2001, 2006; Seo et al., 2007).

1.2 What Determines the Reliability of Visual Perception?

Early abnormal visual experiences during the critical period of development can impact how visual system pathways are formed, and result in perceptual deficits later in life. Pioneering studies by Hubel and Wiesel first described the detrimental effects of monocular deprivation on visual processing in the primary visual cortex (V1) of cats. They showed that following experimentally induced eye closure early in life, very few V1 neurons could be driven by the visually-deprived eye (Wiesel & Hubel, 1963). Deprivation to this extreme is rare in humans and other animals. A more common cause of abnormal early vision is a misalignment of the two eyes (strabismus) which results in imbalanced visual input through the two eyes and a reduced percentage of V1 neurons that receive binocular input. Strabismus often leads to amblyopia, a disorder of spatial vision through the affected eye. Researchers typically utilize a macaque model of strabismic amblyopia to study the neural basis of the visual deficits that accompany this visual disorder (Acar et al., 2019; F. H. Baker et al., 1974; Hallum et al., 2017; Kiorpes, 2006; Kiorpes et al., 1998b; Kiorpes & Daw, 2018). In addition to disrupting basic spatial vision functions like visual acuity and contrast sensitivity (Hess & Howell, 1977; Levi & Harwerth, 1977; McKee et al., 2003), amblyopia has been shown to impact cognitive processes that rely on higher visual system function, namely contour integration (Kozma & Kiorpes, 2003; Levi et al., 2007; Rislove et al., 2010), global motion perception (Kiorpes et al., 2006; Meier et al., 2016), visual decision making (Farzin & Norcia, 2011), and visual attention (Hou et al., 2016; Pham et al., 2018). In

Chapter 2 of this dissertation, to better understand the neural origins of perceptual deficits in amblyopia, we study the effects of abnormal early visual experience on functional interactions in pairs of neurons in the primary visual cortex (V1) of adult macaque monkeys with artificially induced strabismic amblyopia.

Even when the visual system develops normally, a variety of factors can either corrupt or optimize our ability to perceive sensory information in the world around us. It is now well accepted that the ability to detect small changes in a stimulus fluctuates even across repeated identical presentations of that stimulus. This variability in perception has been attributed to fluctuations in the responses of individual neurons, as well as to coordinated fluctuations in neural activity of pairs and even populations of neurons (Averbeck et al., 2006; Cohen & Maunsell, 2010; Renart & Machens, 2014; Shadlen & Newsome, 1998; Waschke et al., 2021). One potential source for these neural fluctuations is the noise in retinal sensory receptors and feedforward afferents that provide stimulus information. Additionally, extra-retinal, internal signals such as covert attention, arousal, and motivation can shape both sensory-evoked responses as well as the ongoing background neural activity upon which sensory stimulus information is superimposed (Jacob et al., 2018; Lee & Dan, 2012; Nienborg & Roelfsema, 2015). Even our own subjective experiences can tell us that our ability to perceive and interpret information worsens with increased drowsiness or fatigue and improves when we are well-rested and attentive. What mediates these transitions in internal state? Previous studies suggest that brain state shifts are, at least in part, mediated by brain-wide projections of several small groups of neurons that produce and release neuromodulators. These include Serotonin-synthesizing neurons of the raphe nuclei, Norepinephrine-producing neurons of the locus coeruleus, Dopamine-synthesizing neurons in 3 cell groups of the ventral midbrain (substantia nigra pars compacta, ventral tegmental area and retrorubral area), and the

Acetylcholine-producing neurons of nuclei in the basal forebrain and the midbrain (Aston-Jones & Cohen, 2005a; Everitt & Robbins, 2003; Harris & Thiele, 2011; Jacob et al., 2018; Lee & Dan, 2012; Robbins & Arnsten, 2009; Thiele & Bellgrove, 2018). In chapters 3 and 4 of this dissertation, we investigate how activation of the locus coeruleus, the primary source of noradrenergic neuromodulation in the central nervous system, relates to fluctuations in cortical population activity patterns and perceptual behavior.

1.3 The Locus Coeruleus – Norepinephrine Neuromodulatory System

The locus coeruleus (LC) is a small nucleus of neurons which produce the neuromodulator substance known as norepinephrine (NE). LC is located in the upper pons region of the brainstem; the nucleus is adjacent and ventral to the floor of the fourth ventricle. LC neurons project throughout the central nervous system and the noradrenergic axon terminals are the exclusive source of norepinephrine in cortical areas (R. Y. Moore & Bloom, 2003; Samuels & Szabadi, 2008). NE, when released via projections of LC neurons to other brain regions, can bind to specific receptors and thus modulate the responses of targeted neurons.

The spiking of individual LC neurons occurs in two distinct patterns: 1) baseline LC activity is typically temporally irregular but continuous, with a firing rate of 1-6 spikes/second while 2) phasic LC activation is higher in frequency (10-20 spikes/second) and characterized by brief bursts of spikes that are temporally clustered together (<300ms). Over the past few decades, different functions have been ascribed to these two modes of firing by LC neurons. However, research is still ongoing to more precisely understand how changes in overall LC activation, and

the accompanying neuromodulatory effects of norepinephrine at target sites, may influence both higher order cognitive processes and more innate aspects of behavior.

1.3.1 Anatomical Organization of the LC-NE System

The locus coeruleus is remarkably well connected, despite having a relatively tiny footprint (~30000 cells across both hemispheres in primates) in the brain (Sharma et al., 2010). LC neurons provide norepinephrine (NE) to the entire central nervous system via diffuse ascending axonal projections to most cortical, and subcortical regions, as well as via descending projections to the spinal cord (Loughlin et al., 1986; Poe et al., 2020; Samuels & Szabadi, 2008). LC receives projections from a diverse array of brain regions; these inputs modulate the activity of LC neurons to different extents and provide information about the current state of cognitive, sensory and autonomic processes throughout the nervous system (Poe et al., 2020; Samuels & Szabadi, 2008; Sara & Bouret, 2012a). Although the location, dense clustering and widespread projection pattern of LC neurons are conserved across laboratory rats, mice, non-human primates and humans, there are undoubtedly aspects of the LC-NE system that are unique to each species (Manger & Eschenko, 2021). Because primate studies of LC anatomy are limited, and recent, more detailed studies of the anatomical connectivity of LC have been done in rodents, we review evidence from both species below. We primarily focus on connections that could mediate the regulation of visual perceptual behavior by LC.

Evidence from early anatomical tracing studies suggests that the dorsal prefrontal cortex (PFC) may the only source of direct cortical projections to the LC, in both primates and rodents (Arnsten & Goldman-Rakic, 1984; Luppi et al., 1995). The LC receives projections from several brain regions which have also been implicated in internal state regulation. These include

projections from the central nucleus of the amygdala, from the paraventricular nucleus of the hypothalamus (PVN), and likely from nuclei of all 3 of the other neuromodulatory systems (reviewed by Samuels & Szabadi, 2008). Inputs from several brainstem regions, including the nucleus gigantis cellularis and the nucleus paragigantocelllaris (part of the RVLM), convey information from the autonomic nervous system about cardiovascular, respiratory and digestive processes (Ennis & Aston-Jones, 1989; Mello-Carpes & Izquierdo, 2013; Samuels & Szabadi, 2008; Sara & Bouret, 2012a; van Bockstaele et al., 1993). There is some evidence for an ascending pathway from the dorsal horn of the spinal cord to the LC, which may serve to provide information about noxious somatosensory stimuli (Samuels & Szabadi, 2008).

LC neurons send projections to most regions in the brain (Berridge & Waterhouse, 2003; Loughlin et al., 1986; R. Y. Moore & Bloom, 2003). Although LC axonal projections are widespread, there is now substantial evidence indicating that the density of innervation by noradrenergic fibers varies across cortical regions. In macaques, the earliest observation of these regional differences came from a study that reported a higher-to-lower gradient of norepinephrine concentration along the fronto-occipital axis, such that frontal and somatosensory regions contain a higher concentration of NE than the occipital and temporal lobes (Brown et al., 1979). Later anatomical tracing and immunohistochemical studies in different monkey species confirmed this innervation pattern, by identifying substantial noradrenergic projections from LC to prefrontal cortex (Lewis & Morrison, 1989; Porrino & Goldman-Rakic, 1982b) and to somatosensory cortex (Morrison & Foote, 1986), but observing limited projections to primary visual cortex, and the primary auditory cortex (Campbell et al., 1987; Levitt et al., 1984; Morrison & Foote, 1986). It is noteworthy that within the primate visual system, LC projections predominately target the prefrontal cortex (PFC) and the superior colliculus (SC), while projections to the primary visual

cortex (V1) and the lateral geniculate nucleus (LGN) of the thalamus are quite sparse (Morrison & Foote, 1986). Others have suggested that such a projection pattern supports a role for the LC-NE system in preferentially modulating visuomotor integration functions of PFC and SC while having a lesser influence on visual input processing at the level of LGN and V1 (Berridge & Waterhouse, 2003; Jacob et al., 2018; Morrison & Foote, 1986). Other noteworthy cortical projection targets of LC include the anterior cingulate cortex and motor cortex (Chandler et al., 2014; Porrino & Goldman-Rakic, 1982b).

In addition to the various cortical targets, LC neurons extensively innervate subcortical regions. There is substantial evidence of direct or indirect LC noradrenergic projections targeting the dorsal motor nucleus of the vagus, the rostroventrolateral medulla (RVLM), and the salivatory nuclei, which are all brainstem regions with autonomic system functions (Samuels & Szabadi, 2008). It is now well accepted that changes in LC activity can influence pupil diameter (Joshi et al., 2016a; Joshi & Gold, 2020). Although we do not yet know the precise anatomical circuitry between LC and regions that control pupil diameter, the effects are thought to be mediated at least in part via direct projections to the intermediolateral cell column (IML) of the spinal cord and potentially direct projections to the Edinger-Westphal nucleus (EWN) (reviewed by Joshi & Gold, 2020). Typically, based on projection patterns and types of adrenergic receptors expressed in targeted regions, LC activation influences autonomic functions by increasing the sympathetic drive and decreasing the parasympathetic drive (Samuels & Szabadi, 2008). Importantly, LC also sends direct or indirect projections to centers of the 3 other neuromodulatory systems, including the ventral tegmental area (VTA), the raphe nuclei, and the basal forebrain (Samuels & Szabadi, 2008; Sara, 2009; Schwarz & Luo, 2015).

In the last few years, several research groups have focused on characterizing the organization of cells within LC (reviewed by Poe et al., 2020; Totah et al., 2019). Until recently, it was widely thought that neurons throughout LC are homogenous in function and projection targets. Early studies of the LC-NE system reported the existence of gap junctions between some LC neurons, as well as a synchronization of activation between (small numbers of) pairs of simultaneously recorded LC neurons (Aston-Jones & Bloom, 1981b, 1981a; Finlayson & Marshall, 1988; Usher et al., 1999a). These findings led to the long-standing, widely restated notions that all or most LC neurons activate in synchrony to enable the simultaneous, brain-wide release of NE and that the main function of LC is to globally regulate arousal state (Aston-Jones & Cohen, 2005a; Aston-Jones & Waterhouse, 2016; Dayan, 2012; Lee & Dan, 2012). Recent methodological advances in neural projection mapping (e.g., MAPseq, Kebschull et al., 2016), cell-type labeling and recordings from multiple neurons have enabled new, more precise experiments which have revealed that the structure within LC is more complex and heterogenous than previously thought. For example, one study characterized interactions across thousands of pairs of LC neurons and found that synchronized spiking occurred only in a small (~15%) percentage of pairs (N. K. Totah et al., 2018). Another group of studies together provide evidence for a modular or ensemble based organization of cells within LC, such that different subsets of LC neurons selectively project to some brain regions but not others (Chandler, 2016; Chandler et al., 2014, 2019; Kebschull et al., 2016; Poe et al., 2020; Uematsu et al., 2017; Waterhouse & Chandler, 2012). Furthermore, there is some evidence that these subpopulations of LC neurons have different behavioral functions associated with their differential projection targets (Chandler, 2016; Chandler et al., 2014, 2019; Hirschberg et al., 2017; Uematsu et al., 2017). These detailed examinations of the anatomical organization of the LC-NE system have so far only been done in rodents, but these

important findings should be considered in experiments and result interpretations across all species.

1.3.2 Noradrenergic Modulation of Target Neuron Responses

Past microdialysis studies confirm that fluctuations in LC activity can generate both sustained and transient changes in norepinephrine (NE) efflux in different target areas, thus altering the amount of modulation delivered to target neurons throughout the day (Berridge & Abercrombie, 1999; Florin-Lechner et al., 1996). The majority of LC axon terminals form conventional synapses where they release NE (Papadopoulos et al., 1989), but some likely have non-synaptic NE release sites as well. There is some evidence that upon release, NE can diffuse through the extracellular space to modulate pre- and postsynaptic sites nearby the NE-containing varicosities (Callado & Stamford, 2000). NE exerts its modulatory effects by binding to adrenergic receptors of 3 different families (alpha-1, alpha-2 and beta), which are expressed in varied patterns throughout the brain. Alpha-1 and beta adrenergic receptors are primarily expressed at postsynaptic sites while alpha-2 receptors are expressed postsynaptically and also presynaptically on noradrenergic axon terminals (reviewed in Berridge & Waterhouse, 2003). Alpha-2 receptors have the highest affinity for NE, while alpha-1 and beta receptors have comparatively lower affinity for NE and require higher NE concentrations to be engaged (reviewed in Amsten & Simon, 2000).

Within cortical sensory regions and thalamus, NE has been shown to have complex effects on cellular excitability that can alter neuronal responses to sensory input. These neuromodulatory effects have been characterized in all 4 sensory modalities and include 1) increasing signal-to-noise ratio via reduction of spontaneous but not stimulus-evoked firing, 2) transforming

subthreshold excitatory inputs into suprathreshold spiking responses, 3) sharpening of tuning curves and 4) amplification of stimulus-evoked excitation (Berridge & Waterhouse, 2003; Devilbiss et al., 2006; Foote et al., 1975; Hurley et al., 2004; Jiang et al., 1996; Manella et al., 2017; Martins & Froemke, 2015; McCormick et al., 1991; McLean & Waterhouse, 1994; Waterhouse et al., 1998; Waterhouse & Navarra, 2019a). Many of these findings are from studies that examined how individual sensory neuron responses are altered following the manipulation of noradrenergic transmission either by electrically stimulating in LC or using iontophoresis to locally alter NE concentration within a sensory region of interest. In contrast, very few studies have considered the effects of changing NE concentration on sensory encoding in populations, or even pairs, of neurons (Devilbiss, 2019; Devilbiss et al., 2006).

Overall, the diversity in NE modulatory effects on target neuron responses likely arises from differences in adrenergic receptor expression throughout the brain, in addition to fluctuations in LC activity that adjust the levels of NE. To this point, a series of studies in primate prefrontal cortex showed that the binding of NE to higher affinity alpha-2 receptors enhances neural activity underlying working memory, while NE effects at alpha-1 and beta receptors dampen behavioral performance in spatial working memory tasks (Amsten & Simon, 2000; Berridge & Spencer, 2016; Mao et al., 1999; Ramos & Arnsten, 2007; Sawaguchi, 1998).

1.3.3 Existing Theories of LC function

As described above, LC neurons receive a range of inputs from many brain regions and have diffuse long-distance projections throughout the central nervous system. LC neurons also modulate the activity of neurons in the autonomic nervous system, which controls the function of internal organs. Such elaborate connectivity allows the LC-NE system to account for changes in

cognitive demands while regulating a myriad of important bodily and neural functions such as respiration, cardiac function, pupil size, and transitions in arousal (Aston-Jones & Cohen, 2005b; Carter et al., 2010; Jahn et al., 2020; Reimer et al., 2014; Samuels & Szabadi, 2008). Additionally, a few recent studies have reported that the magnitude of LC phasic activation signals the amount of physical effort required to complete a task-relevant behavioral response for reward (Bornert & Bouret, 2021; Varazzani et al., 2015). Thus, some researchers have proposed that changes in LC activity can help optimize behavioral responses by mobilizing and coordinating cognitive, autonomic, physical (energy) and visual (pupil) resources under stressful or otherwise demanding conditions (Bornert & Bouret, 2021; Sara & Bouret, 2012a; Varazzani et al., 2015).

As first reported more than 50 years ago (Roussel et al., 1967) and confirmed by many subsequent studies, the changes in LC activity and concurrent adjustments to norepinephrine release undeniably contribute to brain-wide transitions between states of sleep and wakefulness (Aston-Jones & Bloom, 1981a; Berridge et al., 1993; Carter et al., 2010; Hobson et al., 1975; Roussel et al., 1967; Samuels & Szabadi, 2008). Additionally, previous work suggests that the LC-NE system may have an important role in regulating cognitive processes such as perception, decision making, learning, and memory formation (Aston-Jones & Cohen, 2005a; Berridge & Waterhouse, 2003; Foote & Berridge, 2019; Sara, 2009). Many researchers have proposed that the NE-mediated improvements to sensory signal processing support a role for the LC-NE system in enhancing sensory perception (Devilbiss, 2019; Devilbiss et al., 2006; Gelbard-Sagiv et al., 2018; Guedj et al., 2019; Hurley et al., 2004; McBurney-Lin et al., 2019; Sara, 2009; Waterhouse & Navarra, 2019b). Fluctuations in LC activity have been correlated with fluctuations in cognitive behavior on different timescales, from seconds to hours (Aston-Jones & Cohen, 2005b; Berridge & Waterhouse, 2003; McGinley et al., 2015; Sara, 2009; N. K. B. Totah et al., 2019a). For

example, phasic bursts (<300ms) are closely temporally aligned with novel or task-related sensory stimuli and behavioral responses that require an animal's immediate attention (Aston-Jones & Bloom, 1981b; Bouret & Sara, 2004; Foote et al., 1980; Sara & Bouret, 2012a), while slower timescale (minutes to hours) changes in LC baseline activity have been correlated with similarly timed changes in distraction and task-engagement in some behavioral contexts (Aston-Jones & Cohen, 2005a; Usher et al., 1999a). Some have argued the level of LC activity regulates cognitive performance according to the level of arousal, such that moderate LC activation optimizes cognitive resources necessary for the task at hand, while extremely low or high levels of LC activity correspond to disengagement due to drowsiness or mental stress, respectively (Arnsten, 1998; Aston-Jones & Cohen, 2005b; Devilbiss et al., 2006; Usher et al., 1999a).

Despite many existing theories about the function of noradrenergic neuromodulation, our knowledge of how changes in the activation of the LC-NE system may modulate neural computations underlying cognition is only in the early stages. This is because researchers have only recently begun to interpret results from experiments where LC activity (or NE axon activity) is recorded concurrently with cortical activity in animals engaged in cognitive tasks. In chapters 3 and 4 of this dissertation, we explore the significance of LC activation for visual perceptual decision making. Specifically, we examine the relationship between different timescales of fluctuations in the activity of the locus coeruleus, decision relevant processes in prefrontal cortex and variability in visual perceptual behavior.

1.4 Perceptual Decision Making

Perceptual decision making is a sensorimotor process by which an appropriate behavioral response is chosen upon interpreting the available sensory information in the surroundings. A real-world example of perceptual decision making is a driver choosing to stop the car upon noticing a traffic light change from green to yellow. Over the past few decades, researchers have come up with varied experimental paradigms and theoretical models to better understand the neural basis of how perceptual decisions are formed (Gold & Shadlen, 2007; Hanks & Summerfield, 2017; O'Connell et al., 2018). In a laboratory setting, perceptual decision formation is typically studied by recording neural activity in candidate neurons that encode task relevant information, while subjects engage in tasks that require them to make decisions about sensory stimuli and report their choices via overt motor responses such as saccades. Statistical models, such as 'sequential sampling' and 'signal detection theory (SDT)' have been immensely helpful for parsing the decision process into tractable elements. A perceptual decision is now thought to depend on: 1) information or evidence from the sensory stimulus and 2) a decision threshold or criterion which, in dynamic decision models, describes how much sensory evidence needs to accumulate before commitment to a decision, and, in SDT, describes the how strong a sensory signal must be to decide that a stimulus is present (Gold & Shadlen, 2007). Taken together, past experimental studies convincingly show that these decision computations can be implemented by several brain regions with a range of sensorimotor functions (Gold & Shadlen, 2007; Hanks & Summerfield, 2017; O'Connell et al., 2018). Ongoing research aims to better understand sources of variability in perceptual decision making behavior.

In the studies described in chapters 3 and 4 of this thesis, we were interested in relating concurrently recorded population activity in the dorsolateral Prefrontal Cortex (dlPFC), and single

neuron activity in the Locus Coeruleus (LC), to elements of the perceptual decision making process. To accomplish this, our task design was rooted in signal detection theory, which is one method to statistically model the process of perceptual decision formation (Gold & Shadlen, 2007; Macmillan & Creelman, 2004; Shadlen & Kiani, 2013). SDT is typically applied to binary (two-alternative) decisions – for example in a task where the subject must decide whether a change in a stimulus occurred or not. Reporting Yes or No for trials of the two possible stimulus conditions (change present or absent) provides 4 different behavioral outcomes: hit, miss, correct rejection and false alarm. According to the SDT model for perception, a behavioral report about a stimulus in the task depends on noisy internal neural signals that represent sensory evidence. The range of neural responses evoked by change (signal) and no-change (noise) stimuli is represented by overlapping normal distributions. There are two metrics that determine if a subject perceives or misses a stimulus change, these are 1) sensitivity (d') and 2) criterion (c). Behavioral sensitivity is a measure of how well an ideal observer can separate the presence of signal in a sensory stimulus from its absence while decision criterion is akin to a decision rule, conveying how strong or reliable the sensory evidence signal must be before the ideal observer decides to report an orientation change.

Previous work in trained monkeys performing two choice visual discrimination or detection tasks amenable to SDT analysis indicates that sensory evidence for decisions is represented by neurons in visual cortical regions. For example, MT (V5) neurons represent motion direction information (Zeki, 1974), V1/V4 represent orientations (Desimone & Schein, 1987; Hubel & Wiesel, 1959, 1962; HUBEL & WIESEL, 1965; Roe et al., 2016), and responses of neurons in these areas are correlated with the perceptual decisions reported by animals (Britten et al., 1992, 1996; Cumming & Nienborg, 2016; Macke & Nienborg, 2019; Nienborg et al., 2012).

Sensorimotor regions such as dorsolateral prefrontal cortex, lateral intraparietal area and superior colliculus (dlPFC, LIP, SC) are thought to both set the criterion for the sensory evidence required to report a choice, as well as prepare and execute eye movement commands to report the decisions. A recent study reported that electrical stimulation of superior colliculus (SC) neurons led to changes in behavioral decision criterion, providing convincing evidence that SC neural activity can control the position of decision criterion (Crapse et al., 2018). Does it then follow, that SC neurons are exclusively responsible for setting the decision criterion? Not quite. A series of recent studies investigated whether spatial attention-related modulation of neural activity in V4 and dlPFC is linked to distinct behavioral changes on a stimulus change detection task. They found that when subjects attended a cued location in the visual field, the activity of dlPFC neurons with receptive fields at the attended location reflected spatially specific changes in criterion, while activity of visual cortex neurons corresponded to changes in the quality of sensory representation of the attended stimulus (Luo & Maunsell, 2015, 2018). Thus, it is likely that multiple brain regions work together to adjust the decision criterion. Collectively, previous work indicates that process of decision formation involves neural activity across a distributed network of brain regions with sensory, and sensorimotor functions. Modulation of neural responses in any one of these brain regions could result in distinct changes in perceptual decision making behavior.

1.5 Behaviorally Relevant Signals Encoded by Populations of Neurons

Many of the classic past studies of visual processing and perceptual decision making could only gain insights from experiments in which a single neuron was recorded in one brain region at a time. For instance, most of what we know about neural correlates of amblyopia comes from

analyzing trial averaged single neuron responses within V1 or V2. However, it is now known that previously found changes in contrast sensitivity and spatial frequency tuning of single V1 neurons are too small in magnitude to account for the entirety of perceptual deficits revealed by behavioral assessments of monkeys with amblyopia (Bi et al., 2011; Kiorpes et al., 1998a; Shooner et al., 2015b). Recent technological advances have made it possible to record neural activity simultaneously from populations of neurons within and across different brain regions, prompting researchers to test novel theories about the neural basis for visual perception that look beyond single neuron responses.

With new developments in large scale data collection, came the need for advanced analysis methods that can help interpret behaviorally relevant patterns in high-dimensional neural activity. The application of dimensionality reduction methods to neural population activity has been transformative for the field of perceptual decision making, leading to improved models of neural mechanisms supporting perceptual decisions (Cohen & Maunsell, 2010, 2011; Cunningham & Yu, 2014; Engel & Steinmetz, 2019; Najafi & Churchland, 2018; O'Connell et al., 2018; Williamson et al., 2019). For instance, in a recent study from our lab, we applied dimensionality reduction methods to population activity simultaneously recorded in two brain regions and thus uncovered a novel brain-wide slow varying neural signal that can influence decision formation by shifting the likelihood of an impulsive decision and overriding sensory evidence (Cowley et al., 2020). Another recent study identified a similar fluctuation in population activity of motor cortex neurons, that reflected changes in a monkey's engagement in a learning paradigm on a trial-to-trial timescale (Hennig et al., 2021).

Recent neurophysiological studies have reported the presence of multiple behaviorally-related dimensions (e.g., thirst, facial movements) in the population activity of several different

brain regions (Allen et al., 2019; Stringer et al., 2019). A particularly interesting finding was that the representation of sensory stimuli and spontaneous facial movements, such as licking, whisking, and sniffing, was mixed among different dimensions of population activity in mouse visual cortex (Stringer et al., 2019). These findings support the idea that neural encoding of any sensory information is combined with behavioral state variables into a mixed representation. Such findings warrant further investigation into how internal state-regulating signals transmitted by neuromodulatory systems may influence encoding of sensory or goal-related information by populations of neurons in different behavioral contexts, whether during task-related cognitive engagement or in the natural environment. In the studies described in this dissertation, we took advantage of the recent advances in experimental techniques and data analyses to examine how neural signals on multiple processing levels and temporal scales coordinate to influence visual perception and behavior.

2.0 Altered Functional Interactions between Neurons in Primary Visual Cortex of Macaque Monkeys with Experimental Amblyopia

2.1 Introduction

Normal visual system development is dependent on having unobstructed and balanced binocular visual experience during early life. Amblyopia is a disorder of the visual system which often arises when visual input through the two eyes is imbalanced, most commonly through a misalignment of the two eyes (strabismus) or anisometropia (unilateral blur), during a critical window for development. Amblyopic individuals show major impairments in basic spatial vision in the affected eye, including decreased visual acuity and diminished contrast sensitivity that is often particularly acute at high spatial frequencies (Asper et al., 2000; D. H. Baker et al., 2008; Bradley & Freeman, 1981; Hess & Howell, 1977; Levi, 2013; Levi & Harwerth, 1977; McKee et al., 2003; Meier & Giaschi, 2017). Furthermore, several studies suggest that amblyopia is detrimental to cognitive processes that rely on higher visual system function, namely contour integration, global motion sensitivity, visual decision-making, and visual attention (El-Shamayleh et al., 2010; Farzin & Norcia, 2011; Hamm et al., 2014; Hou et al., 2016; Kiorpes, 2006, 2016; Kozma & Kiorpes, 2003; Levi et al., 2007; Meier et al., 2016; Meier & Giaschi, 2017; Pham et al., 2018; Rislove et al., 2010). Deficits in amblyopic vision originate from altered neural activity in the primary visual cortex (V1), and cortical areas downstream of V1, rather than from abnormalities in the eye or the visual thalamus (Bi et al., 2011; Blakemore & Vital-Durand, 1986; Hallum et al., 2017; Hubel & Wiesel, 1965, 1977; Kiorpes et al., 1998b; Movshon et al., 1987; Shooner et al., 2015b; E. L. 3rd Smith et al., 1997; Tao et al., 2014; Wiesel, 1982).

Previous studies using macaque models of amblyopia provide evidence for some functional reorganization of ocular dominance in amblyopic V1 (Adams et al., 2015; M. L. Crawford et al., 1989; M. L. J. Crawford & Harwerth, 2004; Fenstemaker et al., 2001; Hendrickson et al., 1987; Horton et al., 1997; LeVay et al., 1980; Tychsen et al., 2004; Tychsen & Burkhalter, 1992, 1997), including a significant loss in the proportion of binocularly activated cells and – in severe amblyopia – a reduced proportion of neurons that respond to amblyopic eye stimulation (Kiorpes et al., 1998b; Schröder et al., 2002; Shooner et al., 2015a; E. L. 3rd Smith et al., 1997). Additionally, several studies report changes in spatial frequency tuning, as well as a loss of contrast sensitivity in some V1 neurons that receive input from the amblyopic eye in monkeys (Kiorpes et al., 1998b; Movshon et al., 1987) and in cats (Chino et al., 1983; Crewther & Crewther, 1990). Overall, these changes in the functional properties of V1 neurons suggest that the representation of visual input from the amblyopic eye across the cortical neuronal population is distorted.

Early studies on the neural basis of amblyopia hypothesized that the perceptual deficits in amblyopes arise directly from corresponding losses in responsivity of single neurons in primary visual cortex (Wiesel, 1982; WIESEL & HUBEL, 1963). However, it is now clear that the magnitude of these single neuron changes cannot account for the entirety of spatial vision deficits revealed by behavioral assessments of amblyopes (Bi et al., 2011; Kiorpes et al., 1998b; Shooner et al., 2015a). There are two additional neurophysiological mechanisms that could contribute to amblyopia: (1) neural deficits more profound than those seen in V1 may arise in downstream visual areas (Bi et al., 2011; El-Shamayleh et al., 2010; Kiorpes, 2016; Kiorpes et al., 1998b; Tao et al., 2014; H. Wang et al., 2017) and (2) impaired visual representation might result from changes in the structure of activity in populations of V1 neurons (Kiorpes, 2016; Roelfsema et al., 1994; Shooner et al., 2015a).

Here we seek evidence for this second mechanism, and investigate whether activity correlations between neurons are altered in amblyopic V1 during visual stimulus processing. We recorded from populations of V1 neurons in macaque monkeys that had developed amblyopia as a result of surgically-induced strabismus (as in Kiorpes et al., 1998). We measured correlation in the trial-to-trial variability (hereafter referred to as "correlation") in the responses of pairs of neurons to an identical visual stimulus presented to either the non-amblyopic (fellow) or amblyopic, deviating eye. Similar to the firing rate of single neurons, the strength of correlated variability in normal visual cortex has been shown to change due to a number of factors, including the contrast of a visual stimulus (Kohn & Smith, 2005), the animal's attentional state (Cohen & Maunsell, 2009a; Mitchell et al., 2009; Snyder et al., 2016), and over the course of perceptual learning (Gu et al., 2011; Ni et al., 2018). In our experiments, comparing correlation measurements for stimuli presented to the two eyes allowed us to determine whether the functional circuitry used for processing amblyopic eye visual input is altered compared to that supporting fellow eye processing. We found that correlation indeed changes depending on which eye receives the visual stimulus, an effect that was not present in a control animal. Overall, stimuli presented to the amblyopic eye evoked correlations that were more prominent in pairs of neurons with similar orientation tuning and eye preference. When stimulus contrast was increased, pairs of neurons driven through the fellow eye tended to decorrelate, whereas the high levels of correlation remained elevated for neurons driven by the affected eye. Our findings are consistent with the hypothesis that the abnormalities in amblyopic vision may in part be explained by changes in the strength and pattern of functional interactions among neurons in primary visual cortex.

2.2 Methods

Subjects. We studied four adult macaque monkeys (Macaca nemestrina), three female and one male. One animal remained a visually normal, untreated control while three of the animals developed strabismic amblyopia as a result of surgical intervention at 2-3 weeks of age. Specifically we resected the medial rectus muscle and transected the lateral rectus muscle of one eye in order to induce strabismus. All of the animals underwent behavioral testing to verify the presence or absence of amblyopia. All procedures were approved by the Institutional Animal Care and Use Committee of New York University and were in compliance with the guidelines set forth in the United States Public Health Service Guide for the Care and Use of Laboratory Animals.

Behavioral testing. We tested the visual sensitivity of each animal by evaluating their performance on a spatial two-alternative forced-choice detection task. Behavioral testing was conducted at the age of 1.5 years or older, and the acute experiments took place at the age of 7 years or older. On each trial in this task, a sinusoidal grating was presented on the left or the right side of a computer screen while the animal freely viewed the screen. The animal had to correctly indicate the location of the grating stimulus by pressing the corresponding lever in order to receive a juice reward. The gratings varied in spatial frequency and contrast level: we tested 5 contrast levels at each of 3-6 different spatial frequencies and collected at least 40 repeats of each stimulus combination. We then determined the lowest contrast the animal could detect at each spatial frequency (threshold contrast) and constructed contrast sensitivity functions for each animal's right and left eyes. A detailed account of the procedures we used for behavioral assessment in this study can be found in previous reports (Kiorpes et al., 1998b; Kozma & Kiorpes, 2003).

Electrophysiological recording. The techniques we used for acute physiological recordings have been described in detail previously (M. A. Smith & Kohn, 2008). Briefly, anesthesia was

induced with ketamine HCl (10 mg/kg) and animals were maintained during preparatory surgery with isoflurane (1.5-2.5% in 95% O2). Anesthesia during recordings was maintained with continuous administration of sufentanil citrate (6-18 μg/kg/hr, adjusted as needed for each animal). Vecuronium bromide (Norcuron, 0.1 mg/kg/hr) was used to suppress eye movements and ensure stable eye position during visual stimulation and recordings. Drugs were administrated in normosol with dextrose (2.5%) to maintain physiological ion balance. Physiological signs (ECG, blood pressure, SpO2, end-tidal CO2, EEG, temperature, and urinary output and osmolarity) were continuously monitored to ensure adequate anesthesia and animal well-being. Temperature was maintained at 36-37 C°.

Recordings of neural activity were made from 100-electrode "Utah" arrays (Blackrock Microsystems) using methods reported previously (Kelly et al., 2007; M. A. Smith & Kohn, 2008). Each array was composed of a 10x10 grid of 1 mm long silicon microelectrodes, spaced by 400 um (16 mm^2 recording area). Each microelectrode in the array typically had an impedance of 200-800 kOhm (measured with a 1 kHz sinusoidal current), and signals were amplified and bandpass filtered (250 Hz to 7.5 kHz) by a Blackrock Microsystems Cerebus system. We targeted the superficial layers by inserting the arrays 0.6 mm into cortex using a pneumatic insertion device (Rousche & Normann, 1992).

Our full data set consisted of acute recordings from 7 microelectrode arrays across 3 amblyopic macaque monkeys and 4 arrays in 1 control monkey. One of the amblyopic animals (EM 640) had 4 array implants (3, 8, 14 and 51 neurons); one (JS 579) had 2 array implants (34 and 68 neurons), and the third (HN 580) had 1 array implant (30 neurons). The control animal had 4 implants (4, 7, 6, and 16 neurons). For animals with multiple implants in a single hemisphere, the array was removed and shifted to a different, non-overlapping region of cortex prior to

reimplantation. We did not notice any substantial differences in recording quality across arrays moved to different locations. Arrays were inserted within a 10 mm craniotomy made in the skull, centered 10 mm lateral to the midline and 10 mm posterior to the lunate sulcus. The resulting receptive fields lay within 5° of the fovea.

Visual stimulation. We presented stimuli on a gamma-corrected CRT monitor (Eizo T966), with spatial resolution 1280 x 960 pixels, temporal resolution 120 Hz, and mean luminance 40 cd/m^2. Viewing distance was 1.14 m or 2.28 m. Stimuli were generated using an Apple Macintosh computer running Expo (http://corevision.cns.nyu.edu).

We used a binocular mirror system to align each eye's fovea on separate locations on the display monitor, so that stimuli presented in the field of view of one eye did not encroach on the field of view of the other eye. This setup enabled us to show stimuli to the receptive fields for the right and left eye independently. We mapped the neurons' spatial receptive fields by presenting small, drifting gratings (0.6 degrees; 250 ms duration) at a range of spatial positions in order to ensure accurate placement of visual stimuli within the recorded neurons' receptive fields. During experimental sessions, we presented full-contrast drifting sinusoidal gratings at 12 orientations spaced equally (30˚) in the field of view of either the right or the left eye on alternating trials. Each stimulus was 8–10 deg in diameter and was presented within a circular aperture surrounded by a gray field of mean luminance. Each stimulus orientation was repeated 100 times for each eye. Periods of stimulus presentation lasted 1.28 seconds and were separated by 1.5 s intervals during which we presented a homogeneous gray screen of mean luminance. In one of the amblyopic animals (4 separate array implants) and the control animal, we presented the drifting sinusoidal gratings at 12 orientations and 3 contrast levels (100%, 50%, 12%). In these cases, stimuli were presented for 1 second and each stimulus orientation was repeated 50 times at each of three

contrasts. The spatial frequency (1.3 c/deg) and drift rate (6.25 Hz) values for the grating stimuli were chosen to correspond to the typical preference of parafoveal V1 neurons (Foster et al., 1985; M. A. Smith et al., 2002) and to be well within the spatial frequency range where we could behaviorally demonstrate contrast sensitivity in both eyes.

Spike sorting and analysis criteria. Our spike sorting procedures have been described in detail previously (M. A. Smith & Kohn, 2008). In brief, waveform segments exceeding a threshold (based on a multiple of the r.m.s. noise on each channel) were digitized at 30 kHz and stored for offline analysis. We first employed an automated algorithm to cluster similarly shaped waveforms (Shoham et al., 2003) and then manually refined the algorithm's output for each electrode. This manual process took into account the waveform shape, principal component analysis, and inter-spike interval distribution using custom spike sorting software written in Matlab (https://github.com/smithlabvision/spikesort). After offline sorting, we computed a signal to noise ratio metric for each candidate unit (Kelly et al., 2007) and discarded any candidate units with SNR below 2.75 as multi-unit recordings. We kept all neurons for which the best grating stimulus evoked a response of more than 2 spikes/second for either the fellow or amblyopic eye. We considered the remaining candidate waveforms (240 units total across sessions) to be high-quality, well isolated single units and we included these units in all further analyses.

Fano factor. The Fano factor (FF) is defined as across-trial spike count variance divided by mean spike count. We calculated the mean and variance of spike counts for each neuron across 50 repeat trials of an identical high contrast stimulus (stimuli of each orientation were considered as a separate group of 50 repeats). For each neuron-stimulus group of 50 trials, we calculated the mean and variance of spike counts in 100-ms time windows starting at stimulus onset (time 0) and sliding every 50 ms until 850 ms post-stimulus onset. For example, for a time bin of 0-100 ms

relative to stimulus onset, counts were made within that 100-ms window at the beginning of each of the 50 trials of each neuron-stimulus pairing, and the mean and the variance were calculated from the resulting set of 50 numbers.

Measurements of the Fano factor are known to be influenced by variability in firing rates: the Fano factor declines as the mean firing rate increases. It is important to take this into account when comparing Fano factor at different time points throughout the trial or for different behavioral conditions to ensure that any significant differences in FF are not simply a consequence of large changes in mean firing rate (Churchland et al., 2010). To control for the possible effect of changing firing rates on FF measurements, we used a "mean-matching" method which keeps the population distribution of mean firing rates (but not variances) constant across the analyzed time points and eye stimulation conditions (Churchland et al., 2010). For each eye condition, the mean-matching algorithm first assembled a scatter of the mean rate for each neuron-stimulus set of trials plotted against the variance for each neuron-stimulus pairing, doing so at each time bin. Then, the algorithm selected the greatest common distribution of mean rates across the time points and eye conditions. Then, independently at each time point, neuron-stimulus data points were randomly eliminated if they fell outside the common distribution, and thus not considered in FF calculation for that time point for each eye condition. Importantly, for each eye condition, different neuron-stimulus data points were eliminated, but an equal number of data points remained in subdistributions for the two eye conditions after the elimination. FF was then computed for each eye condition from the remaining neuron-stimulus points as the slope of the regression relating the variance to the mean. The elimination procedure was repeated 10 times, and the resulting FF value for each time point and eye condition was an average of the 10 iterations. We adapted the code

provided in the "Variance Toolbox" for MATLAB by M.M. Churchland to do the mean-matching procedure across behavioral conditions in addition to across time points (Churchland et al., 2010).

Measures of correlation. Here we provide a brief description of correlation analyses performed for this study. A detailed discussion can be found in two previous publications (Kohn & Smith, 2005; M. A. Smith & Kohn, 2008). The r_{sc}, also known as spike count correlation or noise correlation, captures the degree to which trial-to-trial fluctuations in responses are shared by two neurons. Quantifying the magnitude of the correlation in trial-to-trial response variability is achieved by computing the Pearson correlation coefficient of evoked spike counts of two cells to many presentations of an identical stimulus. For each session, we paired each neuron with all of the other simultaneously recorded neurons, but excluded any pairs of neurons from the same electrode. We then combined all the pairs from all of the recording sessions in the amblyopic animals, and separately, the control animal. This resulted in 4630 pairs across the 3 amblyopic animals and 155 pairs in one control animal. For each stimulus orientation, we normalized the response to a mean of zero and unit variance (Z-score), and calculated r_{sc} after combining response z-scores across all stimuli. We removed trials on which the response of either neuron was > 3 SDs different from its mean (Zohary et al., 1994) to avoid contamination by outlier responses. We also compared our measures of response correlation to the tuning similarity of the two neurons, which we calculated as the Pearson correlation between the mean response of each cell to each of the tested orientations (termed r_{signal}). For neurons with similar orientation tuning r_{signal} is closer to 1, while neurons with dissimilar tuning have r_{signal} values approaching −1.

Curve fitting: We fit the raw data in Figure 4C with the equation:

$$r_{sc} = [a - b(distance)]^{+} e^{\frac{rsignal-1}{\tau}} + c$$

in order to estimate the parameters a (y-intercept), b (slope), τ (exponential decay constant) and c (baseline value). We used the Matlab function lsqcurvefit, with initialization parameters based on the fit parameters estimated for r_{sc} , r_{signal} and distance data in our previous work in visually normal animals (M. A. Smith & Kohn, 2008). The utilized initialization values were: a = 0.225, b = 0.048, T = 1.87, c = 0.09.

Ocular dominance analysis. For each unit, we first obtained the average firing rate response to each of the 12 orientations of high contrast gratings, then subtracted the baseline firing rate measured during the interstimulus intervals. Next, we determined each unit's eye preference by comparing the maximum mean response elicited by visual stimulation of the fellow eye (R_f) with the same unit's maximum response to visual stimulation of the amblyopic eye (R_a). Specifically, we computed an ocular dominance index (ODI) defined as ODI = $(R_f - R_a)/(R_f + R_a)$. The ODI values ranged from -1 to 1, with more negative values signifying a cell's preference for amblyopic eye stimulation, and more positive values indicating a preference for the fellow eye. For the pairwise analyses, we measured the difference between the ODI values of the cells constituting each pair, such that cells with a very similar eye preference had an ODI difference close to 0, and cells preferring opposite eyes had an ODI difference close to 2.

Statistical significance tests. All indications of variation in the graphs and text are standard errors with paired t-tests, unless otherwise noted.

We used a bootstrapping method for statistical testing of the relationships between r_{sc} and r_{signal}. Specifically, for 1000 iterations, we sampled with replacement from a pool of matched r_{sc} and r_{signal} values computed for each pair of neurons, separately for each eye condition. Using the "polyfit" function in Matlab, we then computed the slope of a line fit through the scatter of r_{sc} values plotted against the corresponding r_{signal} values for the neuronal pairs used on each sampling

iteration. Thus, for each eye stimulation condition, we collected 1000 estimates of the slope of the linear relationship between r_{sc} and r_{signal}. We then looked at confidence interval bounds to test for a statistically significant difference between the bootstrapped distributions of slope values computed for amblyopic vs. fellow eye stimulation. We also performed the same bootstrapping procedure to assess whether the relationship between r_{sc} and eye preference was significantly different between fellow and amblyopic eye conditions. We used non-smoothed data for this statistical analysis.

We also used bootstrapping for statistical testing of the inter-ocular difference in delta $r_{sc.}$ Briefly, we calculated Δr_{sc} in our data set by subtracting the high contrast r_{sc} value of each neuronal pair from the low contrast r_{sc} value attained for the same pair of neurons. We then performed 1000 iterations of randomly sampling with replacement from the pool of pairs of neurons (1381 pairs total). Each pair of neurons was associated with a high contrast and low contrast r_{sc} value that we could use to compute $\Delta r_{sc.}$ For each eye condition, on each iteration, we computed the average of the sample of Δr_{sc} values. In the end we collected a distribution of 1000 average Δr_{sc} values for each eye condition. We compared these distributions of Δr_{sc} values using confidence interval bounds.

Decoding stimulus orientation. Within 4 separate recording sessions, we randomly subdivided the spiking data in our two eye conditions such that a subset of the trials was used to train the classifier and the held-out trials were used to assess classification performance. We did 3 rounds of cross-validation such that 3 different random subsets of trials were used for training the classifier. For 3 of the recording sessions (JS 579 and EM 640), we show the average classification performance of 20 classifiers each trained and tested on the responses of 30 randomly selected V1 neurons in each session. In the fourth session (subject HN 580), we only recorded from 30 neurons

in total, and thus for this session we assessed performance of just one classifier from 3 rounds of cross-validation. For each round of cross-validation that we performed for each group of 30 neurons, we calculated the classification accuracy of the trained classifier as the proportion of held-out, testing trials that were correctly classified - meaning these trials were assigned their true class labels by the classifier. The remaining three of the total seven sessions had comparatively few simultaneously recorded cells (~10) and thus were not included in this decoding analysis.

As we had a total of 12 stimulus orientations, for each testing trial, a trained multi-class classifier was tasked with deciding which one of 12 orientations (classes) was most fitting given the V1 population activity on that trial. We used the Error-Correcting Output Coding method (ECOC) which decomposed our multi-class classification problem into many binary classification tasks solved by binary SVM classifiers. In the ECOC framework, the final decision about the class label for a piece of data is achieved by considering the output or "vote" of each subservient binary classifier.

2.3 Results

The overall goal of our study was to examine whether neuronal interactions are altered within primary visual cortex of strabismic amblyopes. To this end, we recorded from populations of V1 neurons using 100-electrode "Utah" arrays while a visual stimulus was separately presented to the amblyopic or the fellow, non-amblyopic eye of anesthetized macaque monkeys. We then evaluated the strength and pattern of correlation in the recorded populations in order to determine if functional interactions among neurons differed during visual stimulation of each eye.

2.3.1 Behavioral Deficits in Amblyopic Monkeys

Prior to the neural recordings, we characterized the behavioral extent of the amblyopic visual deficits by constructing spatial contrast sensitivity functions for each eye in the amblyopic animals. The fitted curves were used to estimate the optimal spatial frequency and peak contrast sensitivity. For the three strabismic amblyopes, reduced contrast sensitivity and spatial resolution in the amblyopic eye was evident from the reduced peak and spatial extent of the fitted curve (Figure 1). The control animal was tested binocularly and confirmed to be visually normal (Figure 1). Based on these behavioral assessments, we concluded that all three of our experimental animals had severe strabismic amblyopia.

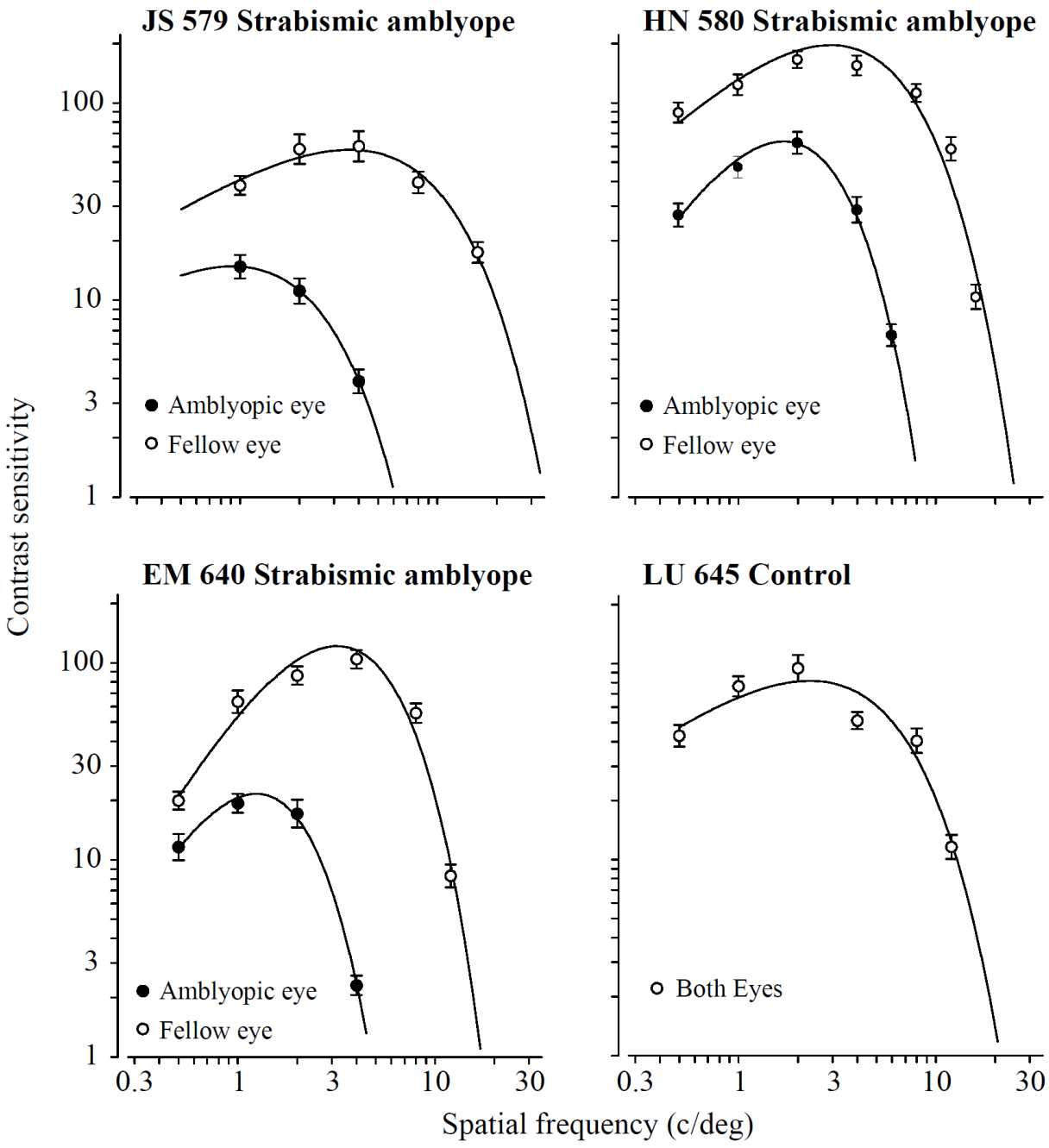

Figure 1. Behavioral assessment of strabismic amblyopes and visually normal animals.
Spatial contrast sensitivity functions, plotted separately for the amblyopic eye (filled symbols) and fellow eye (unoperated, normal eye; open symbols). The four panels show plots for 3 strabismic amblyopes and 1 control, visually normal animal. Behavioral sensitivity loss in the amblyopic eye was observed for all 3 amblyopes: the peak contrast sensitivity was both decreased and shifted to lower spatial frequencies for the amblyopic eyes compared to the fellow eyes.

2.3.2 Amblyopia Affects Individual Neuronal Responsivity

We first studied the changes in single neuron responses in amblyopic primary visual cortex. We recorded from "Utah" arrays while a drifting sinusoidal grating was presented to either the fellow or amblyopic eye of an anesthesized monkey. We presented full-contrast gratings of 12 different orientations to either the amblyopic or fellow eye of three monkeys. For comparison, we also analyzed neural responses to the full-contrast stimuli shown to the right or left eye of the control animal.

We found that most V1 neuronal firing rates were substantially lower during amblyopic eye stimulation compared to fellow eye stimulation (Figure 2A-B). Over the whole population of recorded neurons, the mean maximum spike count across 1-second stimuli presented to the fellow eye was 15.08 ± 1.1 sp/s, compared to 9.56 ± 0.96 sp/s for the same 1-second stimuli presented to the amblyopic eye ($p<0.0001$, Figure 2B). In the control animal, considering all the recorded neurons, there was no statistically significant difference in maximum evoked firing rates for left versus right eye stimulation (Figure 2C, 9.61 ± 1.67 vs. 9.65 ± 1.55 sp/s, $p=0.92$).

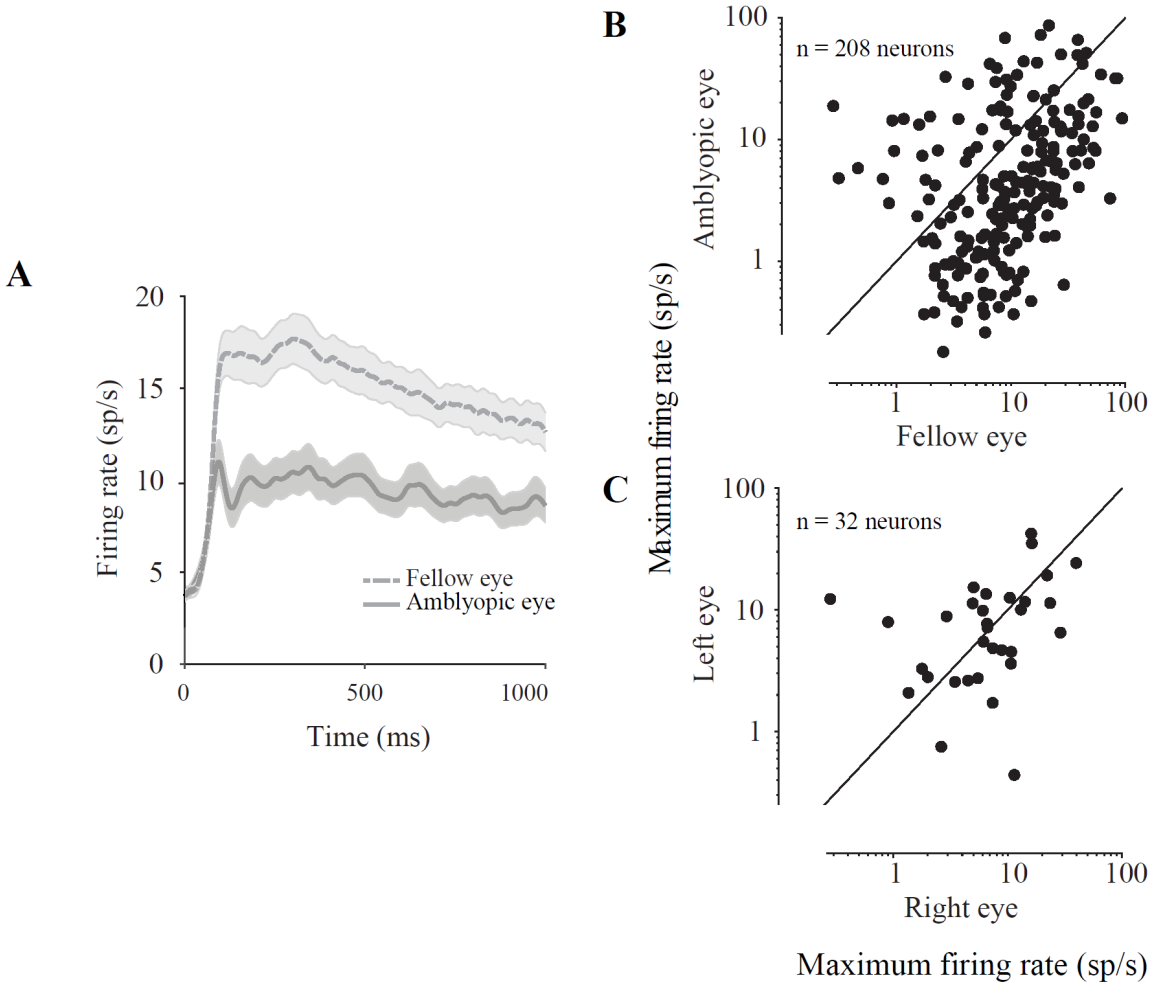

Figure 2. Comparison of neuronal firing rates in response to normal and amblyopic eye stimulation.

(A) Peristimulus time histograms (PSTHs) show the population average responses to fellow (dashed line) and amblyopic (solid line) eye stimulation. For each neuron, we computed a PSTH for the one stimulus orientation that evoked the highest response from that neuron, then we averaged across all recorded neurons. Shading represents ± 1 SEM (n = 208 neurons). Neuronal firing rates were greatly diminished upon amblyopic eye stimulation. (B) Each point in the scatter diagram represents the maximum firing rate (spike count during 1 second of stimulus presentation) of each recorded neuron across 12 tested orientations of drifting gratings. The maximum firing rates in response to stimulation of the fellow eye are plotted against the maximum firing rates evoked by amblyopic eye stimulation. The majority of recorded neurons showed decreased responsivity to amblyopic eye stimulation as compared to fellow eye stimulation. Combined across animals, a total of 208 neurons were recorded from V1 of amblyopic animals. (C) Same as in (B), except data for the control animal are shown. A total of 32 neurons were recorded in the control, visually normal animal. There was no observed difference in the maximum firing rates elicited by stimulation of normal right and left eyes.

2.3.3 Amblyopia Alters Both Response Variability and Coordinated Population Activity in V1

It is well known that both the spontaneous and evoked responses of individual neurons are variable even across repeated trials of identical visual stimulation conditions (Arieli et al., 1996; Shadlen & Newsome, 1998; Tolhurst et al., 1983). Recent neurophysiological studies have found that in many primate visual areas, the ongoing response variability declines with the onset of a stimulus (Churchland et al., 2010), suggesting that sensory inputs stabilize cortical activity which could in turn improve the reliability of transmitted sensory information. In amblyopia, it is possible that abnormally increased neuronal response variability during stimulus processing contributes to vision problems(Levi et al., 2008). In fact, a recent study compared the amount of spiking noise between V2 neurons of amblyopic and visually normal animals, and found that response variability was increased in amblyopic V2 during spontaneous activity and for low contrast visual stimulation (Y. Wang et al., 2017).

We quantified whether trial-to-trial response variability of individual neurons in V1 differs between amblyopic and fellow eyes by measuring the Fano factor (FF), or the variance-to-mean ratio, for spiking responses elicited by high contrast stimulation of each eye. Importantly, we utilized a mean matching procedure in our calculation of FF, where we used different subgroups of neurons across different time points and eye stimulation conditions to keep the mean firing rates constant (see Methods). This method ensured that the computed FF values were independent of the any large changes in firing rates between the eye stimulation conditions, or over the course of stimulus presentation.

We assessed the temporal evolution of FF throughout the stimulus duration by calculating FF in 100 ms time windows at multiple time points over the 1 second stimulus. We found that for

both eye conditions, there was a sharp decrease in FF after stimulus onset that was consistent with the previously observed time course of FF in a study of numerous cortical areas (Figure 3A;(Churchland et al., 2010)). However, we observed that FF for amblyopic eye stimulation remained significantly higher than FF for fellow eye throughout the whole stimulus duration (Figure 3A), indicating that a high level of spiking variability persists in V1 neurons during processing of visual stimuli presented to the amblyopic eye.

A small portion of the individual neuron response variability, or noise, is known to be shared between neighboring neurons in cortex. Numerous recent studies have been devoted to understanding how stimulus information is embedded in the population code. In particular, the pattern of correlated variability and its dependence on the stimulus-response structure have been shown in theoretical studies to have potential importance for the information in the population code (Averbeck et al., 2006; Kohn et al., 2016). We reasoned that amblyopia could alter the activity pattern and level of interaction in networks of V1 neurons, and might thereby influence information encoding and behavioral performance.

We measured the correlated variability of neural responses to quantify the interactions in pairs of simultaneously recorded V1 neurons. The degree to which trial-to-trial fluctuations in responses are shared by two neurons can be quantified by computing the Pearson correlation of spike count responses to many presentations of the same stimulus (termed spike count correlation, r_{sc}, or noise correlation). In Figure 3B, the scatter plot depicts z-transformed spike count responses of two example recorded V1 neurons to an identical stimulus presented to the fellow eye on many trials. The depicted pair of neurons has a positive r_{sc} of 0.31, indicating that responses of these two neurons tend to fluctuate up and down together across trials. We measured correlations over the

entire stimulus window (1 second), for all pairs of neurons recorded either during amblyopic or fellow eye stimulation (see Methods).

Correlations for pairs of neurons were significantly larger when a stimulus was presented to the amblyopic eye compared to the fellow eye (Figure 3C; mean r_{sc} 0.21 (0.17 SD) vs mean r_{sc} 0.16 (0.14 SD); $p<0.00001$). Because we randomized the visual stimulus between the eyes across trials, we were able to make this comparison directly in the same neurons. This difference in r_{sc} between amblyopic and fellow eye stimulation provides evidence for altered functional interactions in the same population of neurons. Furthermore, our finding of a higher (mean matched) Fano factor for amblyopic compared to fellow eye stimulation suggests that the changes in covariance among the V1 neuron responses must be quite large, leading to increased noise correlations despite a concomitant increased variance of individual neuronal responses to amblyopic eye stimulation. There was no apparent difference in r_{sc} between the stimulation of the right and the left eyes in the control animal (Figure 3D; mean r_{sc} 0.16 (0.17 SD) vs mean r_{sc} 0.13 (0.15 SD); $p=0.06$). In both the control and amblyopic animals, our recordings were targeted to the superficial layers of V1, where previous studies have reported r_{sc} values higher than in the intermediate and deep layers (Hansen et al., 2012; M. A. Smith & Sommer, 2013). The distribution of r_{sc} values we observed across our animals is consistent with the range of values reported by previous studies using similar and different recording preparations in V1 of primates (Cohen & Kohn, 2011a; Gutnisky & Dragoi, 2008; Kohn & Smith, 2005; Reich et al., 2001; M. A. Smith & Kohn, 2008).

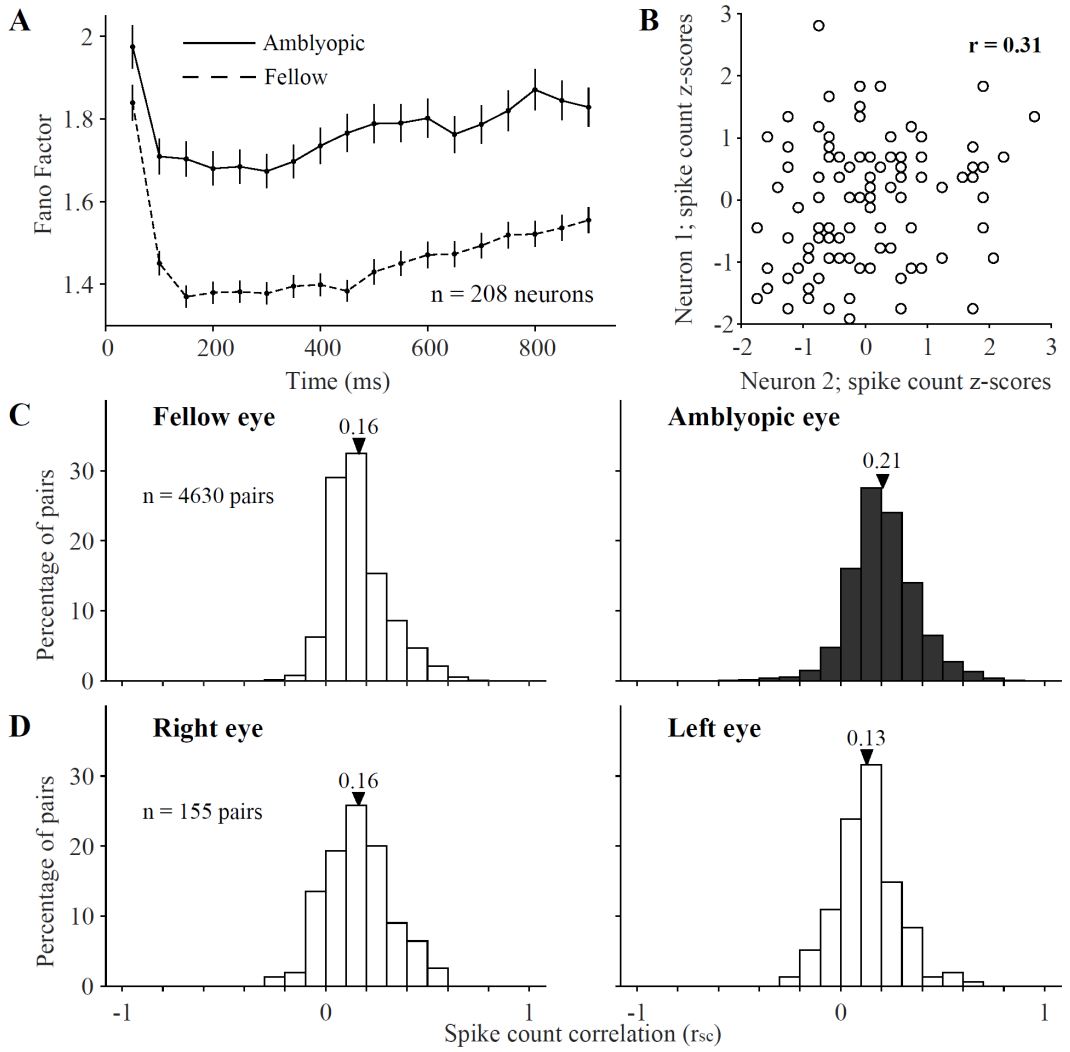

Figure 3. Effect of amblyopia on individual and shared variability of responses to full contrast stimuli in a population of V1 neurons.

Effect of amblyopia on individual and shared variability of responses to full contrast stimuli in a population of V1 neurons**.** (A) Mean-matched Fano factor is increased for amblyopic compared to fellow eye stimulation at different time points throughout stimulus presentation. Error bars represent 95% confidence intervals. (B) The scatter plot shows the aggregate, z-transformed, single trial responses of an example pair of recorded V1 neurons to 100 repeat presentations of a single identical full contrast stimulus. Both of the neurons' responses were 'noisy', varying from trial to trial. Spike count correlation (r_{sc}), also known as noise correlation, is computed as the Pearson's correlation coefficient (r) of the responses of two cells to repeated presentations of an identical stimulus. (C) Shown are the distributions of r_{sc} computed across 4630 pairs of neurons. The mean of each r_{sc} distribution is indicated with a triangle. Spike count correlation was computed separately for neuronal responses evoked by visual stimulation of the amblyopic (filled) and fellow (white) eyes. For each neuronal pair, we calculated the r_{sc} after combining response z-scores across all stimulus orientations. Spike count correlation was significantly increased for pairs of neurons responding to amblyopic eye stimulation, compared to fellow eye stimulation ($p<0.00001$). (D) Same as in (C), except r_{sc} was computed for 155 pairs of neurons in the control, visually normal animal when either the right or the left eye was stimulated. We did not observe a statistically significant difference in average r_{sc} between right and left eyes of the control animal ($p = 0.06$).

2.3.4 Stimulus-dependent Correlation Structure is Modified in Amblyopic V1

Several experimental and theoretical studies suggest that the structure of correlations – the dependence of correlations on the functional properties and physical location of neurons – can have a strong influence on the information encoded by the population (Averbeck et al., 2006; Kohn et al., 2016). Previous work in normal macaque V1 and V4 has shown that correlations are highest for pairs of neurons that are near each other and that have similar orientation tuning preferences (Kohn & Smith, 2005; Ruff & Cohen, 2016; M. A. Smith & Kohn, 2008; M. A. Smith & Sommer, 2013). Here, we investigated whether the correlation structure observed in visual cortex of normal animals is maintained in the cortex of amblyopes. To do this, we first examined if r_{sc} measurements differed depending on the distance between the neurons in each pair. We found that r_{sc} was largest for pairs of neurons near each other, compared to pairs of neurons farther apart, for both fellow and amblyopic eye stimulation (Figure 4A & C). Thus, for cortical processing of visual information received through the amblyopic eye, correlations were increased for all pairs of neurons, regardless of the distance between them.

We next investigated whether the relationship between tuning similarity and the magnitude of correlations was altered in the cortex of amblyopes. We used sinusoidal gratings of 12 different orientations to engage neurons with varied orientation preferences, which enabled us to assess the tuning similarity of each pair of neurons. Tuning similarity was quantified by calculating r_{signal}, the Pearson correlation of the mean responses of two neurons to each of 12 stimulus orientations. To test how functional interactions varied among neurons with different tuning preferences, we calculated r_{sc} as a function of r_{signal}. As in previous studies, we found that r_{sc} was highest for neurons with similar tuning (positive r_{signal}), and lowest for neurons with opposite tuning preferences (negative r_{signal}), for both fellow and amblyopic eye stimulation (Figure 4B). However, for the

amblyopic eye, the relationship between r_{sc} and r_{signal} was significantly stronger compared to the fellow eye ($p < 0.05$; see Methods for details of bootstrapping and statistical testing), such that pairs of similarly tuned neurons exhibited the largest difference in r_{sc} between the amblyopic and fellow eye stimulation conditions (Figure 4B&C). That is, pairs of similarly tuned neurons show the largest increase in r_{sc} between fellow and amblyopic eye stimulation. So, both raw correlation for stimulation of each eye as well as the difference in correlation between activity evoked by stimulation of the two eyes depend on tuning similarity of a pair of neurons. In the control animal, we found that r_{sc} was highest for neurons with similar tuning and lowest for neurons with opposite tuning preferences, for both left and right eye stimulation, as previously reported in normal animals.

The summary color maps in Figure 4C depict the dependence of r_{sc} on distance and r_{signal} for amblyopic and fellow eye visual stimulation. In a previous study of V1 neurons in visually normal animals, we found that the dependence of r_{sc} on both cortical distance and tuning similarity is well characterized by a product of two functions:

$$r_{sc} = [a - b(distance)]^{+} e^{\frac{rsignal-1}{\tau}} + c$$

where the linear term represents the decay of r_{sc} with distance, the exponential decay represents how r_{sc} declines with r_{signal}, and $[\ ]^{+}$ indicates that negative values of the linear terms are set to 0 (Smith and Kohn 2008). We fit the data from our amblyopic animals in Figure 4C with this same equation. For fellow eye condition, the linear decay had an intercept (a) of 0.121 ± 0.038 (95% confidence interval), and a slope (b) of 0.048 ± 0.02 mm^{-1} while the exponential decay constant (τ) was 0.936 ± 0.47 (unitless) and the baseline (c) added to the product of the functions was 0.149 ± 0.006. For the amblyopic eye, the linear decay had an intercept (a) of 0.267 ± 0.055 (95% confidence interval), and a slope (b) of 0.038 ± 0.019 mm^{-1} while the exponential decay

constant (τ) was 0.67 ± 0.3 and the baseline (c) added to the product of the functions was 0.151 ± 0.026. The intercept, slope and baseline values for both of the eye conditions were similar to those reported for V1 neurons of normal animals in our previous work(M. A. Smith & Kohn, 2008). This similarity indicates that the relationship between distance and r_{sc} in amblyopic animals of this study is not altered compared to normal animals of our previous study. On the other hand, the value of τ was lower for the amblyopic animals of this study compared to the value (1.87 ± 0.67) reported in our previous work in normal animals. A smaller value of τ indicates that the rate at which r_{sc} values decline as r_{signal} values decrease is faster in amblyopes, which is consistent with our analysis of the relationship between r_{sc} and r_{signal} in Figure 4B. Overall, our results suggest that amblyopia affects not only the overall level of correlation, but also the extent to which neurons interact with their neighbors of both similar and dissimilar stimulus preferences.

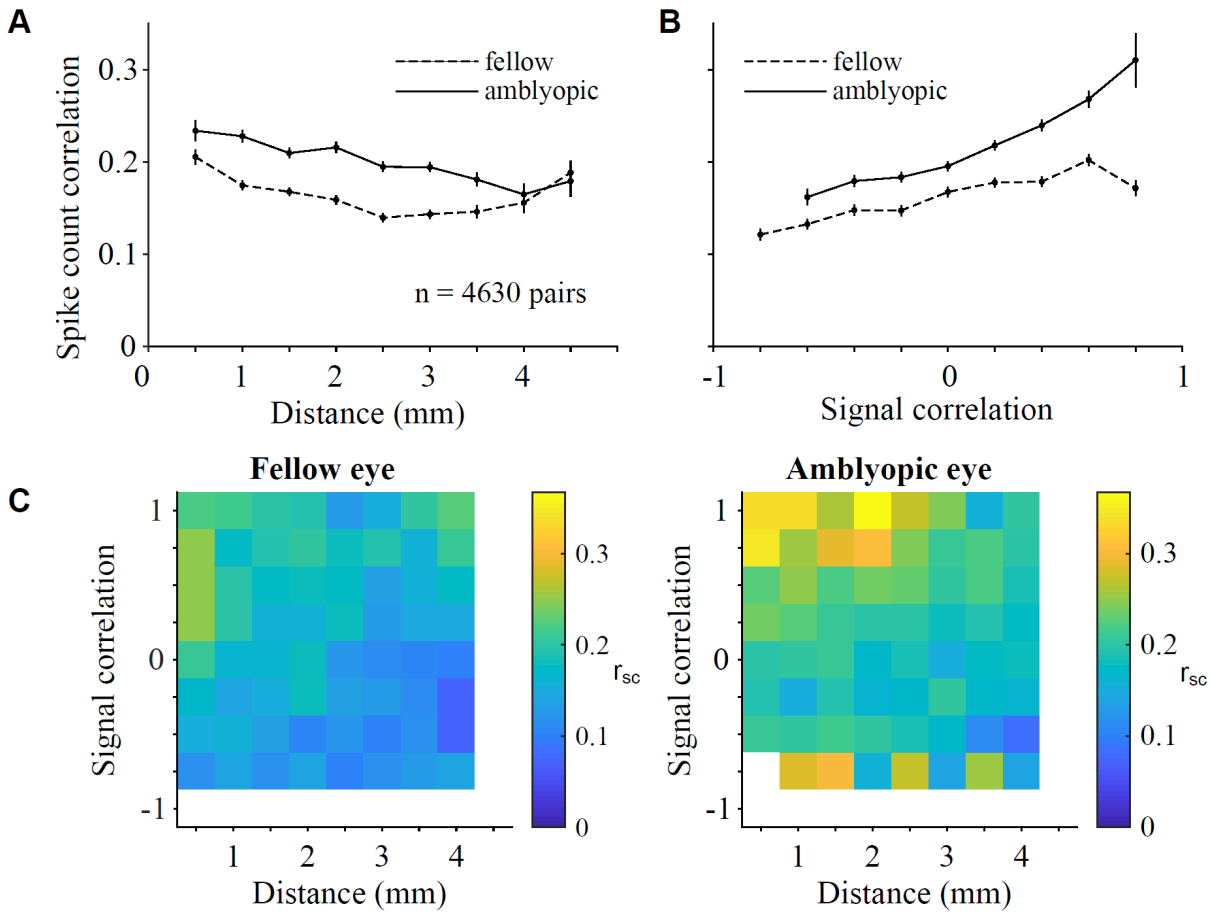

Figure 4. Dependence of r_{sc} on distance and tuning similarity in amblyopic V1.
Dependence of rsc on distance and tuning similarity in amblyopic V1. (A) Stimuli presented to the amblyopic eye (solid line) resulted in higher spike count correlation over all possible distances between recorded neurons, as compared to fellow eye stimulation (dashed line). Mean spike count correlation is plotted as a function of the distance between the array electrodes that contain the neurons in each assessed pair. The distance bins start at 0 mm and extend to 4.5 mm in 0.5 mm increments. The average of the rsc values for neuronal pairs included in each bin is plotted at the end value for each bin. Error bars represent ± 1 SEM . (B) For fellow and amblyopic eye stimulation, mean spike count correlation is plotted as a function of signal correlation, which can be thought of as similarity in orientation tuning of the two neurons. The rsignal bins start at -1.0 and extend to 1.0 in 0.2 increments. The average of the rsc values for neuronal pairs included in each bin is plotted at the start value for each bin. As has been reported previously, spike count correlation increased with signal correlation. Furthermore, for the amblyopic eye, the relationship between rsc and rsignal was significantly stronger compared to the fellow eye ($p<0.05$), indicating that similarly tuned neurons exhibit the largest increase in shared trial-to-trial variability. Error bars represent ± 1 SEM (C) Summary color maps illustrate the relationships between distance, spike count correlation and signal correlation for fellow vs. amblyopic eye stimulation. The scale of the colors is indicated by the bar on the right. rsignal bins start at -1 and extend to 1 in 0.25 increments.

2.3.5 Increased Correlations Predominate among Amblyopic V1 Neurons that Preferentially Respond to Fellow Eye

In strabismic amblyopic monkeys, binocular organization in V1 is disrupted, such that the ocular dominance distribution becomes U-shaped with a significant reduction in binocularly activated cells (F. H. Baker et al., 1974; Kiorpes et al., 1998b; E. L. 3rd Smith et al., 1997; Wiesel, 1982). Additionally, several studies report a decrease in the number of cortical neurons that preferentially respond to visual stimulation through the amblyopic over the fellow eye (M. L. Crawford & von Noorden, 1979; Hubel & Wiesel, 1965; Kiorpes et al., 1998b; Movshon et al., 1987; Schröder et al., 2002; Shooner et al., 2015a). Specific changes in the circuitry underlying the eye preference and binocular responsivity of V1 neurons could be reflected in an altered pattern of pairwise interactions in the population. Therefore, we next examined whether our observed changes in spike count correlation were associated with eye preference changes of individual neurons in amblyopic V1.

For each cell, we first computed an ocular dominance index (ODI) as a measure of the cell's eye preference. ODI distributions in each amblyopic animal ranged between the values of -1 and 1, with more negative and positive values indicating higher responsivity to visual stimuli viewed through the amblyopic or fellow eye, respectively. Figure 5A shows a distribution of ODI values for 208 neurons recorded from the 3 amblyopic animals. We observed an ocular dominance bias toward positive values, indicating that the majority of cells fired more strongly in response to visual stimulation of the fellow eye than the amblyopic eye (141 neurons with ODI value > 0.2 and 36 neurons with ODI value < -0.2). There were relatively few binocularly activated V1 neurons in our amblyopic animals (31 neurons with ODI values within +/- 0.2 of 0).

We next investigated whether the magnitude of spiking correlations was dependent on the eye from which each neuron received its dominant input. In this analysis, we measured correlations in pairs of neurons as a function of the difference in eye preference between the cells in each pair, termed ODI difference. Differences in ODI ranged from 0 to 2, where cells that preferred the same eye had an ODI difference of 0, while cells that preferred opposite eyes had an ODI difference of 2. Because of the ocular dominance bias in our neuronal population, the majority of neuronal pairs with an ODI difference close to 0 preferred the fellow eye. We first analyzed the magnitude of correlation as a function of the ODI difference, and found that there was a negative relationship in both the fellow (Figure 5B) and amblyopic (Figure 5C) eye, indicating that pairs of neurons that preferred the same eye had higher correlations than pairs of neurons that had opposite eye preferences. This effect could be due simply to the lower mean firing rates among pairs of neurons that preferred quite dissimilar stimuli. For the fellow eye, this was indeed the case – the correlation tracked the geometric mean firing rate of the pairs of neurons. However, for the amblyopic eye there was a particularly high level of correlation among neurons that preferred input from the same eye (ODI difference < 0.8) that could not be explained by the firing rates. When comparing the same pairs of neurons under different eye stimulation conditions, the neuronal pairs with an ODI difference < 0.8 had decreased responsivity but higher correlations during amblyopic eye stimulation, compared to fellow eye stimulation. Accordingly, we found that the relationship between eye preference similarity and the magnitude of correlations in pairs of neurons was significantly different between the two eyes (stronger for the amblyopic eye, $p<0.05$; see Methods for details on bootstrapping and statistical testing). These results indicate that in amblyopia there is not only a weaker representation of the amblyopic eye at the single neuron level in V1, as has

been shown before, but also that the ocular dominance changes in individual neurons are related to changes in functional interactions among those neurons.

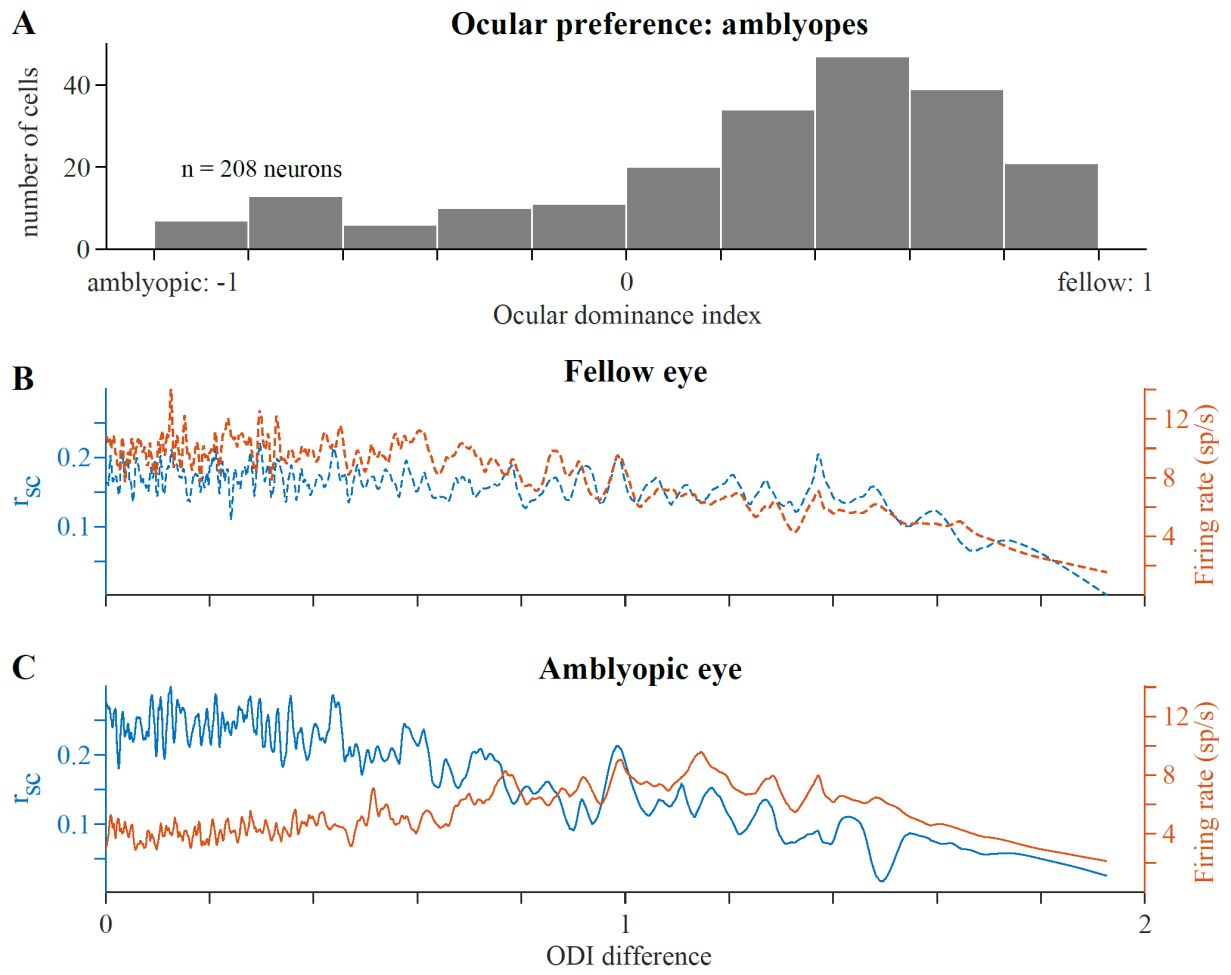

Figure 5. Relationship between ocular dominance changes and increased correlations in amblyopic V1.

Relationship between ocular dominance changes and increased correlations in amblyopic V1. (A) A histogram showing the ocular dominance index (ODI) values for all 208 neurons recorded across the 3 amblyopic animals. Neurons with ODI values closer to -1 preferentially responded to visual input through the amblyopic eye, while neurons with ODI values closer to 1 had higher responsivity to fellow eye visual stimulation. The ODI values were unevenly distributed, and biased toward the fellow eye (ODI < -0.2: 36 neurons; -0.2<ODI<0.2: 31 neurons; ODI>0.2: 141 neurons). (B) For fellow eye visual stimulation, spike count correlation values (left y-axis) and firing rates (right y-axis) are plotted as a function of the difference in ODI values of the neurons in each pair. An ODI difference closer to 0 indicates that the neurons composing the pair have the same ocular preference. The traces shown were produced by smoothing over the data points with a sliding window (size of window = 15 data points). (C) same as in (B), but considering V1 responses to visual stimulation through the amblyopic eye. Neurons with similar ODIs had higher correlations during amblyopic eye stimulation, compared to the level of correlations in the same neuron pairs during fellow eye stimulation ($p < 0.05$).

2.3.6 Decoding Stimulus Orientation from Amblyopic V1 Population Activity

The modifications in pattern and strength of functional interactions that we observed in amblyopic V1 could degrade the encoding of stimuli presented to the amblyopic eye. Therefore, we compared how well the recorded network of V1 neurons represented stimulus information when high contrast visual input was delivered through the amblyopic versus the fellow eye. We used a statistical classification method to decode stimulus orientation from the activity of simultaneously recorded V1 neurons (see Methods for details). As we had a total of 12 stimulus orientations, for each testing trial, a trained multi-class classifier was tasked with deciding which one of 12 possible classes was most consistent with the V1 population activity on that trial. Using this classification analysis, we explored whether visual stimulus information was harder to read out from V1 population activity when the amblyopic eye provided the input.

We found that classification accuracy was substantially decreased when a classifier was trained and tested on neuronal responses during amblyopic eye stimulation compared to training and testing on V1 responses to fellow eye stimulation. Figure 6 shows decoding accuracy for fellow versus amblyopic eye stimulation trials for four different recording sessions across 3 animals. While decoding performance remained above chance (8.33%) for both of the eyes in all four examined sessions, accuracy was consistently reduced when decoding from neural responses to amblyopic eye visual input. Importantly, classification performance is dependent on the response properties and orientation tuning of the recorded neuronal population. For instance, we observed different decoding accuracies for two recording sessions that were conducted in the same animal (JS579) because the sampling of neurons was different.

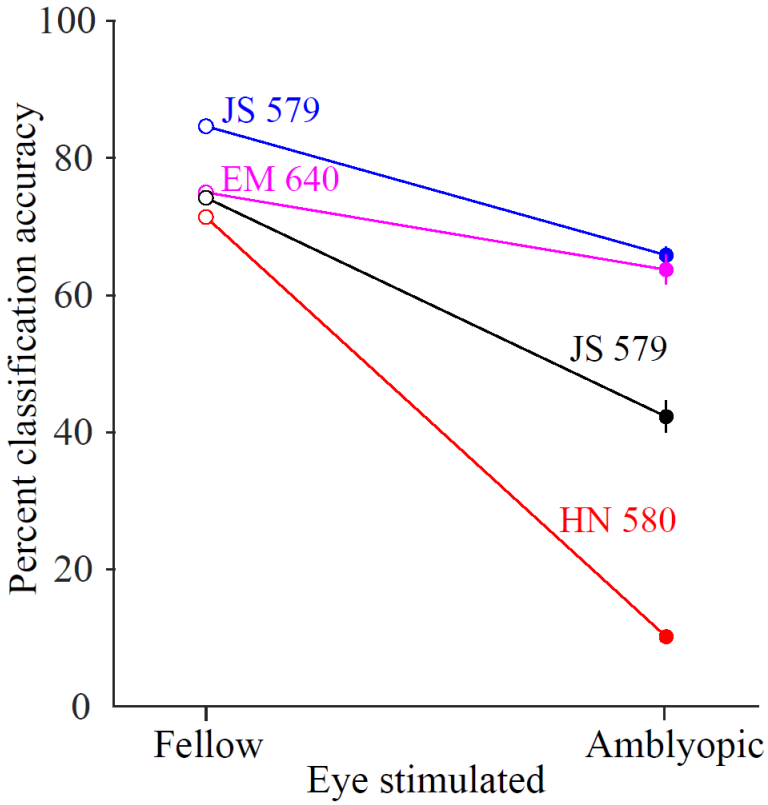

Figure 6. Decoding grating orientation from fellow or amblyopic eye stimulation.
Decoding grating orientation from fellow or amblyopic eye stimulation. When trained and tested on neuronal responses during amblyopic eye stimulation, the decoding accuracy was decreased compared to when a decoder is trained and tested on responses to fellow eye stimulation. The four colors correspond to decoding results from neuronal responses on 4 different array implants across 3 animals.

2.3.7 Effect of Stimulus Contrast on Correlated Variability in Amblyopic V1

Despite previous work, our understanding of the neural basis for diminished contrast sensitivity in amblyopes remains incomplete. It is possible that in amblyopia, a deficit in global network responsivity to contrast is more pronounced than individual neuron response deficits. Importantly, studies in visually normal animals have shown that stimulus contrast can affect the level of interactions in a neuronal population. For instance, correlations in pairs of V1 neurons depend on stimulus contrast, such that r_{sc} is significantly larger for low contrast stimuli than high contrast stimuli (Kohn & Smith, 2005). This suggests that spontaneous cortical activity has a considerable amount of inherent correlated variability which can be reduced by strong stimulus drive (Churchland et al., 2010; M. A. Smith & Kohn, 2008; Snyder et al., 2014). Developmental abnormalities in the visual cortex of amblyopes could affect how networks of cortical neurons interpret the strength of stimulus drive provided by high vs. low contrast stimuli. Based on these observations in normal animals, we wondered how the amount of stimulus drive to the amblyopic eye affects the strength of correlated variability in V1.

We presented full (100%), medium (50%) and low (12%) contrast gratings of 12 different orientations, separately to the amblyopic or fellow eye of one of the amblyopic monkeys. We then measured the correlation in response variability of 1381 neuronal pairs in the recorded neuronal population for each stimulus contrast presented to each of the two eyes. Because r_{sc} values for neuronal pairs are known to depend on the firing rates of constituent neurons (Cohen & Kohn, 2011b), for this analysis, we binned the computed r_{sc} values by geometric mean firing rate of neuronal pairs. This method allowed us to study the effect of stimulus contrast on correlated variability in amblyopic V1 while accounting for the wide range of responsivity observed across the recorded individual neurons (Figure 2B).

In agreement with the results of Kohn and Smith (2005), when we analyzed the V1 population response on trials with fellow eye stimulation, lowering stimulus contrast significantly increased mean r_{sc} for all neural pairs regardless of their geometric mean firing rate (Figure 7A). Interestingly, for stimuli presented to the amblyopic eye, r_{sc} was relatively insensitive to the level of contrast (Figure 7B). That is, a full contrast stimulus viewed by the amblyopic eye did not substantially reduce the amount of correlated variability in most V1 neurons (except those with very high firing rates) compared to a lower contrast stimulus. This is apparent when viewing a contrast response function for correlation (Figure 8), where the relatively flat lines in low-firing rate pairs of neurons for amblyopic eye stimulation indicate a lack of contrast sensitivity of correlation.

We observed that the mean r_{sc} values for high firing neuronal pairs responding to fellow eye stimulation were higher than the r_{sc} values in the highest firing rate bins for the amblyopic eye condition (Figure 7). Because some neurons in our population retained high firing rates to stimuli shown to the amblyopic eye, it is expected that the r_{sc} values for neuronal pairs in the high firing rate bin would be more similar to those for fellow eye. Additionally, although most neurons we recorded had a significantly higher r_{sc} for amblyopic than fellow eye stimulation, the ocular preferences of the neurons can play a role in how responsive the neurons are to each eye, and thus can influence the relative difference in r_{sc} magnitude between amblyopic and fellow eyes. For instance, if there are two neurons that have a slight preference for the right (fellow) eye, they will have higher firing rates (and a higher r_{sc} value) in response to right (fellow) eye visual stimulation compared to left (amblyopic) eye visual stimulation. In such a scenario, the effect of increased r_{sc} during amblyopic eye stimulation would not be as apparent.

We next quantified the differential effect of stimulus contrast on the amount of correlated variability for the fellow versus the amblyopic eye. For each neuron pair, we computed the difference in r_{sc} between high and low contrast (Δr_{sc}) for each eye condition. Since Δr_{sc} is computed by subtracting high contrast r_{sc} values from low contrast r_{sc} values, the closer Δr_{sc} is to 0, the more similar are the r_{sc} values computed during high and low contrast stimulation. This metric revealed that indeed, the Δr_{sc} distribution for amblyopic eye stimulation was shifted closer to 0, and was significantly different from the Δr_{sc} distribution computed for fellow eye stimulation (amblyopic mean = -0.1017, fellow mean = -0.1523; $p<0.05$; based on confidence intervals of bootstrapped, mean Δr_{sc} distributions). Furthermore, we also found a significant difference in the strength of this interocular disparity between the amblyopes and the control animal ($p<0.0001$). Thus, for stimulus processing through the amblyopic eye, neurons had not only impaired contrast sensitivity measured one cell at a time (Kiorpes et al., 1998b; Movshon et al., 1987), but also maintained high levels of correlated variability even in the presence of strong stimulus input.

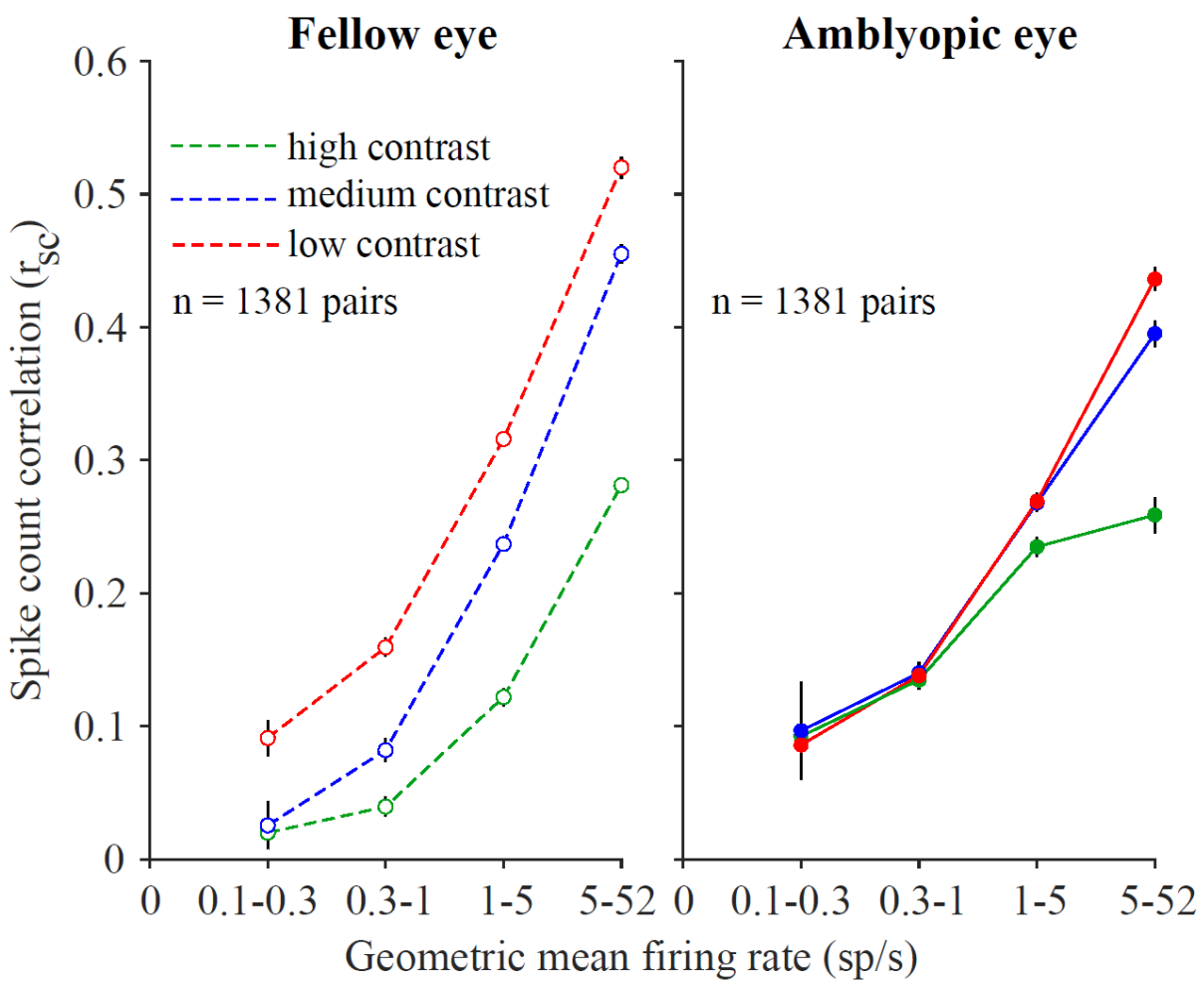

Figure 7.
The average of the r_{sc} values for neuronal pairs in each geometric mean firing rate bin is plotted, for grating stimuli of high (green, 100%), medium (blue, 50%), and low (red, 12%) contrasts. Error bars represent s.e.m. For the fellow eye, lowering stimulus contrast significantly increased mean r_{sc} at all firing rates, while with amblyopic eye stimulation, r_{sc} was relatively unaffected by stimulus contrast. Computing the difference in r_{sc} between high and low contrast (Δr_{sc}) for all 1381 neuron pairs revealed a significant inter-ocular disparity in Δr_{sc} in the amblyopic animal ($p<0.05$; based on confidence intervals of bootstrapped, mean Δr_{sc} distributions).

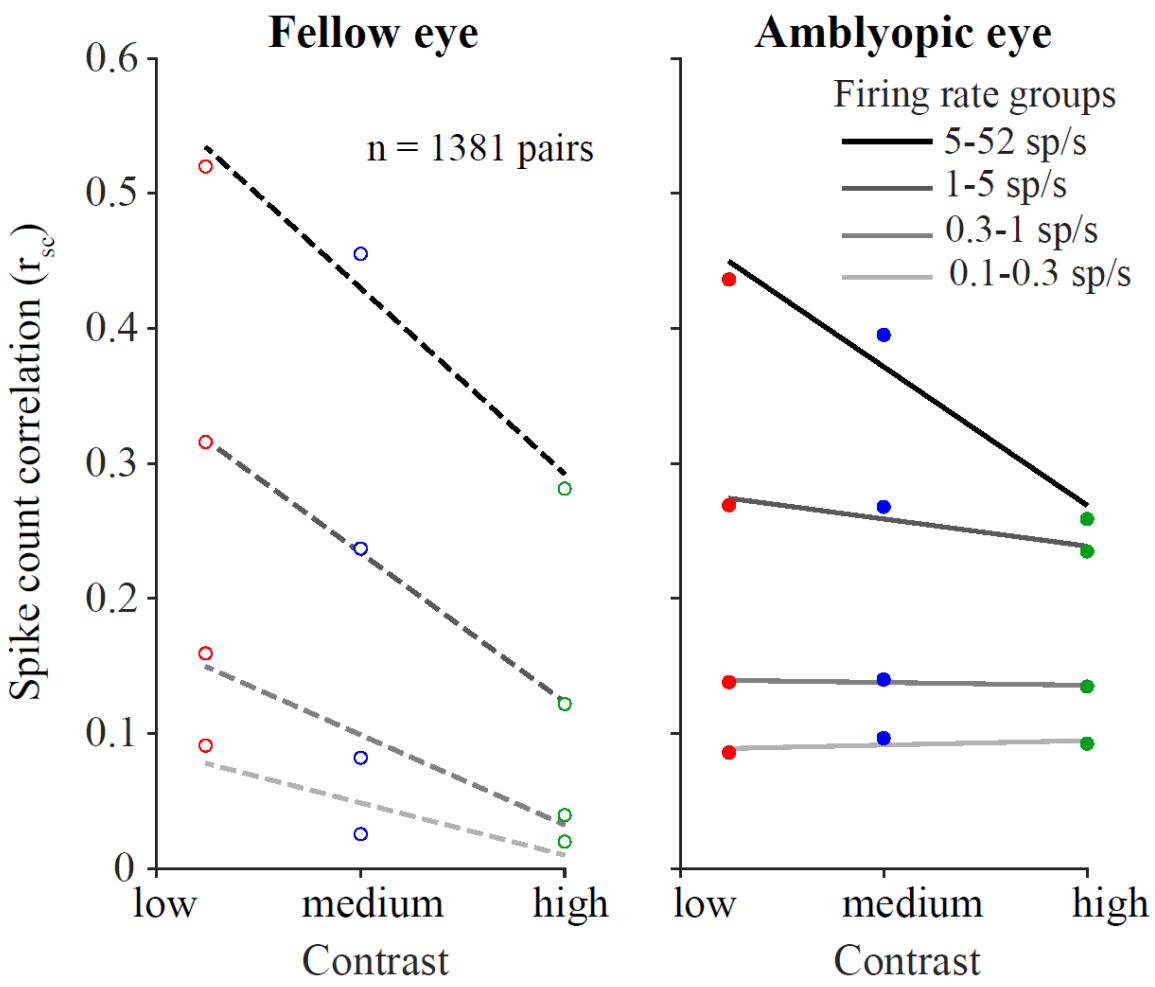

Figure 8. Dependence of spike count correlation on stimulus contrast.
Amblyopic eye stimulation resulted in similar r_{sc} across three stimulus contrasts (100%, 50% and 12%). r_{sc} values are binned according to the mean firing rate for each neuronal pair, and the average r_{sc} value per firing rate bin is plotted as a function of contrast.

2.4 Discussion

Our goal in this study was to gain insight into the neural basis of amblyopia by looking for abnormalities beyond those already known to affect individual neuronal responses. We recorded simultaneously from tens of neurons in the primary visual cortex of monkeys with strabismic amblyopia, which allowed us to measure the functional interactions between pairs of neurons during visual stimulation of the fellow, non-amblyopic eye versus the amblyopic eye of each animal. Our primary finding was that the structure of correlated trial-to-trial response variability among V1 neurons was altered in amblyopic compared to fellow eye stimulation. Specifically, stimulation of the amblyopic eye resulted in stronger correlations that were restricted to neurons with similar orientation tuning and similar eye preference, and these correlations were relatively insensitive to stimulus drive. To examine the consequence of these changes for stimulus representation in networks of amblyopic V1 neurons, we decoded grating orientation from simultaneously recorded populations of neurons. The accuracy of decoding stimulus orientation for amblyopic eye stimulation was reduced compared to decoding the same stimuli from neural activity in response to fellow eye stimulation. Taken together, these results demonstrate profound shifts in the functional response properties and interactions among neurons in amblyopic cortex when the stimulus is presented to the amblyopic eye.

2.4.1 Altered Circuitry in V1 of Amblyopes

What do our observed differences in r_{sc} between the two eyes suggest about circuits of V1 neurons that process visual information received from amblyopic eye? To answer this question, it is first necessary to consider the physiological sources of correlated variability (for review see

Doiron et al., 2016). Correlations in pairs of neurons are thought to arise in part from common afferent projections to the two neurons (Shadlen & Newsome, 1998). Correlations can also arise from feedback (top down) signals (Cumming & Nienborg, 2016), feedforward processing of stimuli (Kanitscheider et al., 2015), recurrent connectivity in local circuits (Doiron et al., 2016), and from variable synaptic transmission due to the dynamics of vesicle release (Doiron et al., 2016). Changes in correlated variability may therefore reflect reorganization in the underlying circuitry, and correlation analysis has previously proved useful for assessing changes in functional connectivity (Cohen & Newsome, 2008; Greschner et al., 2011; Reid & Alonso, 1995).

In our study of amblyopic V1, we found that during amblyopic eye stimulation, there was elevated pairwise correlation in V1 neuronal responses, and that this remained unchanged across low, medium and high stimulus drive to the amblyopic eye. Our results suggest that in amblyopic visual systems, networks of V1 neurons have altered connectivity and function abnormally when processing visual information received through the amblyopic eye. In particular, our observation that increased correlation persists across a range of stimulus intensities shown to the amblyopic eye suggests that V1 neurons may not fully engage in processing stimulus information received through an amblyopic eye. Previous studies measuring individual neuronal contrast response functions have found that few amblyopic V1 neurons have reduced contrast sensitivity at high spatial frequencies, and that the observed reduction in neuronal contrast sensitivity is not enough to account for contrast perception deficits found in amblyopic animals (Kiorpes et al., 1998b; Movshon et al., 1987; Shooner et al., 2015a). However, a recent study (Y. Wang et al., 2017) found that contrast response functions for V2 neurons responding to amblyopic eye stimulation in anisometropic amblyopes were abnormal. Our findings indicate that amblyopia-related contrast

processing deficits could manifest both downstream of V1 and at the level of neuronal correlations in V1.

According to our results, it is likely that visual stimuli received through the amblyopic eye have a weaker influence in the visual cortex due to both single-neuron and network level changes following a shift in ocular dominance towards the fellow eye. In the amblyopic animals of this study, the majority of the recorded V1 neurons preferentially responded to stimulus drive through the fellow eye, and there were few binocularly responsive neurons. Furthermore, the difference in correlated variability and firing rates between amblyopic and fellow eye stimulation was restricted to pairs of cells that had the same eye preference. Together, these results are consistent with a re-wiring scheme in which a substantial portion of the neurons lose amblyopic eye inputs but gain or retain fellow eye inputs during abnormal visual experience. Anatomically, the representation of the amblyopic eye in pairs of V1 neurons could decline as a result of altered lateral connections in V1, from reduced thalamocortical projections that carry amblyopic eye information, or both. Studies of horizontal connections in amblyopic macaques and cats have reported reduced connectivity between cells located in opposite ocular dominance columns in the superficial layers of V1, but connectivity between neurons in columns dominated by the same eye is normal (Löwel, 1994; Löwel & Singer, 1992; Trachtenberg & Stryker, 2001; Tychsen et al., 2004; Tychsen & Burkhalter, 1992, 1997). At a coarse level, the structure of thalamocortical inputs remains largely normal in amblyopic monkeys (Adams et al., 2015; Fenstemaker et al., 2001; Hendrickson et al., 1987). But even with structurally intact thalamocortical projections, the effectiveness of thalamocortical drive to V1 could be reduced specifically for inputs from the amblyopic eye if there were changes in how cortical circuits receive and process these inputs. To that point, we recently described local circuit changes in V1, in particular, reduction in excitatory drive to

amblyopic eye neurons resulting in a change in E/I balance, that could explain the abnormal response to contrast variation during amblyopic eye viewing (Hallum et al., 2017; Shooner et al., 2015a, 2017).

When considering changes across the entire population of neurons, it is evident that the effect of amblyopia is heterogenous across the V1 population. For instance, although most neurons exhibited a higher level of correlations and lower firing rates for amblyopic eye stimulation, a subgroup of neurons retained normal responsivity and continued to respond well to stimulation of the amblyopic eye. Specifically, neuronal pairs with the highest firing rates did not show an increase in correlation compared to the same high firing neuronal pairs responding to fellow eye stimulation (Figures 5 and 7). This observation is consistent with prior reports that some neurons in amblyopic cortex retain normal response properties. For example, some neurons in amblyopic cortex in monkeys maintained high responsivity to high spatial frequencies while other neurons had altered responsivity (Kiorpes et al., 1998a; Movshon et al., 1987). This co-existence of normally responsive and altered cells in amblyopic V1 highlights the importance of considering pairwise interactions in the context of the properties of the cells in each pair, which can reveal subgroups of neurons (and types of visual stimulus information) that are particularly affected.

2.4.2 Decoding Information from V1 Populations

A number of studies suggest that correlated variability between sensory neurons might be especially important for encoding of stimulus information in populations of neurons (Abbott & Dayan, 1999; Averbeck et al., 2006; Cohen & Kohn, 2011b; Cohen & Maunsell, 2009a). Furthermore, there is some evidence for a direct link between changes in correlated variability and shifts in psychophysical performance (Beaman et al., 2017; Cohen & Maunsell, 2009a; Zohary et

al., 1994). Importantly, not only the amount of correlated variability in a given network, but also the particular neurons that have altered interactions, matters for stimulus representation. Here, we found that the increase in correlations was highest for pairs of similarly tuned neurons. A common finding of theoretical and experimental studies is that an increase in amount of shared noise between similarly tuned neurons is detrimental for population coding (Averbeck et al., 2006; Ecker et al., 2011; Jeanne et al., 2013). Our results thus indicate that stimulus representation is degraded in populations of V1 neurons that process visual stimuli shown to the amblyopic eye, and that this effect is greater than would be expected simply from the reduced responses observed in individual neurons.

Our decoding analysis demonstrates that, as expected, stimulus information is harder to read out from V1 population activity when amblyopic eye rather than the fellow, non-amblyopic eye provides the visual input. Classification accuracy was consistently reduced when decoding stimulus orientation from neural responses to amblyopic compared to fellow eye stimulation. This is consistent with the idea that stimulus representation in V1 is impaired for amblyopic eye signals, which can in turn lead to downstream errors in information processing. Interestingly, amblyopic observers have global perceptual deficits that are not simply predicted by single neuron changes in V1 (Kozma & Kiorpes, 2003). For instance, strabismic amblyopes have impaired performance in contour integration, a task that requires identifying a curve imbedded in a noisy background (Kozma & Kiorpes, 2003; Levi et al., 2007). In this study we found a larger increase in correlations between similarly tuned neurons compared to neurons with dissimilar tuning during amblyopic eye stimulation. Perhaps deficits in contour integration in amblyopia arise from decreased accuracy in coordinating V1 representations of neighboring, similarly oriented pieces of the contour. Overall, our findings indicate that to more conclusively define the neurophysiological correlates

of visual deficits in amblyopia, it is important to consider population-level processing of visual information and not just the properties of single neurons.

2.4.3 Theories for the Neural Basis of Amblyopia

Previous work provides evidence for at least four neurophysiological correlates of amblyopic visual deficits, including 1) altered responsivity and tuning of single neurons in V1, 2) neural changes in visual areas downstream of V1, 3) reduced cortical representation of the amblyopic eye ("undersampling") and 4) topographical jitter, or disorder in neural map of visual space (Kiorpes, 2006, 2016; Kiorpes et al., 1998b; Levi, 2013; Y. Wang et al., 2017). In this study we found that the strength and pattern of functional interactions in pairs of neurons in the primary visual cortex was different when processing amblyopic eye and fellow eye inputs. We therefore conclude that abnormalities in visual representation at the level of V1 neuron populations may constitute a fifth factor contributing to amblyopic visual deficits. Further work will be needed to determine the relative contributions of these factors to amblyopic visual losses.

3.0 Phasic Activation of Locus Coeruleus Neurons During Perceptual Decision Making

3.1 Introduction

Phasic activation of locus coeruleus (LC) neurons is triggered by salient sensory stimuli that may require an immediate behavioral response. Pioneering studies of LC activity first reported that phasic bursts of spikes occur in response to startling, noxious, or otherwise novel sensory stimuli (Aston-Jones & Bloom, 1981b; Foote et al., 1980; Grant et al., 1988). More recent work has focused on uncovering the putative role of LC phasic activation under cognitively-demanding circumstances such as decision making, working memory, perceptual learning, and other goal-directed behavior (Arnsten et al., 2012; Aston-Jones & Cohen, 2005a; Glennon et al., 2019a; Robbins & Arnsten, 2009; Sara, 2009; Sara & Bouret, 2012a). However, the exact contribution of LC phasic responses to these important cognitive processes is not yet understood. Our goal in this study was to clarify the role of LC phasic activation during perceptual decision making.

As the field currently stands, most of what is known about the potential influence of the LC-NE system on visual perception and decision making is based on three different research approaches. Firstly, electrophysiological studies of LC activity in animals engaged in simple decision tasks have observed task-related phasic LC activation by sensory cues, target (but not distractor) sensory stimuli and motor responses (Aston-Jones et al., 1994; Clayton et al., 2004; Kalwani et al., 2014; Rajkowski et al., 2004). Secondly, a large body of work has established that increased NE transmission can improve stimulus information processing, by improving the signal-to-noise ratio (SNR) of sensory stimulus evoked responses and sharpening sensory tuning curves, among other modulatory effects (Waterhouse & Navarra, 2019). Thirdly, several studies observed

that systemic pharmacological manipulations of NE transmission alter behavioral performance on more complex perceptual tasks (e.g., Gelbard-Sagiv et al., 2018; Guedj et al., 2019). Although these previous findings imply that the LC-NE system may influence perceptual decision making behavior, it is not yet clear whether LC phasic activation is linked to sensory, motor or both components of the decision process. It is also possible that LC phasic activation is generally associated with any behavior that requires contextually-important sensorimotor processing, regardless of whether that behavior is instinctive or related to cognitive task demands (e.g., Bouret & Richmond, 2009).

To better understand the significance of LC phasic activation for perceptual decision making, we recorded from single LC neurons in two macaque monkeys while they performed a visual, 2-AFC, orientation change detection task in which perceptual decisions were reported by saccadic eye movements. We hypothesized that during perceptual decision making under normal physiological conditions, LC phasic responses during sensory information presentation may function to improve the subject's perceptual accuracy. Importantly, the trials in our task were structured such that the stimuli containing the sensory evidence for a decision were temporally distinct from the saccade target stimuli for reporting decisions. This task structure allowed us to thoroughly examine whether LC phasic responses are important for sensory or motor or both aspects of the perceptual decision making process. Additionally, our task design allowed us to relate physiological LC phasic activation to psychophysical performance, which is essential for assessing whether LC activation could influence perceptual ability.

We found that LC neurons did not respond to the sensory stimuli which contained the information used by monkeys to form their perceptual decisions. Furthermore, we did not observe any relationship between LC phasic response magnitude and variability in perceptual accuracy of

the monkeys. However, we consistently observed choice saccade-aligned phasic activation in both monkeys. Additionally, we found separate LC phasic responses that were closely aligned with microsaccades which occurred after the monkey was presented with saccade target stimuli but was not yet cued to execute the motor response for reporting the decision. Overall, our findings clarify the role of LC phasic activation during perceptual decision making and provide novel evidence in support of a more general role of LC phasic activation in facilitating motor preparation and execution processes triggered by behaviorally-important sensory events.

3.2 Methods

3.2.1 Subjects

Two adult rhesus macaques (Macaca Mulatta) were used for this study. One of the monkeys was female (Monkey Do) and the other monkey was male (Monkey Wa). Before beginning behavioral training, we affixed a titatnium headpost to the skull of each monkey for the purpose of immobilizing the head during experiments. Experimental procedures were approved by the Carnegie Mellon University Institutional Animal Care and Use Committee and were in compliance with the United States Public Health Service Guide for the Care and Use of Laboratory Animals.

3.2.2 Electrophysiology

After initial training, each monkey was implanted with a recording chamber (Crist) that provided access to the Locus Coeruleus. The chamber was placed on the midline (ML 0mm) and

tilted in the AP plane at an angle of 30 degrees from vertical with the center of the chamber aimed at a location 8 mm above inter-aural zero. Each recording session began by lowering a single tungsten microelectrode (FHC; initial impedance 0.5 - 1 megaohm) through a sharp trans-dural guide tube. In both monkeys, the long guide tube length allowed the electrode to travel straight and come out approximately 23 mm below the dural surface. Next, the electrode was carefully advanced in depth through brain tissue, first at larger increments of 30um and later in smaller increments of 5um, while monitoring the neural activity to assess response characteristics of encountered neurons. A custom-made microdrive controlled by custom-written MATLAB software was used to lower the electrode. Day-to-day, electrode trajectories could be reproduced reliably by placing a grid inside the chamber. Our grids had 1mm spacing between the hole locations.

We used several strategies to find and validate the location of LC in the chamber. In both monkeys, we searched for and recorded from LC units located to the left of the midline. We first confirmed the chamber grid locations of the Superior and Inferior Colliculi (SC, IC). With our chamber positioning, the caudal edge of the SC (confirmed by evoking >30º amplitude saccades with electrical microstimulation) was located a couple of grid holes anterior to grid holes whose trajectories hit LC. Electrical stimulation of caudal SC neurons located in a grid location approximately 2 mm left of the midline evoked large upward saccades (>30º amplitude, angled at +25º) while stimulation of SC neurons in a grid location ~3mm left of the midline evoked downward saccades. We used the topography of SC neurons to estimate the mediolateral position of LC in the chamber grid at ~2mm left of the midline. IC neurons, identified by their obvious response tuning to different sound frequencies, were located in a couple of grid holes posterior to caudal SC. We also located the trochlear decussation and the trigeminal nerve/nucleus (me5/Me5),

which reside in close proximity to LC. We identified the trochlear decussation by observing characteristic 'buzzing', high firing rate, ramp-and-hold responses to saccades with downward and diagonal direction components. We identified the me5 axonal tract by observing neural signals closely aligned with mouth movements made by the monkeys. Finally, with the knowledge of the positioning of the landmark brain regions described above, we searched for a cluster of neurons with response characteristics matching known LC response properties from previous studies. Potential LC units were checked for waveform shape, low firing rate, sensitivity to startling/loud noises, and sleep-wake transitions in response rates (as reported by previous studies, e.g,, Aston-Jones et al., 1994; Bouret & Richmond, 2009; Kalwani et al., 2014)). Typically, the electrode had to be advanced another 7-9mm past the guide tube exit, before reaching LC. In both monkeys, all LC units were found in 2 grid holes spaced 1mm apart and located 1-2mm to the left of midline (presumably left hemisphere LC units). In monkey Do, we performed an MRI which confirmed that the trajectory of the recording chamber encompassed LC and showed that the visible electrode trajectories led to the generally correct region in the pons (see Results, Figure 9A). In Monkey Wa, we recorded in two putative LC sites before, during and after an intramuscular injection of the α2-noradrenergic receptor agonist Clonidine (see Results, Figure 9B).

During data collection sessions, the response properties of each potential LC unit were tested before beginning the experiment. Recorded neural activity was band-pass filtered (0.3 – 7,500 Hz), digitized at 30 kHz, and amplified by a Grapevine system (Ripple, Salt Lake City, UT). Waveforms that crossed a threshold were recorded, saved and stored for offline classification. We manually set the threshold to allow recording of some noise and multi-unit activity in addition to the isolated single unit activity. We used custom spike-sorting software written in MATLAB (https://github.com/smithlabvision/spikesort) to manually sort putative LC waveforms based on

shape and inter-spike interval distributions (Kelly et al., 2007). For analyses, we included both well-isolated single units as well as multi-unit activity in cases where the waveforms of the involved units were practically indistinguishable in shape. We present results obtained from 23 separate sessions in Monkey Wa during task version 1, 20 separate sessions in Monkey Do during task version 1, and 12 separate sessions in Monkey Wa during task version 2.

3.2.3 Behavior

During the experiments, stimuli were displayed on a 21" CRT monitor (resolution of 1024x768 pixels; refresh rate of 100 Hz), with a viewing distance of 36 cm. The visual stimuli were generated using custom software written in MATLAB (MathWorks, Natick, MA) and Psychophysics Toolbox extensions (Brainard, 1997, Kleiner et al., 2007, Pelli, 1997). We measured pupil diameter and eye position using an infrared eye tracking system (EyeLink 1000; SR Research, Ottawa, Ontario). On trials with correct behavioral outcomes, monkeys were rewarded with 2 drops of water delivered through a juice tube.

Behavioral Task: Version 1. The 2 monkeys performed the change detection task shown in Figure 10. A trial began when the monkey fixated on a dot at the center of the screen. After a randomized time period (400-600 ms), two drifting grating stimuli appear on the right and left sides of the screen, but the animal had to maintain central fixation. In this first presentation, the grating stimuli were 'samples' and each has a particular orientation (L: 135deg, R: 45deg). These same sample grating stimuli were shown in each trial over the course of the session. The sample stimuli remained on screen for 350 ms, at which point they disappeared but the animal still maintained central fixation. After a randomized time period (200-400 ms), a 'test' grating stimulus appeared on the right OR the left side only, with a 0.5 probability of appearing on either side. This

'test' stimulus could have the same or a different orientation as the 'sample' stimulus that was first presented on that side of the screen. After 350 ms the second 'test' stimulus disappeared. Next, there was a variable delay period before the fixation point disappeared, and a green and red target circle appeared on the screen. The green target represented a "yes, change occurred" choice while the red target represented a "no change" choice. The disappearance of the central fixation point instructed the animal to report its choice with an eye movement to the green or red target. The position of the green and red targets between bottom and top locations was randomized session to session in monkey Do, and randomized trial to trial in monkey Wa. Among the "change present" trials, the amplitude of the orientation change was selected randomly from 4 possible levels that were chosen based on the animal's performance. "Change present" and "change absent" trials occurred with an equal likelihood. The animal received the same reward if he correctly indicated orientation change or no change, regardless of whether the stimulus was on left or right side. Such task structure ensured that the animal's behavioral strategy fluctuated naturally and was not biased by task conditions or selective signals such as spatial attention. Throughout each session, we used an inter-trial interval of 1 second.

Behavioral Task: Version 2. Monkey Wa completed an additional 12 experimental sessions where he performed an alternate version of the change detection task (see Figure 16A). In this second version of the task, when the red and green targets appeared towards the end of each trial, the central fixation point remained on the screen for an additional randomized time period (350 – 550ms). Next, the fixation point disappeared (but the red and green targets remained on screen), cueing the monkey that it's time to make the choice saccade. This version of the task was similar in all other ways to the first version described above.

3.2.4 Data Analysis

LC activity. Baseline LC firing rates were computed in a 500 ms window during the initial fixation period in a trial, when no stimuli other than the fixation point were present on the screen. To compute LC firing rate responses to the 'first stimulus grating', or 'second stimulus grating', we used a 350 ms window aligned on the onset of the first or second orientation grating. We used a time window of +/- 200 ms centered on saccade onset for computing individual LC neuron firing rate responses to saccades indicating the monkeys' choices on the task. To assess the individual neuron responses to choice target onset, we computed LC firing rates in a window of 0-300 ms aligned on choice target onset.

For calculation of individual neuron PETHs, we first counted spikes for each LC neuron in 20 ms bins within particular time windows during fixation (0 - 500 ms relative to fixation point onset), orientation grating stimuli (-200 to 500 ms relative to stimulus onset), the choice period (-200 to 300 ms relative to choice target onset), and choice saccades (-400 to 400 ms relative to saccade onset). To standardize a PETH for each LC neuron, we computed the mean and standard deviation of the distribution of each neuron's baseline (fixation) responses across all completed trials in each session and then used these values for standardizing (z-scoring) each neuron's responses to the different trial events. Thus, the assigned z-scores conveyed the number of standard deviations by which a neuron's response to a trial event exceeded its baseline response. We compiled population PETHs across the standardized PETHs of individual neurons.

Microsaccade detection. We used the 2D-velocity based algorithm developed by (Engbert & Kliegl, 2003) to determine a velocity threshold that eye movements had to exceed to be classified as potential microsaccades. For each completed trial, we computed the velocity threshold as a multiple (4) of the standard deviation of the distribution of velocities across a time period

starting at -300 ms relative to the onset of the first stimulus grating and ending at fixation point offset (the 'go' cue for making a larger saccade). We defined microsaccades as any eye movements with a velocity between this lower bound threshold and an upper bound of 100º/sec. We removed any eye movements with an amplitude of greater than 1º, or a duration of less than 6 ms. We visually inspected eye position traces in some sessions, in order to verify the validity of our microsaccade detection method.

Quantifying behavioral performance. In the orientation change detection task used in this study, monkeys could report Yes (green) or No (red) decisions about the presence or absence of a stimulus change on each trial. This task design is rooted in signal detection theory and yields 4 possible behavioral outcomes: correct (hit), correct reject, miss, and false alarm (FA). Hit and miss outcomes occurred when a change in stimulus orientation occurred and the monkey made a saccade to the green ('yes') or red ('no') choice target, respectively. Correct reject and false alarm outcomes occurred when there was no change in the stimulus orientation, and the monkey made a saccade to the red ('no') or green ('yes') choice target, respectively. We used these trial outcomes to quantify behavioral performance. Hit rate was calculated for each session as the number of hit trials divided by the total number of trials on which a stimulus change happened (hit + miss trials). False alarm rate was calculated as the number of false alarm trials divided by the total number of trials on which a stimulus change did not happen (false alarm + correct reject trials). Criterion (c) and sensitivity (d') were computed using signal detection theory. Sensitivity was approximated as d' = invcdf(Hit Rate) – invcdf(FA Rate), where invcdf is the inverse cumulative density function of the normal distribution. A larger d' value indicates better sensitivity to stimulus change. Criterion was approximated as c = -0.5 *(invcdf(Hit Rate) + invcdf(FA Rate)). A criterion value of 0 indicates that a subject has no bias for reporting the absence or presence of change in a

stimulus. When $c < 0$, the subject is biased towards reporting that there was a stimulus change (green, 'yes') and when $c > 0$, the subject is biased towards reporting that there was no stimulus change (red, 'no'). For psychometric functions shown in Figure 10, we calculated d' and criterion from Hit and FA rates associated with each amplitude of the orientation change.

Statistical significance tests. To assess whether the magnitude of each neuron's response to a trial event (i.e., grating stimulus, choice targets, saccade) was significantly different from its baseline response, we used the paired-sample t-test (Figures 11, 16). To compare population (non-standardized) LC firing rate responses across different amplitudes of orientation changes or across behavioral outcomes (Figures 12, 13), we used a one-way ANOVA with Tukey-Kramer post hoc comparisons to test for significant differences between groups (at $p<0.05$). To assess whether each neuron's response to choice microsaccades was significantly different from its response to 'other' microsaccades (Figure 17), we used a two-sample t-test (with the Welch's correction for the assumption of equal variances) because we had unequal sample sizes. We did not use statistical methods to predetermine sample sizes of LC neurons or animals, but our sample sizes are similar to those reported in previous studies of single LC neuron recordings in non-human primates (e.g., (Bouret & Richmond, 2015; Kalwani et al., 2014; Varazzani et al., 2015).

3.3 Results

3.3.1 Identification of LC Units

We recorded the activity of a total of 76 single LC neurons in two monkeys (n = 29 in Monkey Do during Task 1; n = 31 in Monkey Wa during Task 1; n = 16 in Monkey Wa during

Task 2). Before beginning data collection experiments, we located LC by mapping the locations of the Superior Colliculus, Inferior Colliculus, trochlear decussation, and the tract of the trigeminal nerve (me5) in our recording chamber. These brainstem regions are typically considered good landmarks for finding LC because of their distinctive response characteristics and close proximity to the noradrenergic nucleus (see Methods for more details). Figure 9A shows a MRI image taken in Monkey Do after chamber implantation and several sessions of brain region mapping. The MRI confirmed that the positioning of the recording chamber allowed for electrode trajectories to pass through the estimated position of LC.

To further validate that we indeed correctly mapped the location of LC, on two separate days we administered an intramuscular injection of clonidine, an alpha-2-adrenergic receptor agonist, at a dose of 5ug/kg to Monkey Wa while the electrode was resting in putative LC (Grant et al., 1988). We recorded the activity of putative LC units before, during and after the administration of clonidine. Consistent with previous reports of the effects of clonidine on LC activity, we observed that a few minutes after the injection, neural firing and pupil diameter decreased and the animal became noticeably drowsy, keeping his eyes closed for extended periods of time (Figure 9B). After about an hour, LC activity ramped back up as the animal regained alertness and began to engage in a visual perception task (Figure 9B).

In the beginning of each data collection session, we identified LC neurons based on several previously established characteristics: low spontaneous firing rates, broad and biphasic waveforms (cite), burst responses to startling sensory stimuli (e.g., knocking on door), and notable changes in responsivity as animals transitioned between periods of drowsiness and alert wakefulness.

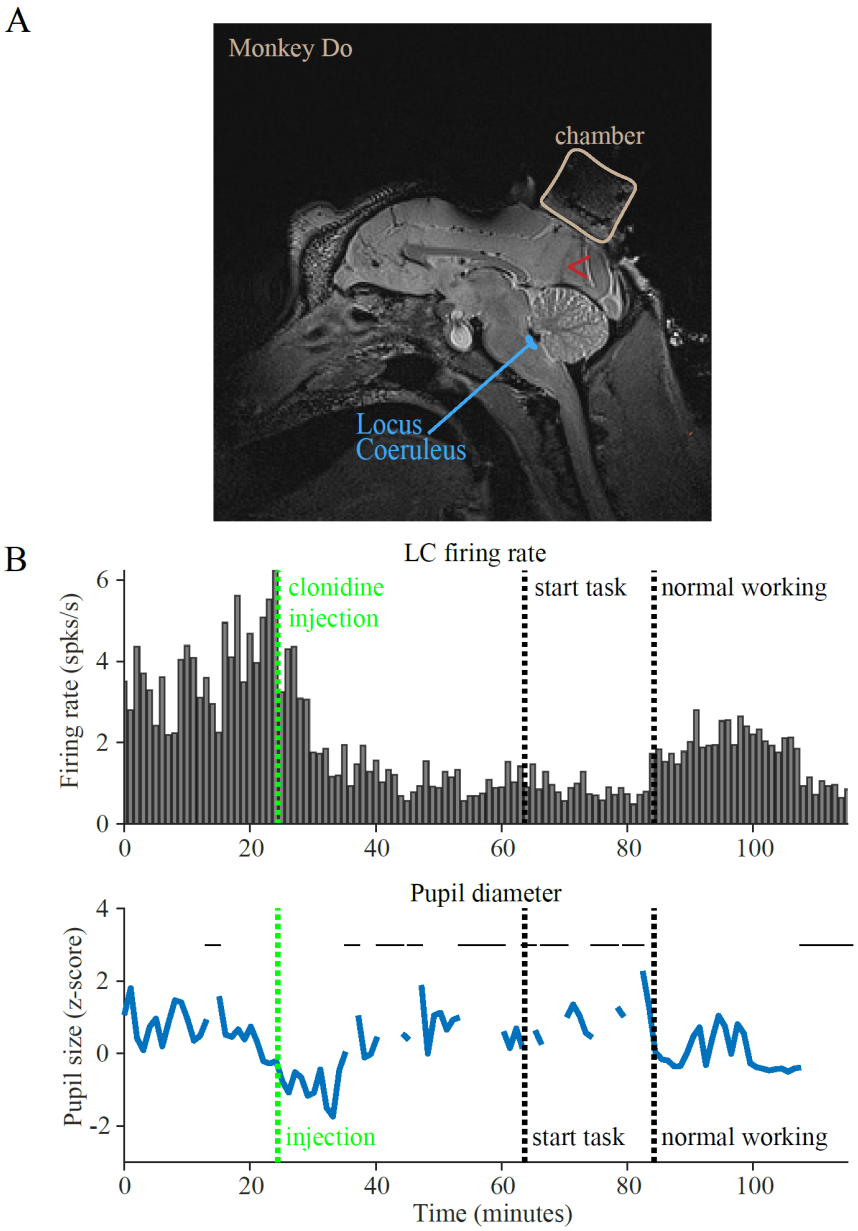

Figure 9. Confirming Locus Coeruleus (LC) location.
(A) Magnetic resonance image (MRI) in the sagittal plane shows that the placement of the recording chamber (tan outline) allowed electrode trajectories down to the approximate location of LC (blue spot) in the brainstem of Monkey Do. Red arrowhead points to the lesion made by repeated guide tube and electrode trajectories down to LC. (B) Pharmacological test of a putative LC neuron with systemic injection of an alpha-2 adrenergic receptor agonist (clonidine, 5*u*g/kg) in Monkey Wa. After a brief increase in activity at the time of the injection (green line), there was a prolonged (~ 1 hour) decrease in the responsivity of the LC neuron. The decrease in activity was accompanied by a decrease in baseline pupil diameter and an overall drowsiness in the monkey (detectable as prolonged drooping or closing of the eye lids, indicated by horizontal black lines at the top of the 'pupil diameter' plot). After ~1 hour, LC activity ramped back up just as the monkey was awake enough to engage in the change detection task.

3.3.2 Task Performance

We trained two monkeys to perform a 2 alternative forced choice (2AFC) orientation change detection task depicted in Figure 10. The monkeys reported the presence or absence of a change in the orientation of a drifting grating by making a saccade to either a green target (Yes) or a red target (No). We varied the difficulty of the orientation change to introduce some perceptual uncertainty as to whether each trial's choice is correct or not. To analyze the monkeys' behavioral performance, we applied signal detection theory, which is a method to statistically model the process of perceptual decision formation (Gold & Shadlen, 2007; Macmillan & Creelman, 2004; Shadlen & Kiani, 2013). SDT is typically applied to binary (two-alternative) decisions, as in our task where the animal had to decide whether a change in orientation occurred or not. Reporting Yes (green) or No (red) for trials of the two possible stimulus conditions (change present or absent) provides 4 different behavioral outcomes on this task: hits, misses, correct rejections and false alarms (Figure 10A). According to the SDT model for perception, a behavioral report about a stimulus in the task depends on noisy internal neural signals that represent sensory evidence from the presented stimulus. The range of neural responses evoked by change (signal) and no-change (noise) stimuli is represented by overlapping normal distributions. There are two metrics that determine if a subject perceives or misses a stimulus change, these are 1) sensitivity (d') and 2) criterion (c). Behavioral sensitivity is a measure of how well an ideal observer can separate the presence of signal from its absence while decision criterion conveys how strong the internal signal must be before the ideal observer decides to report a change.

Because changes in behavioral performance of the task could be due to change in either criterion or sensitivity, we evaluated both parameters in both monkeys. We measured each monkey's ability to detect orientation changes of different difficulties by calculating sensitivity

(d'), and found that both monkeys had higher sensitivity to larger orientation changes, and lower sensitivity to smaller orientation changes (Figure 10B,C). Both monkeys had increased criterion at smaller change amplitudes and decreased criterion at larger change amplitudes (Figure 10B,C). These behavioral results are consistent with those reported by previous studies that utilized a similar task structure (Crapse et al., 2018). We conclude that the two monkeys utilized comparable decision making strategies to perform the task adequately, and as expected.

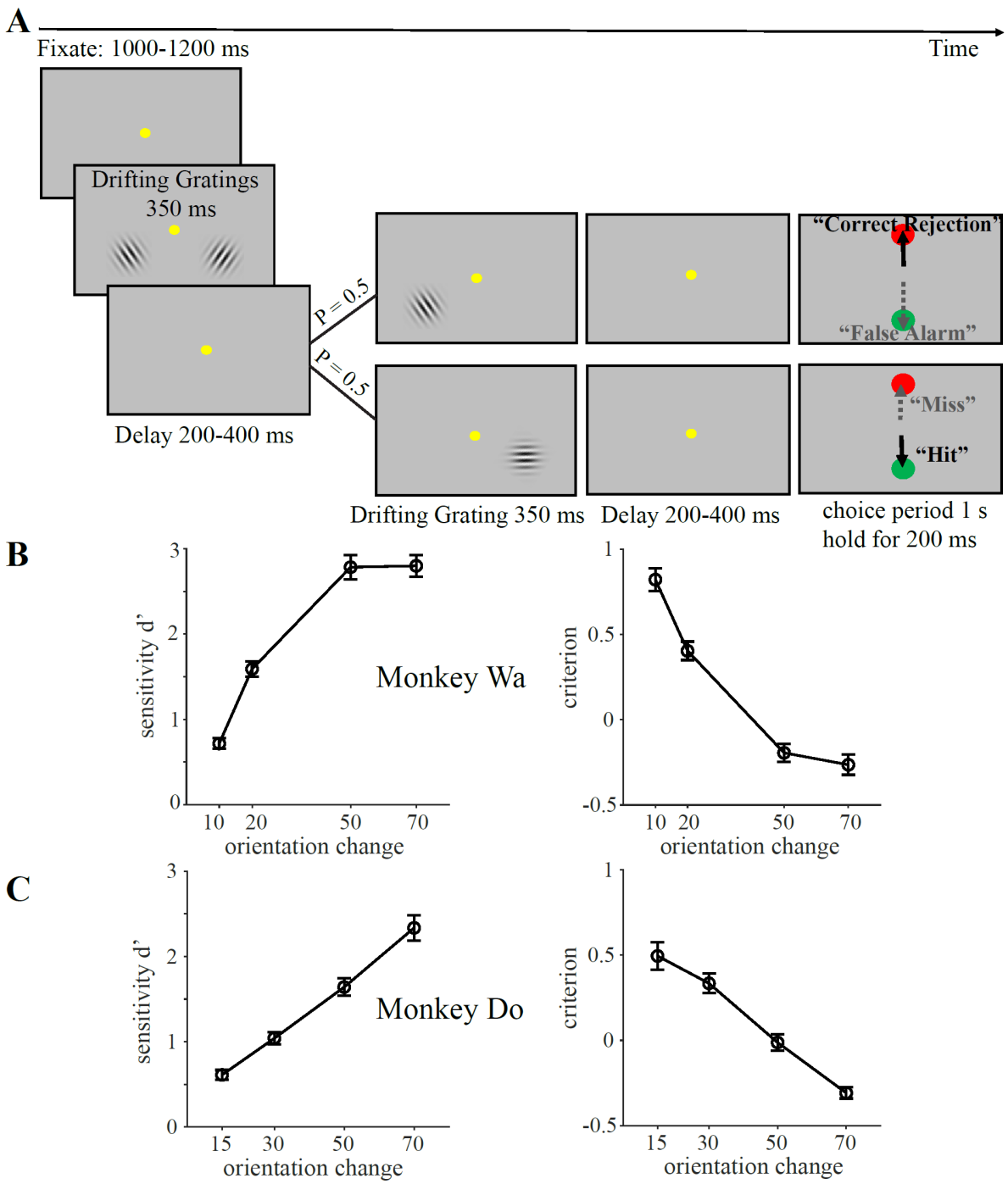

Figure 10. Behavioral task and performance.
(A) An example trial in the perceptual decision making task. Monkeys reported whether they detected a change in the orientation of the grating by making a saccade to 1 of the 2 colored choice targets. Correct decisions were followed by juice reward within 1 second of the choice saccades. (B,C) Average psychometric functions across sessions for Monkey Wa (B) and Monkey Do (C). The signal detection parameters sensitivity (d') and criterion are plotted as a function of the difficulty (amplitude) of the orientation change.

3.3.3 Task-related LC Phasic Activation

Collectively, past studies of the LC-NE system have led researchers to theorize that LC phasic responses could play an important role in decision making (Aston-Jones & Cohen, 2005a; Sara, 2009), but evidence for a specific function remains scarce. It is well accepted that there are several stages to the perceptual decision making process, including sensory evidence evaluation, sensory-motor transformation, and motor prep/execution. Importantly, the timing of these stages was indistinguishable in previous decision making paradigms used for studying LC activity. To more definitively connect the timing of changes in LC activity with a specific element of the perceptual decision formation process, we designed our task structure such that the stimuli containing the sensory evidence for a perceptual decision (the drifting gratings) were temporally distinct from the saccade target stimuli (green and red circles) for reporting choices.

While monkeys performed the task, the majority of LC neurons responded only during the choice period, right around the time of the saccade by which the monkeys reported their perceptual decision on each trial. Figure 11C demonstrates that out of 60 recorded LC units, 53 neurons had responses aligned to choice saccade onset that were significantly higher than baseline responses during initial fixations at the beginning of trials ($p < 0.05$, paired sample t-test). In each monkey, a high proportion of LC neurons showed significant peri-saccadic activation during the choice period: 30/31 in Monkey Wa and 23/29 in Monkey Do. In Monkey Do, 2 LC neurons actually had a peri-saccadic response that was significantly lower than baseline. We observed that a small subset of LC neurons (11/60) had significantly greater responses aligned to onset of the first stimulus grating, compared to baseline ($p < 0.05$, paired sample t-test; Figure 11A). Additionally, 26 of the recorded LC units had responses to the onset of the stimulus 2 grating that were significantly elevated above baseline ($p<0.05$, paired sample t-test; Figure 11B). We confirmed

that saccades to choice targets prompted the highest LC activation; the saccade-aligned responses were significantly greater than stimulus 2 or stimulus 1 aligned responses in 53/60 LC neurons ($p < 0.05$, paired sample t-test).

We also examined the average response dynamics across the whole population of recorded LC units. To compile the population response, we first standardized the firing rate of every neuron to the mean and standard deviation of the distribution of baseline firing rates across all completed trials (see Methods). Figures 11D-F show the average perievent time histograms (PETHs) of standardized LC responses aligned to the onsets of 3 important trial events: grating 1, grating 2 and choice period saccade. Consistent with our finding of increased firing by the majority of individual LC neurons around choice saccade onset, we observed a prominent buildup of the population activity beginning approximately 200 ms before the saccade onset (Figure 11F). The increase in activity lasted through the saccade and gradually decreased during a 200 ms period following the saccade. Population activity remained at baseline levels during stimulus gratings 1 and 2 (Figure 11D,E). Additionally, we separately examined the activity of the 26 LC neurons with significantly elevated firing rates during the second grating, but we did not observe an obvious transient increase in activity in the population PETH or individual neuron spike rasters. We conclude that this subset of LC neurons had generally increased activity during the second grating stimulus, but not phasic responses.

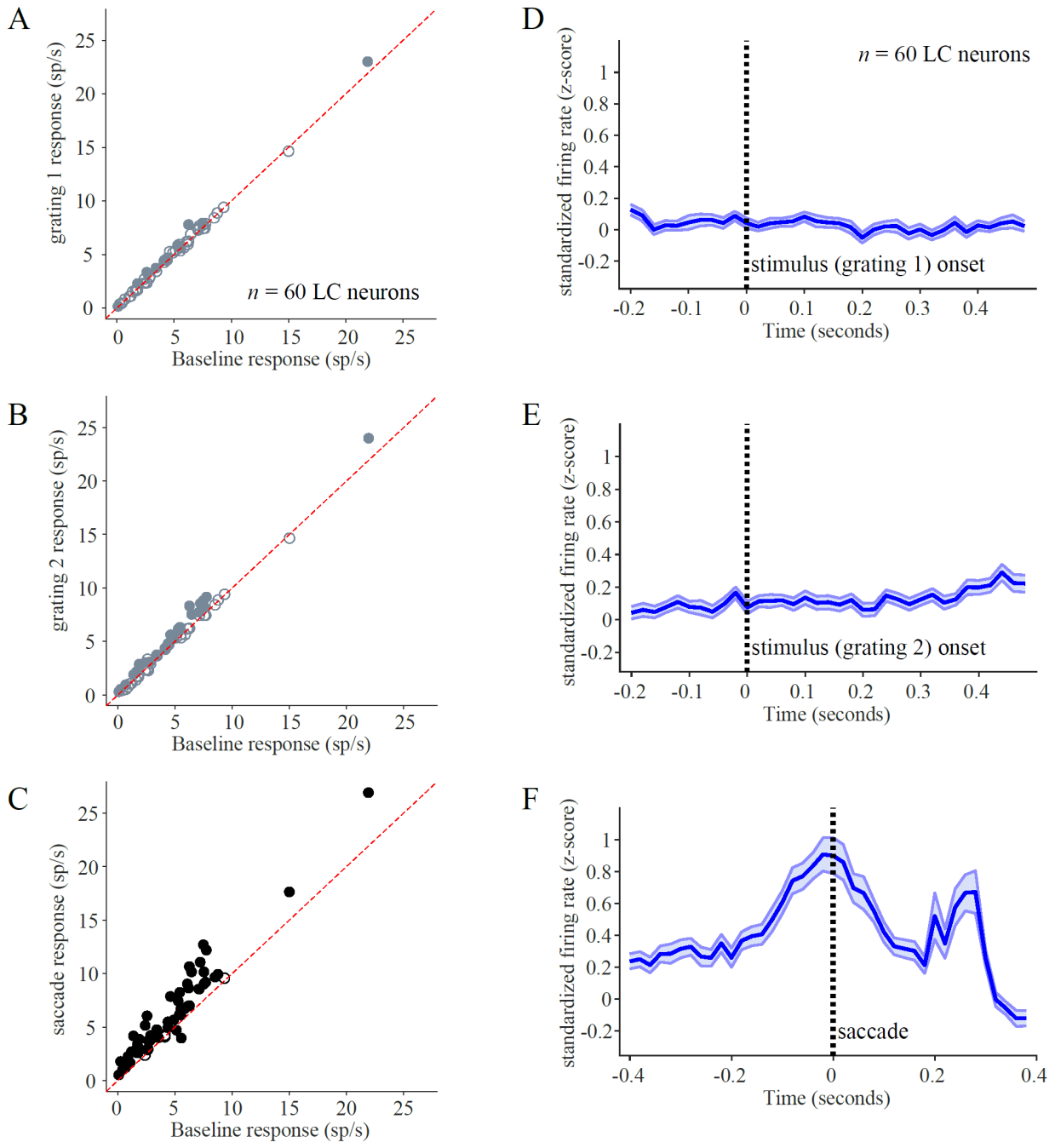

Figure 11. Task-related LC phasic activation.
(A-C) Scatter plots depict the responses of all recorded individual LC neurons aligned to the first stimulus grating onset (A), the second stimulus grating onset (B) and the saccade indicating the monkey's choice (C), as compared to the respective baseline responses (x-axis). Solid points represent LC responses significantly different from baseline (paired t-test, $p < 0.05$). The majority of the 60 recorded LC neurons showed significant activation around the time of the choice saccade. (D-F) Average PETHs across all standardized LC responses (blue bold line and shading represent mean +/- SEM across PETHs of individual neurons) aligned on onset of first stimulus grating (D), onset of second stimulus grating (E) and choice saccade onset (F).

3.3.4 Impact of LC Phasic Responses on Perceptual Behavior

Previous studies have found that increasing extracellular norepinephrine concentration, via stimulating LC or by pharmacological means, can enhance responses of individual sensory neurons to sensory inputs. Additionally, computational models and a few studies in different species (rodents, monkeys, humans) have suggested that boosting NE transmission may optimize behavioral performance in perceptual tasks (Avery et al., 2013; Gelbard-Sagiv et al., 2018; Guedj et al., 2019; Martins & Froemke, 2015; Safaai et al., 2015; Servan-Schreiber et al., 1990). Taken together, previous findings imply that the LC-NE system may modulate perceptual processes. However, manipulation studies offer just a limited perspective for understanding how normal fluctuations in LC discharge and NE efflux may impact perceptual ability. Furthermore, despite numerous theories proposing a function for LC in perception and decision making, there is a currently a shortage of studies of LC activity in the context of demanding perceptual tasks that allow for the use of psychophysical measures to precisely quantify perceptual accuracy (Aston-Jones & Cohen, 2005a; Sara, 2009; Waterhouse & Navarra, 2019a). To address this gap, we recorded physiological LC activity in the context of a task that required monkeys to first interpret perceived visual information of varied difficulty and subsequently report their decisions (Figure 10A). In the following set of results, we investigate whether LC phasic bursts have short time scale effects (within trial, <1 second) on specific elements of perceptual decision making behavior, including perceptual uncertainty, reaction times, perceptual sensitivity and criterion (as defined by SDT).

3.3.4.1 LC Phasic Responses Are Not Modulated by Behavioral Outcome

To introduce some uncertainty into the decision making process, we varied the difficulty of the orientation changes that the monkeys had to detect. Accordingly, on some of the trials the monkeys were unsure of whether they saw a stimulus change or not, resulting in incorrect 'false alarm' change detections or 'missed' orientation changes. We considered whether LC phasic responses are modulated as a function of different behavioral outcomes of the monkeys' choices. We grouped trials by the 4 possible behavioral outcomes on the task: correct detections, misses, correct rejects, and false alarms and compared LC population average responses between the conditions. Figure 12 shows that saccade-aligned LC phasic responses appear qualitatively similar in magnitude and temporal evolution across the 4 behavioral outcomes. Indeed, we found that the magnitude of LC phasic activation was statistically indistinguishable across behavioral outcomes. This was true for both LC responses aligned to stimulus 2 grating as well as LC responses aligned on choice saccade onset (grating 2: one-way ANOVA, post-hoc comparisons, all $p>0.05$; saccade: one-way ANOVA, post-hoc comparisons, all $p>0.05$). Additionally, we verified that the subset of 26 stimulus 2-responsive LC neurons did not differ in responsivity across behavioral outcomes (grating 2-aligned: one-way ANOVA, post-hoc comparisons, all $p>0.05$; saccade-aligned: one-way ANOVA, post-hoc comparisons, all $p>0.05$). The similarity of LC responses across behavioral outcomes suggests that LC phasic activation in this task is not related to any certainty or uncertainty the monkey has about its decision.

Additionally, we considered whether baseline LC firing rate (computed during the initial fixation period in each trial) differed between incorrect and correct behavioral outcome trials. In both monkeys, the average baseline firing rate across all recorded neurons was not significantly

different between correct (hits and correct rejections) and incorrect (false alarms and misses) trials (Monkey Wa: population mean firing rate on incorrect trials (3.9 sp/s) vs population mean firing rate on correct trials (3.9 sp/s), $p = 0.87$, paired t-test; Monkey Do: population mean firing rate on incorrect trials (2.7 sp/s) vs population mean firing rate on correct trials (2.8 sp/s), $p = 0.81$, paired t-test). Therefore, we conclude that the baseline (tonic) LC firing rate did not predict the behavioral outcome of the monkey's perceptual decision process on each trial of the task.

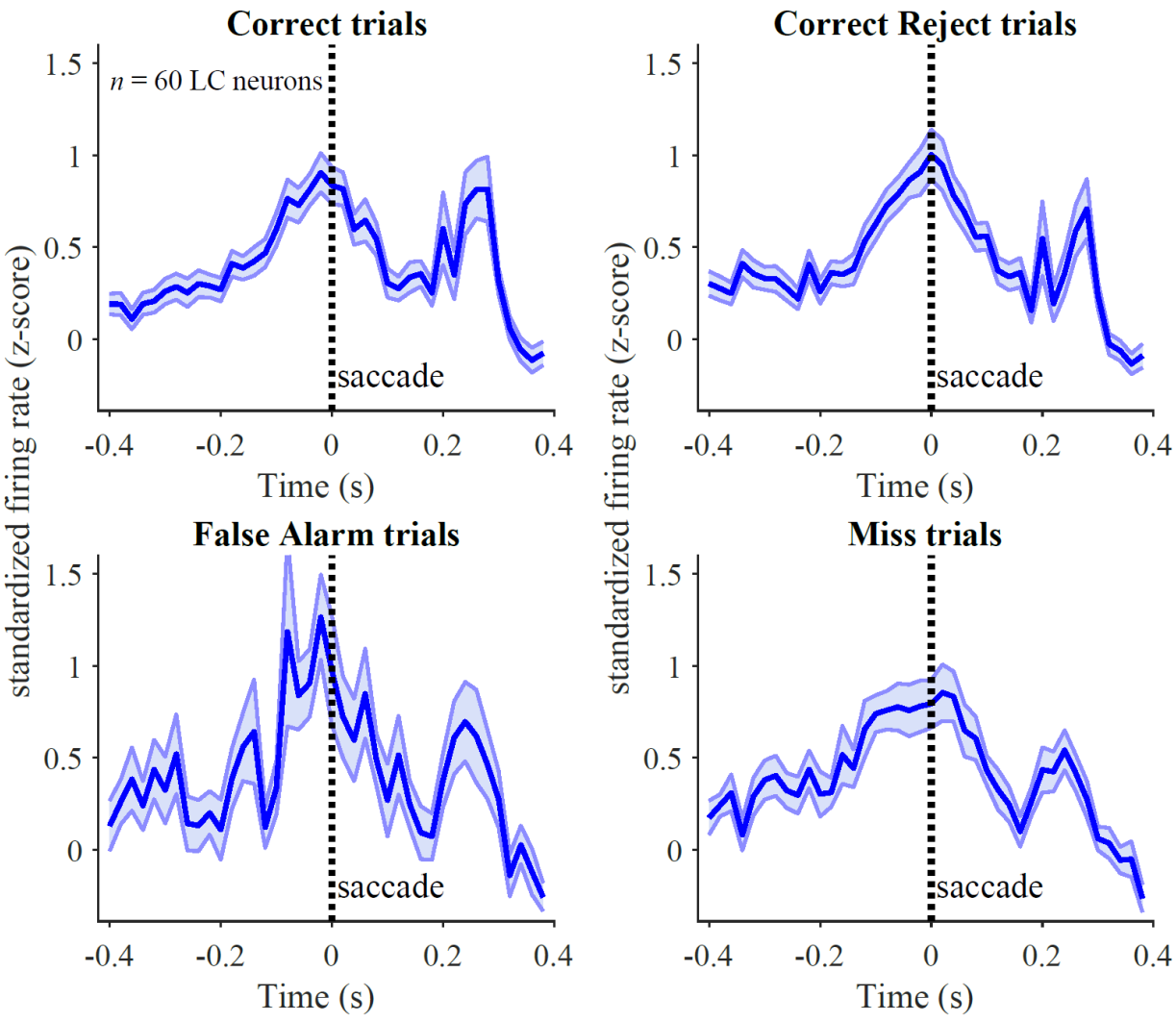

Figure 12. LC phasic activation across different behavioral outcomes.
Each panel depicts a LC population average PETH compiled across trials that resulted in 1 of the 4 possible behavioral outcomes in the orientation change detection task: correct, correct reject, false alarm, or miss. Shown PETHs were averaged across all standardized LC responses (blue bold line and shading represent mean +/- SEM across PETHs of all individual neurons across both monkeys) aligned on onset of the choice saccade. The magnitude of LC phasic activation was statistically indistinguishable across behavioral outcomes (one-way ANOVA, post-hoc comparisons, all $p>0.05$).

3.3.4.2 Relating LC Phasic Responses to Behavioral Sensitivity and Criterion

As described in section 3.3.2 on task performance, both of the monkeys were less accurate at correctly detecting smaller amplitude orientation changes in the drifting grating stimuli. Since the monkeys' choices were based on the available sensory information in presented visual stimuli, NE-mediated changes in how these stimuli are processed by brain regions along the visual pathway could affect the animal's behavioral performance. We hypothesized that LC phasic activation (and accompanying changes in NE efflux across the brain) during our perceptual decision making task may function to improve an animal's perceptual accuracy.

We first asked whether LC phasic response modulation reflected differences in the monkeys' behavioral sensitivity across change amplitudes. For instance, the magnitude of LC phasic activation could increase during harder change detections, resulting in improved SNR of visual cortex neuron responses, one of the known effects following increased NE transmission. Alternatively, LC phasic responses might track the monkeys' behavioral sensitivity, with higher responses corresponding to improved detection ability of larger amplitude changes. We compared LC population average firing rates across the four orientation change difficulties that occurred in each monkey's task. Because the range of orientation change amplitudes used for Monkey Wa differed from the range used for Monkey Do, for this analysis we considered LC neurons recorded in each animal as separate populations. In both monkeys, we found that LC population average firing rates were equal across correct detections of each of the four orientation change difficulties (Figure 13; grating 2 aligned: one-way ANOVA, post-hoc comparisons, all $p>0.05$ in Monkey Wa and Monkey Do; saccade-aligned: one-way ANOVA, post-hoc comparisons, all $p>0.05$ in Monkey Wa and Monkey Do). This result implies that LC phasic responses are not encoding the perceptual difficulty of the stimulus change detections, nor are they related to the monkey's ability to detect

stimulus changes of different difficulties. However, LC phasic activation during our task could be related to other aspects of perceptual decision making.

Several studies, including one from our lab, have shown that perceptual performance fluctuates over the course of a session (Cowley et al., 2020) . Thus we next considered whether trial-to-trial fluctuations in magnitude of LC phasic responses reflected changes in the monkeys' perceptual decision making behavior over the course of a session. We measured detection sensitivity (d') and criterion within windows of 50 trials, shifting the analysis window in 1 trial increments over the course of each session. This yielded an estimate of the animal's perceptual state for each trial. Figure 14A demonstrates an example session where both sensitivity and criterion fluctuated over the time that Monkey Wa performed the change detection task. We found similar behavioral variability over the course of most of the recording sessions in both monkeys. We then grouped all within-trial LC responses by whether they occurred in a period of time when sensitivity or criterion was lower or higher than the median for the session. This median-based grouping strategy allowed us to split trials into two equally-sized data sets in each session.

Figure 14 shows saccade-aligned PETHs of LC responses during high and low d' trials (Figure 14B) as well as high and low criterion trials (Figure 14C), combined across sessions and monkeys. We found no difference in the average LC population response (aligned to saccade or stimulus 2) between low d' vs high d' groups of trials (n=60 neurons in low and high d' conditions, paired t-test to compare population means; aligned to saccade, $p = 0.90$; aligned to stimulus 2, $p = 0.96$). Similarly, we found no difference in the average LC population response (aligned to saccade or to stimulus 2) between low criterion vs high criterion groups of trials (paired t-test; aligned to saccade, $p = 0.41$; aligned to stimulus 2, $p = 0.20$). Thus, although we consistently observed LC phasic responses around decision reports during our perceptual decision making task,

these phasic signals did not appear to encode anything related to how accurately the monkeys process and interpret the sensory evidence provided by the presented visual stimuli.

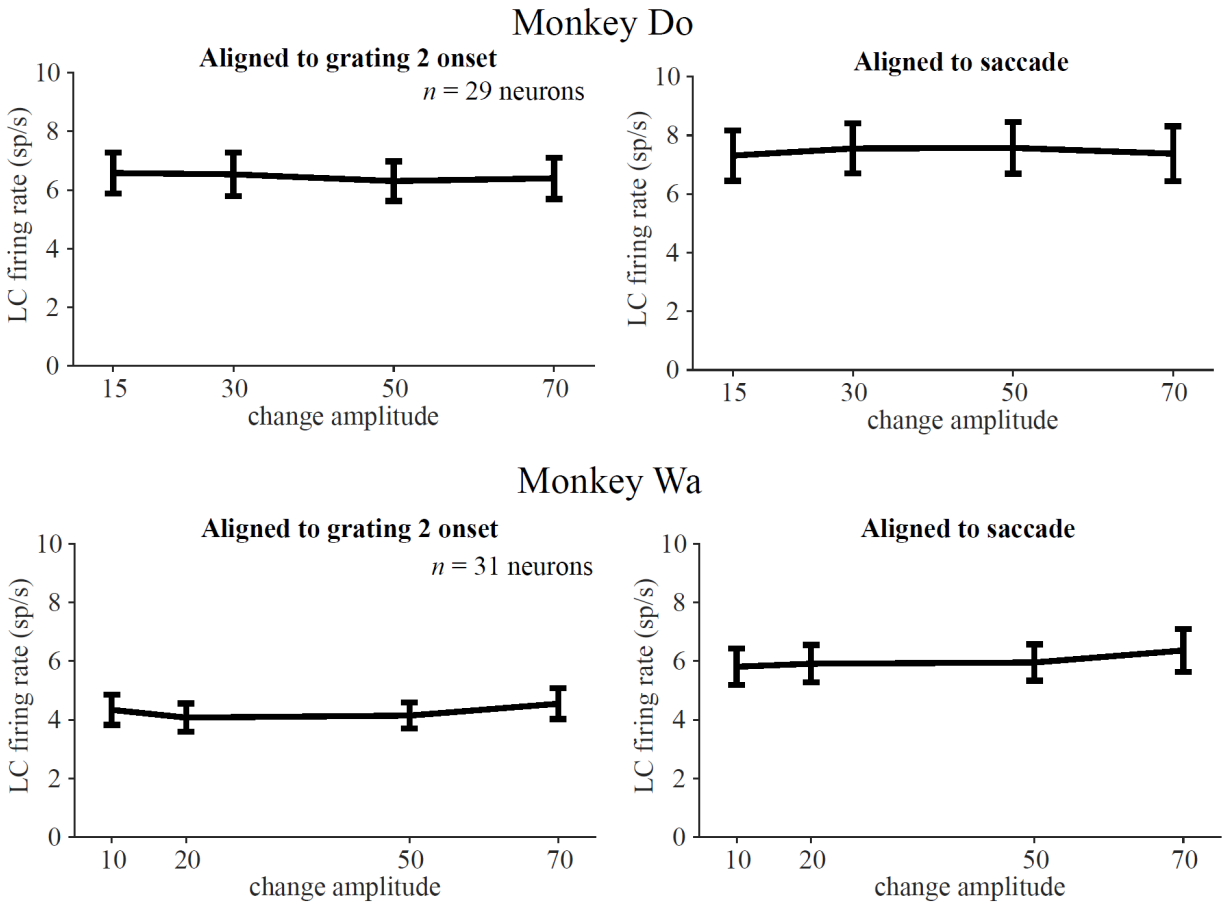

Figure 13. LC population average responses to different amplitudes of orientation changes.
In each monkey, LC population average firing rates were equal when compared across correct detections of each of the four orientation change difficulties. Panels on the left depict population average responses aligned on onset of the second stimulus grating, during which the orientation change occurred (one-way ANOVA, post-hoc comparisons, all $p>0.05$ in Monkey Wa and Monkey Do; errorbars represent +/- SEM across all individual LC neurons recorded in a monkey). Panels on the right depict population average responses aligned on onset of the choice saccade (one-way ANOVA, post-hoc comparisons, all $p>0.05$ in Monkey Wa and Monkey Do).

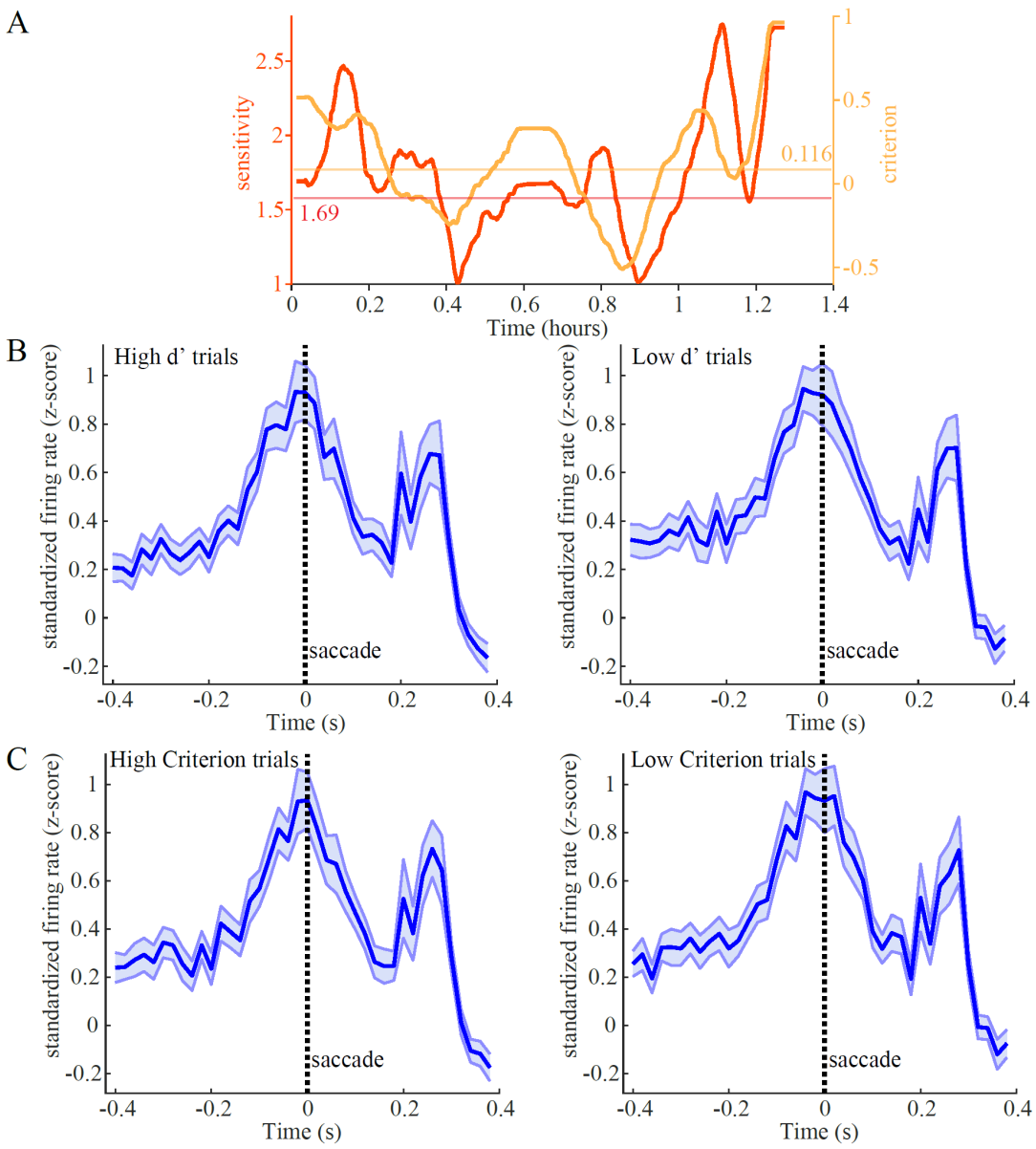

Figure 14. Comparing LC phasic activation between periods of high and low perceptual sensitivity or criterion.

(A) Changes in sensitivity (d', red) and criterion (orange) across time in an example session. Behavioral parameters were estimated in moving 50-trial bins over the course of each session. Horizontal lines signify the median d' (red) and criterion (orange) for the example session. Trials were grouped into high or low d' or criterion groups based on the median. Depicted shifts in behavioral parameters across time are representative of most sessions in both monkeys. (B) LC population average PETHs compiled across high d' (left) and low d' (right) trials (blue bold line and shading represent mean +/- SEM across PETHs of all individual neurons across both monkeys). Saccade-aligned phasic activation was equal between low d' vs high d' groups of trials (paired *t*-test to compare population means between low and high d' groups, p =0.90). (C) same as (B) but comparing saccade-aligned phasic activation between high and low criterion groups of trials (no significant difference, paired *t*-test, p = 0.41).

3.3.4.3 LC Phasic Responses Do Not Predict Behavioral Response Times

We next considered whether the latency or magnitude of LC phasic activation during the choice period is related to behavioral response times (RT). For each monkey, we grouped all completed trials within each session based on whether a trial's RT was higher or lower than the median RT of the session. The mean 'long' and 'short' RTs were comparable between the two monkeys, so we pooled the data for the following LC response analyses (Monkey Wa: 207 ms and 174 ms; Monkey Do: 236.1 ms and 169 ms). Across sessions and monkeys, the mean 'short' RT was 170.6 ms and the mean 'long' RT was 223.5 ms (Figure 15C). Upon a qualitative examination of LC activity aligned on the onset of the choice targets, we did not observe an obvious difference in the magnitude or latency of population average LC phasic responses between short vs long RT trials (Figure 15A). Quantitatively, also there was no significant difference in LC firing rates aligned on the choice period onset when compared between long and short RT groups (paired t-test, $p = 0.89$). Upon inspecting saccade-aligned PETHs, we observed that LC activity on shorter RT trials increased at an earlier latency compared to longer RT trials, about 150 ms before the saccade. Otherwise, the saccade-aligned LC phasic responses appeared nearly identical between the short and long RT trials. There was no significant difference in the magnitude of the saccade-aligned LC responses when compared between long and short RT groups (Figure 15B; paired t-test, $p = 0.5$).

The difference in response times observed across trials likely stems from trial-to-trial variability in decision processes. For instance, the RTs could be affected by the difficulty of the sensory information interpretation. Indeed, in each monkey, we found that the average response time for correct detections of easy orientation changes was significantly shorter compared to average response time for detections of hard orientation changes (Monkey Wa: 184 ms vs 190.2

ms, paired t-test to compare means across sessions, p = 0.016; Monkey Do: 161.5 ms vs 195.3 ms, paired t-test, p = 1.2e-16). Additionally, we found that in both monkeys, average RTs on correct rewarded trials were slightly shorter than RTs on incorrect unrewarded trials (Monkey Wa: 189 ms vs 194 ms, paired t-test to compare means across sessions, p = 0.021; Monkey Do: 197.8 ms vs 217 ms, paired t-test, p = 5.7e-18). However as shown earlier, we did not observe a significant difference in LC response magnitudes between trials of different behavioral outcomes or different change amplitudes (Figures 12, 13). Thus, our results suggest that while LC phasic responses are closely associated with within-trial task relevant behavioral responses, they do not signal any behavioral meaning for why response times are longer on some trials than others.

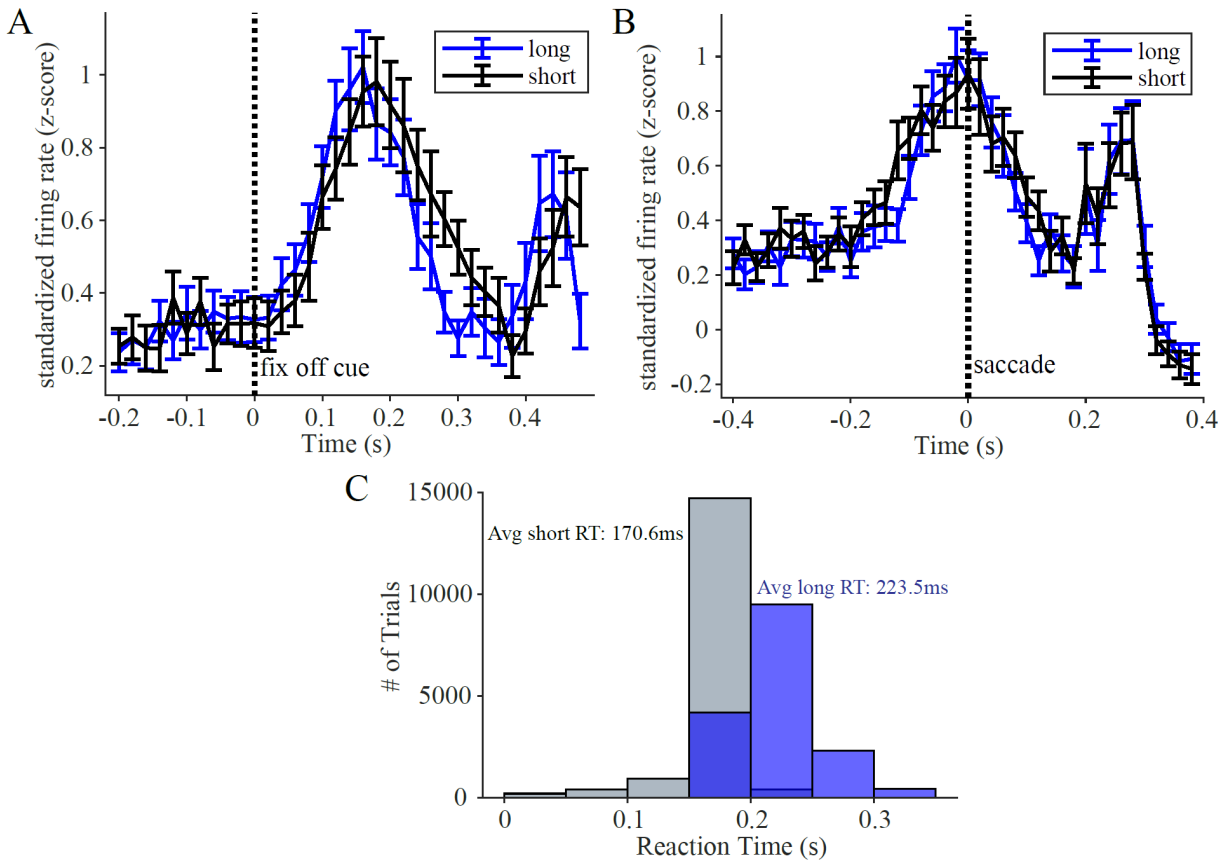

Figure 15. Comparing LC phasic activation between long and short behavioral response times. (A) Average PETHs compiled across choice target-onset aligned LC responses on long (blue) vs short (black) reaction time (RT) trials (lines and error bars represent mean =/- SEM across PETHs of all individual neurons across both monkeys). Target-onset aligned LC firing rates were not significantly different between trials of short vs long RTs (paired t-test, $p = 0.89$). (B) same as (A) but for saccadealigned LC responses; no significant difference between long and short RT trials (paired t-test, $p = 0.5$). (C) Histograms depict averages and distributions of behavioral response times in the short (gray) and long (blue) RT groups across sessions and monkeys. Long and short RT groups were determined by the median RT in each session.

3.3.5 Function of LC Phasic Responses during Choice Period

We next looked more closely into the significance of the peri-saccadic LC phasic responses during the choice period of the task. Overall, the results presented so far suggest that LC phasic responses in this task are more related to the motor aspects of reporting a behaviorally important decision, but not to any decision process elements related to perceiving and interpreting the sensory information. However, we still have not answered the question of whether the observed LC responses during the choice period are sensory, motor, or both in nature. That is, is the phasic activation during the choice period a combination of a sensory response signaling the onset of choice targets and a motor-related activation signaling an impending behavioral act, the saccade? To address this question, we collected an additional data set in Monkey Wa while he performed a slightly altered version of the change detection task (see Methods). Our main goal with the task change was to separate the timing of choice target onset from the 'go cue' signaled by fixation point offset (Figure 16A).

While Monkey Wa performed the task, the majority of recorded LC neurons showed distinct responses for the onset of choice targets and the saccade. Figures 16B,C demonstrate average target onset aligned and saccade aligned PETHs assembled across the activity of 16 LC units recorded during the altered version of the task. We found that 15/16 LC neurons had choice target onset aligned responses that were significantly higher than baseline responses ($p < 0.05$, paired sample t-test). Furthermore, the same 15 LC neurons also had responses aligned to choice saccade onset that were significantly higher than baseline responses ($p < 0.05$, paired sample t-test). We found that 6 out of the 15 neurons had saccade-aligned activation that was higher than target onset – aligned activity ($p<0.05$, paired sample t-test). This result is consistent with a recent

study that showed separable LC phasic responses to task-related sensory and motor events close together in timing during a saccade countermanding task (Kalwani et al., 2014).

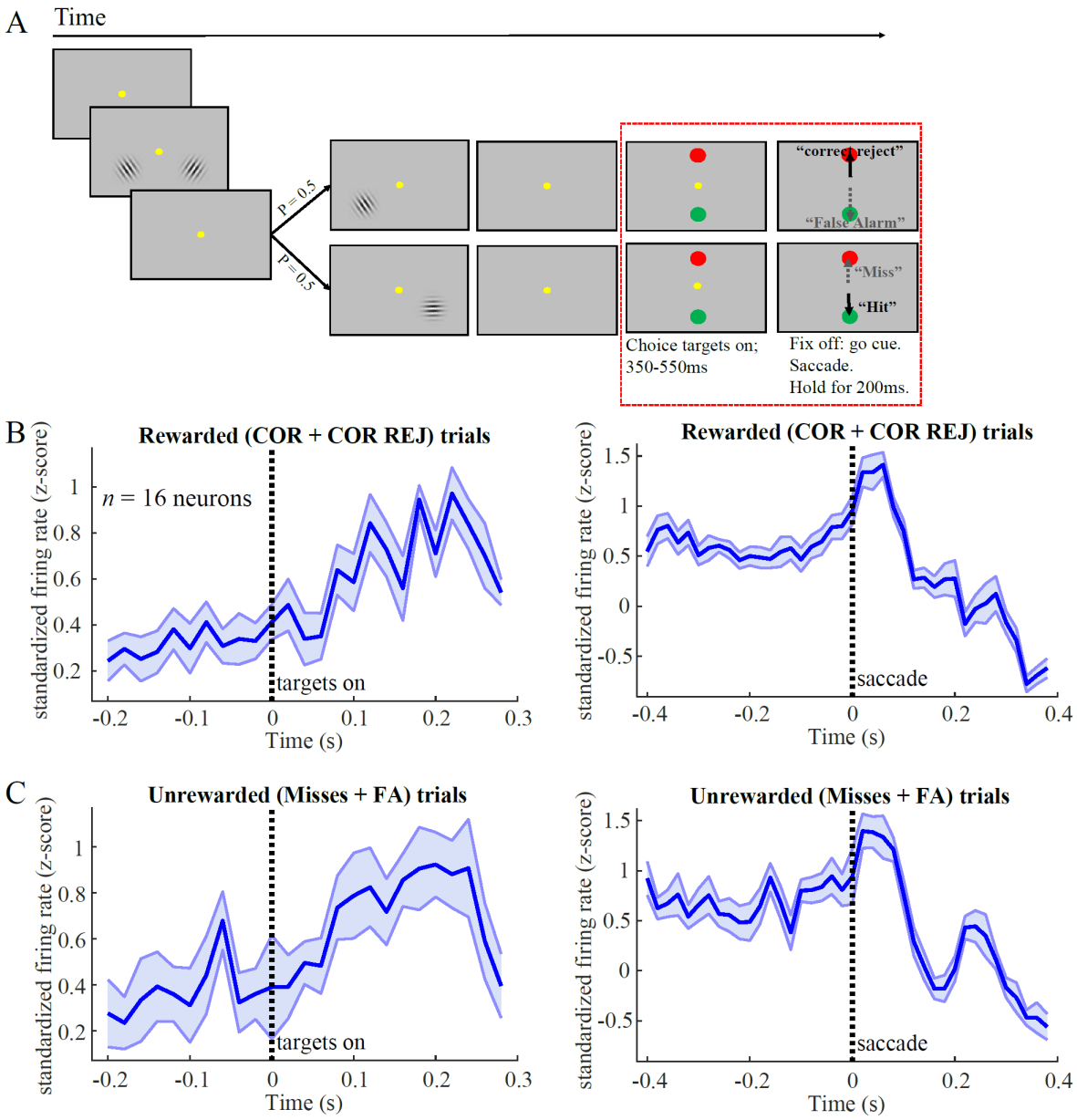

Figure 16. LC phasic activation during the choice period in version 2 of the perceptual decision making task.

(A) An alternate (2nd) version of the orientation change detection task. The red outline shows how the choice period in this task differed in comparison to the first version (depicted in Figure 10A). At the beginning of the choice period, when the red and green choice targets appeared, the fixation point remained on the screen for an additional 350-550ms. The disappearance of the fixation point served as a 'go cue' for the monkey to report its choice via a saccade to one of the choice targets. We recorded the activity of 16 LC neurons across 12 sessions in Monkey Wa as he performed this version of the task. (B) Average PETHs across LC responses aligned on choice target onset (left) and saccade onset (right) in rewarded (correct and correct reject) trials. LC neurons had separate phasic responses to choice target onset and choice saccades. (C) same as (B) but across unrewarded (false alarm and miss) trials. Across all trials (rewarded and unrewarded), 15/16 LC neurons had significantly elevated responses to choice target onset and to saccade onset, compared to baseline responses ($p < 0.05$, paired sample t-test).

Because the monkey could start planning the saccade as soon as the choice targets appeared on the screen, we hypothesized that the observed target onset – aligned LC responses could be related to motor planning rather than the sensory aspects of the choice targets. To address this possibility, we first grouped trials by the amount of variance in the monkey's eye position (fixation variance) throughout the time period between choice target onset and the 'go' cue onset. We found that choice target onset – aligned LC activity was higher in trials with higher fixation variance compared to trials in which the monkey's eye position was more stable during fixation (not shown). Next, we more closely examined traces of horizontal and vertical eye position in each trial in order to detect any small fixational eye movements that the monkey might have made (see Methods). Although monkey Wa maintained fixation throughout each completed trial, we observed that he occasionally made microsaccades which are small (<1º amplitude), rapid, typically involuntary deflections in eye position. We grouped all detected microsaccades in a session by the time at which they occurred in a trial. This allowed us to examine whether there was a significant increase in LC activity when aligned on microsaccade onset, and also whether the magnitude of LC activation varied depending on the timing of the microsaccade within a trial. Figure 17A demonstrates that in monkey Wa, LC phasic activation was tightly linked with the onset of 'choice period' microsaccades, but not microsaccades that occurred during 'other' time periods in the trial (i.e., grating stimuli, initial fixation). We found that 15 of the 16 LC neurons had 'choice period' microsaccade aligned responses that were significantly increased compared to responses aligned on all 'other' microsaccades (unpaired t-test, $p<0.05$). Additionally, figure 17B shows that there was no appreciable build-up in LC activity aligned on microsaccades that occurred specifically during the second stimulus grating. Although the trial structure during the choice period differed between the two task versions, it was identical during the time in a trial before choice period onset.

This allowed us to check whether LC activity aligned on 'other' microsaccades was similar across the two monkeys. As observed in Monkey Wa, there was no increase in LC activity aligned on microsaccades that occurred outside of the choice period in Monkey Do (Figure 17C).

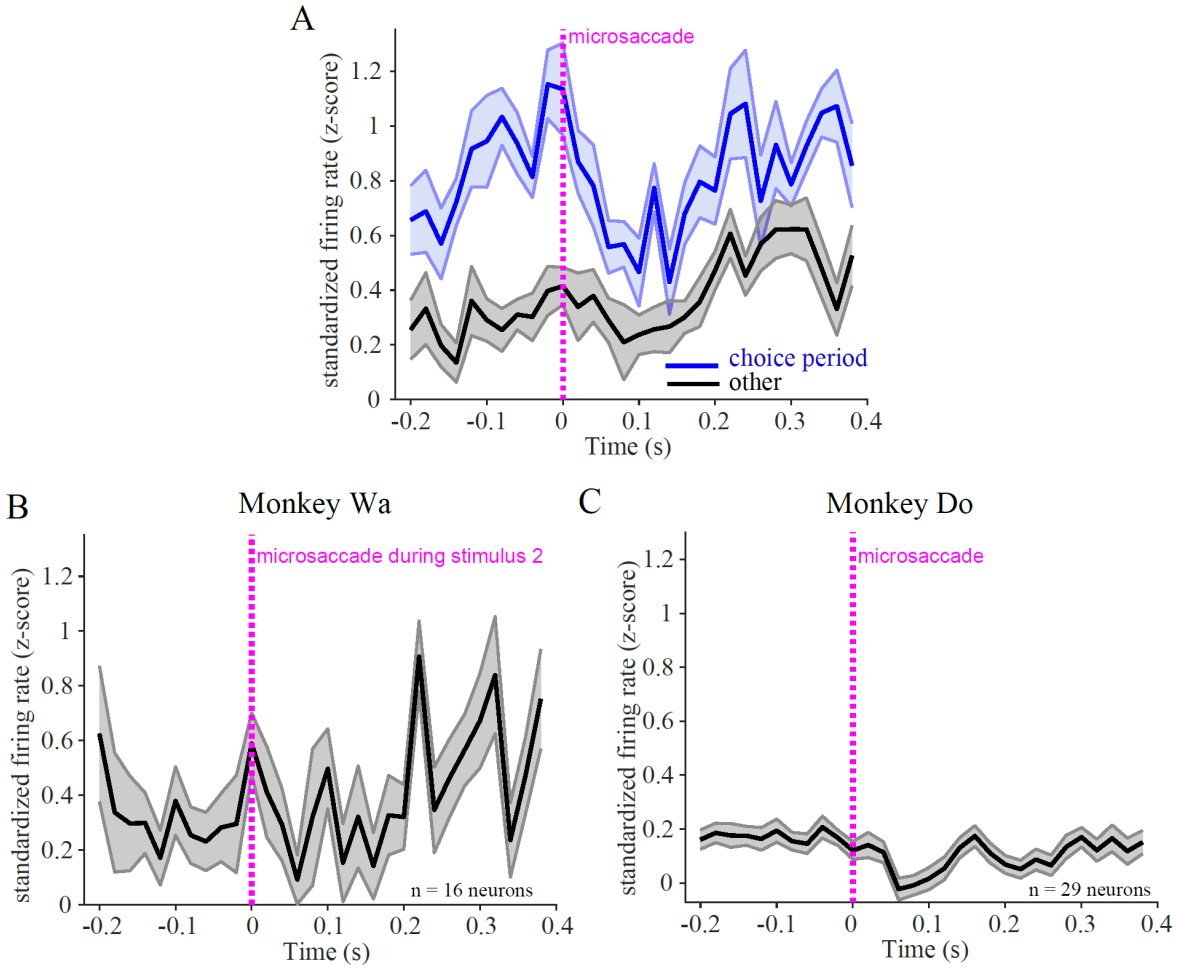

Figure 17. Microsaccade-related phasic activation of LC neurons.
(A) Average PETHs across LC responses aligned on microsaccades that occurred during different time periods in trials. Blue line and shading represent mean response +/- SEM for LC activity aligned on microsaccades that occurred during the choice period. Black line and shading represent mean response +/- SEM for LC activity aligned on microsaccades that occurred at all other times within trials (e.g. stimulus gratings, interstimulus intervals). 15/16 LC neurons had 'choice period' microsaccade aligned firing rates that were significantly increased compared to their responses aligned on all 'other' microsaccades (unpaired t-test, $p < 0.05$). (B) Average PETH across LC responses aligned on microsaccades that occurred during the second stimulus grating, in Monkey Wa. (C) Average PETH shows no increase in LC responses aligned on microsaccades that occurred outside of the choice period in Monkey Do (black line and shading represent mean +/- SEM across 29 LC neurons recorded in Monkey Do during the original version of the orientation change detection task).

3.4 Discussion

We examined the function of LC phasic activation in 2 monkeys during performance of a demanding perceptual decision making task. Our main findings are as follows. The timing of LC phasic responses was closely associated with saccadic eye movements used by the monkeys to report their decisions, but the magnitude of phasic activation was equal regardless of whether animals were correct or incorrect in their choices. LC neurons did not activate appreciably during presentation of sensory information evaluated by the monkeys in order to form their perceptual decisions. Furthermore, we did not observe any relationship between LC phasic response magnitude and perceptual accuracy on the task. Finally, in addition to choice saccade-aligned phasic activation, we found separate LC phasic responses that were closely aligned with microsaccades which occurred after the monkey was presented with saccade target stimuli but was not yet cued to execute the motor response for reporting the decision. Our results clarify the role of LC phasic responses during perceptual decision making and provide new evidence in support of the view that LC phasic responses function to orient and prepare an organism for a contextually appropriate and important behavioral response.

3.4.1 Significance of LC Phasic Activation for Sensory Perception and Decision Making

To date, perhaps the most direct examination of LC phasic activation during decision making was done by a study where physiological LC activity was recorded while monkeys evaluated the directional orientation of presented visual stimuli (Clayton et al., 2004). The authors found that the LC phasic responses were tightly linked with the variable timing of hand movements by which the monkeys reported their decisions trial to trial. Based on these findings, the authors

proposed that LC phasic responses facilitate the execution of a behavioral response following the commitment to a particular decision. However, this and other previous studies of LC activity during decision making (Aston-Jones et al., 1994; Clayton et al., 2004; Rajkowski et al., 2004; Usher et al., 1999a) utilized a task structure that did not allow for a conclusive assessment as to whether the observed LC phasic activation may be a combination of sensory information processing and motor components of a decision process. To address this point of confusion, we structured trials in our task such that the stimuli containing the sensory evidence for a decision were temporally distinct from the saccade target stimuli for reporting choices. Our finding that LC phasic responses occurred only in close alignment with eye movements during a specified decision reporting period allows us to definitively conclude that LC phasic responses do not occur in time to modulate the sensory processing and interpretation of the presented stimuli within the same trial.

We found that the magnitude of LC phasic activation remained the same despite obvious changes in the monkeys' change detection performance as measured by computing sensitivity and criterion in sliding windows throughout sessions (Figure 14). At first glance, our results appear to contradict a series of previous studies which reported that changes in baseline and phasic patterns of LC activity were closely correlated with fluctuations in behavioral performance as measured by the frequency of False Alarms errors on a simple visual stimulus detection task (Aston-Jones et al., 1994; Usher et al., 1999a). However, when we compare our task design to the above mentioned studies, it becomes apparent that the divergence in results can be explained by different interpretations of behavioral performance, originating in different evaluation methods. The previously used detection task required monkeys to respond to infrequent target stimuli but withhold responses to more frequent distractors. In that context of a continuous stream of task

stimuli, periods of increased false alarms and poor behavioral performance can be interpreted as high arousal-related disengagement from the task, as suggested by the authors themselves (Aston-Jones & Cohen, 2005a). In contrast, we reason that disengagement in the context of our task would manifest as fewer completed trials (a decreased willingness to wait the length of a trial) rather than more frequent incorrect judgements about stimuli (false alarms or misses). Errors on our task likely occurred because of variation in perceptual ability rather than distraction or disengagement since monkeys had to commit to fixating through a relatively long perceptually demanding trial before they could report a correct or incorrect choice. Thus, our results clarify previous conclusions about the relationship between LC activity levels and behavioral performance, showing that LC phasic activation does not signal changes in a subject's perceptual accuracy.

Our results do not preclude the possibility that changes in LC activity patterns can reflect arousal-related changes in behavioral performance. The above-mentioned previous findings (Aston-Jones et al., 1994; Usher et al., 1999a) formed the base for the prominent theory that transitions in LC activity patterns adaptively regulate behavior. This theory proposes that intermediate baseline LC activity and increased phasic activation serve to optimize performance on a current task, while elevated baseline activity and decreased phasic activation correspond to poor task performance, promoting increased distraction and exploration of other behavioral options (Aston-Jones & Cohen, 2005a). However, in our data, we did not find a difference in average LC baseline firing rates (computed during initial fixations within trials) when we compared responsivity between correct and incorrect behavioral outcome trials. A few previous studies also failed to observe a relationship between baseline (tonic) LC firing rates and various metrics of behavioral performance (Kalwani et al., 2014; Rajkowski et al., 2004). It has been suggested that more extreme changes in arousal are required for the larger fluctuations in LC tonic

activity that could influence an animal's behavior (Aston-Jones & Cohen, 2005a). In contrast, LC activity appears to span some optimal range within trials of more perceptually challenging tasks such as ours, perhaps because considerable concentration is required for performing the task well enough to earn some reward.

Many previous studies have focused on manipulating either Locus Coeruleus activity or cortical NE concentration to elucidate the cellular and circuit mechanisms by which the LC-NE system might influence behavior. Increased NE transmission has been shown to improve the signal- to-noise ratio (SNR) of sensory stimulus evoked responses, alter sensory tuning curves, lower thresholds for sensory-evoked responses (gating), and enhance spike synchrony (Waterhouse & Navarra, 2019). Together these previous findings prompted the prevalent theory that the LC-NE mediated improvements to sensory signal processing can alter perceptual behavior (Sara, 2009; Waterhouse & Navarra, 2019b). Only recently, investigators have begun to rigorously test this theory by linking changes in LC activity to simultaneously recorded cortical neuron responses in awake rodents engaged in a perceptual task (Martins & Froemke, 2015; Yang et al., 2021). So far one major study has demonstrated that pairing electrical stimulation of LC with sounds not only induced tuning changes in neurons located in the primary auditory cortex but also improved auditory perception in rodents (Martins & Froemke, 2015).

Since LC phasic activation is associated with transient but substantial increases in NE efflux (Berridge & Abercrombie, 1999; Florin-Lechner et al., 1996), we hypothesized that LC phasic responses function to improve perceptual performance within trials of our perceptual decision making task. However, our results decisively indicate that the LC phasic responses we observed during our task do not have any short time scale effects (within trial, <2 sec) on perceptual decision making behavior (Figures 12-15). Although previous studies have provided some

evidence that activating the LC-NE system has an enhancing effect on sensory signal processing and/or perception (Gelbard-Sagiv et al., 2018; Glennon et al., 2019b; Guedj et al., 2019; Martins & Froemke, 2015; Waterhouse & Navarra, 2019b), all of these investigations manipulated NE transmission whereas we assessed the relationship between physiological phasic LC activation and perceptual ability. Manipulations of the LC-NE system likely have prolonged effects on NE concentration in projection-targeted brain regions. Indeed, a previous study reported that cortical neuron response changes and perceptual performance improvements lasted hours to days after repeated LC microstimulation (Martins & Froemke, 2015). Since effects of LC activity on behavior can differ between experiments like ours where physiological activity is monitored and experiments where LC activity is manipulated, it is important to continue to study and compare findings about the LC-NE system in both contexts.

3.4.2 LC Phasic Activation Prepares an Animal for Important Behavioral Responses

Initial studies of the LC-NE system showed that unconditioned novel, salient or noxious stimuli of all sensory modalities evoke phasic responses, prompting hypotheses about the role of LC phasic activation in facilitating the processing of behaviorally important sensory information (Aston-Jones & Bloom, 1981a; Berridge & Waterhouse, 2003; Foote et al., 1980). More recent studies have shown that LC responses in various contexts including decision making are more closely linked to the animal's behavioral response (Bouret & Sara, 2004; Clayton et al., 2004; Rajkowski et al., 2004). Furthermore, a number of recent studies have shown that LC neurons can have separable phasic responses to task-related conditioned sensory stimuli and behavioral action onset (Bouret & Richmond, 2009; Bouret & Sara, 2004; Kalwani et al., 2014; Varazzani et al., 2015). Similarly, in the second version of our task, we first observed an increased firing rate about

100 ms after the onset of the choice targets, followed by another phasic activation around the onset of a saccade to one of the choice targets (Figure 16). It is noteworthy that in our task, LC neurons selectively responded to the choice targets, but not to the stimulus gratings. That the LC neurons are able to respond differentially to 2 sensory stimuli containing distinct but behaviorally important information, suggests that LC phasic responses are tuned to a specific stimulus meaning. This is in line with previous studies showing that LC phasic activation updates following reversals in task contingencies that change the meaning sensory stimuli (Aston-Jones et al., 1997; Dalley et al., 2001). Based on both previous observations and our results, it can be said that all the sensory stimuli which evoke LC burst responses share the common characteristic of alerting or cueing the animal that a behavioral response may be necessary very soon in time.

What could be the function of these sensory and motor aligned LC phasic responses that are so precisely timed to occur in very specific behavioral contexts? The timing of phasic bursts could be merely correlated with important sensory cues and motor events because LC receives diverse afferent inputs that transmit contextually important information for the task at hand (Poe et al., 2020; Sara, 2009; Sara & Bouret, 2012b). However, our results show that LC activation preceded the onset of microsaccades and saccades during the choice period, suggesting that LC phasic responses occur in time to modulate the preparation of these eye movements. This result is consistent with most previous studies which have shown that the onset of LC phasic activation precedes motor responses (Bouret & Richmond, 2009, 2015; Clayton et al., 2004; Varazzani et al., 2015; Yang et al., 2021), but see (Kalwani et al., 2014). Below, we discuss how our findings provide new evidence in support of the theory that LC phasic bursts facilitate processing in brain regions involved in motor output and autonomic activation, thus preparing the animal for an

appropriate motor response to a behaviorally significant stimulus, whether that's in a task setting or in the natural environment (Bouret & Sara, 2005; Sara & Bouret, 2012b)

We found that in the altered, second version of our task (Figures 16, 17) monkeys tended to make small fixational eye movements (microsaccades) while they waited for the offset of the fixation point which served as the 'go' cue for executing a larger saccade for reporting the decision. Importantly, during that time period, LC phasic activation was more tightly linked to the onset of the microsaccade than the onset of the choice targets (Figure 17A). An important novel finding of our study is that, at least in the context of our task, the visual-stimulus aligned LC phasic activation did not reflect the sensory aspects of the choice targets, but rather signaled a motor process that was likely triggered by the onset of the choice targets. Although the visual function of microsaccades has been debated for decades, the current understanding is that microsaccades and saccades are the same type of eye movement, generated by a common oculomotor pathway (Martinez-Conde et al., 2013). For instance, there is now substantial evidence that neurons throughout the Superior Colliculus represent all saccade directions and amplitudes, with the <1deg amplitudes typical of microsaccades encoded by neurons in the rostral pole of SC (Hafed et al., 2009; Munoz & Wurtz, 1993). Just as saccades have multiple roles in vision, microsaccades may also serve several important functions, including correcting fixation errors (Engbert & Kliegl, 2004), restoring fading vision during fixation (McCamy et al., 2012), sampling the available information in the visual environment (Martinez-Conde et al., 2013), and overtly signaling shifts in covert attention (Engbert & Kliegl, 2003; Hafed & Clark, 2002; Yu et al., 2022).

It is possible that in our task LC activation facilitated microsaccades during the choice period to help the monkey covertly orient to the locations and colors of the two choice target stimuli. Of note, we only observed significant LC activation around microsaccades during the

choice period, but not microsaccades occurring during other times in the trial (Figure 17). Such selective timing implies that LC phasic responses and the corresponding NE release in target regions function to optimize motor preparation for an upcoming important behavioral response, which in our task was a saccade to report a decision. Our interpretation is consistent with previous anatomical tracing studies which have shown that within the primate visual system, LC projections predominately target the prefrontal cortex and tecto-pulvinar structures, while projections to the visual and inferotemporal cortex are comparatively less dense (Arnsten, 1998; Lewis & Morrison, 1989; Morrison & Foote, 1986; Porrino & Goldman-Rakic, 1982a). Others have noted that such a projection pattern supports a role for the LC-NE system in preferentially regulating activity in brain regions with visuomotor and spatial analysis functions, such as the Superior Colliculus (Berridge & Waterhouse, 2003; Morrison & Foote, 1986).

Interestingly, recent studies provide compelling evidence that action-onset aligned LC phasic activation signals the amount of physical effort required for a task-relevant important behavioral response (Bornert & Bouret, 2021; Varazzani et al., 2015). These findings support the theory that motor-related LC phasic activation promotes mobilization of physical (i.e., muscles) and autonomic (i.e., respiratory, cardiac systems) resources to help complete physically effortful actions. Our results are consistent with such an interpretation and extend previous understanding of LC motor-related activity in two important ways. Firstly, it can be said that behavioral responses in the above-mentioned studies were by nature volitional, as monkeys had to exert a specific understood amount of physical force for completing trials. Because microsaccades are typically involuntary, our finding of LC activation around microsaccades provides evidence that LC neurons respond to both voluntary and involuntary motor outputs. Secondly, although the physical effort required for behavioral responses (saccades) was equal across all trials in our task, the monkeys

faced perceptual challenges such as detecting very subtle stimulus changes on some trials. In our results, we demonstrated that LC neurons activated equally for all difficulties of stimulus changes, whether subtle or obvious. In the context of previous findings, we can conclude that although LC neurons encode information about the physical effort required for a behavioral response, they do not encode the amount of perceptual effort necessary for noticing or appropriately responding to a sensory stimulus.

Based on our results, future studies should consider the possibility that any observed stimulus-aligned LC responses are not purely sensory in nature, but instead may be linked to motor preparation processes triggered by the presentation of an important sensory stimulus, as we found in our study (Figures 16, 17). Interestingly, all previous experimental paradigms used for studying LC phasic activation involved some variant of sensory cuing that could in principle trigger small eye, face, or body movements as preparations for impending, larger motor responses. For instance, in early studies of LC activity it is likely that startling or noxious stimuli prompted reflexive responses (e.g., muscle contractions, eye blinks associated with the startle reflex) or fidgeting movements not measured by experimenters. A previous study in rodents showed that LC phasic responses were associated with lipping (a Pavlovian reward expectation response) that occurred at the time of a reward cue and at the time of a task-related motor response (Bouret & Richmond, 2009). However, few other studies of LC phasic activation have considered such potentially task-related small movements in their interpretations of sensory stimulus aligned responses. In future studies, it could be particularly illuminating to align LC activity on occurrences of small body (e.g., licking, fidgeting) and eye movements during task engagement, as some recent studies have done for cortical activity in rodents (Stringer et al., 2019). From the findings presented in this study, we conclude that the relatively brief, discrete LC phasic activations within seconds-long

trials of our perceptual decision making task serve to orient and prepare the animal for an important behavioral response but have no impact on the perceptual accuracy of the animal's decisions.

4.0 Fluctuations in Baseline Activity of Locus Coeruleus Neurons Track Changes in Pupil Diameter and Cortical Population Activity Over Time

4.1 Introduction

In a complex and ever-changing environment, our brains repeatedly carry out the process of perceptual decision making, wherein the available sensory information is encoded, evaluated and used to form an appropriate behavioral response. The accuracy of perceptual decisions fluctuates, in part because the brain does not maintain a constant state of optimal perceptual capacity, but rather cycles between higher and lower states of arousal, distractibility and motivation throughout the day. Neuroscientists have yet to determine how global brain state changes may corrupt or optimize neural computations local to brain regions responsible for perceptual decision making.

Previous studies have established that perceptual decision formation can be separated into several core processing stages that take place across a distributed network of brain regions (Gold & Shadlen, 2007; O'Connell et al., 2018; Shadlen & Kiani, 2013). For decisions about visual stimuli, the visual cortex represents sensory information, while brain regions such as the prefrontal cortex, lateral intraparietal area and superior colliculus (PFC, LIP, SC) are thought to both set the threshold for the sensory evidence required to report a choice, as well as prepare and execute eye movement commands to report the decisions. Changes in brain state could influence perception via adjustments of neuronal responses in any one or potentially all of the involved decision stages. Such a brain-wide signal likely originates in a brain region with diffuse projections that could modulate responsivity of many neurons regardless of their location or stimulus preferences.

A fitting candidate is the locus coeruleus (LC), a group of cells which produce the neuromodulator substance called norepinephrine (NE). LC neurons receive inputs from diverse cortical and subcortical brain regions and have long-distance projections that exclusively control the release of NE throughout the brain (Samuels & Szabadi, 2008; Sara, 2009; Schwarz et al., 2015; Schwarz & Luo, 2015). In rodents, numerous studies have comprehensively established that artificial changes in NE concentration can modulate the gain of neural signals in sensory cortical regions, thus potentially regulating the efficacy of sensory information processing (reviewed by Waterhouse & Navarra, 2019). In primates, previous work has shown that LC is reciprocally interconnected with the anterior cingulate cortex (ACC) and prefrontal cortex (PFC) (Arnsten & Goldman-Rakic, 1984; Porrino & Goldman-Rakic, 1982b), which are brain regions involved in the development of goal-based action plans, an important part of decision making (Arnsten et al., 2012; Clark et al., 2015; Ebitz & Platt, 2015; Funahashi et al., 1991; Kim & Shadlen, 1999; Rainer et al., 1998; Shima & Tanji, 1998).

In addition to targeting brain regions with cognitive functions, LC neurons also project to the spinal cord and groups of cells that comprise the autonomic nervous system, which regulates bodily functions such as heart rate, pupil size and respiration rate (Joshi et al., 2016a; Joshi & Gold, 2020; Samuels & Szabadi, 2008; X. Wang et al., 2014). The LC is part of the reticular formation, a group of brain regions that together regulate the sleep-wake cycle (Moruzzi & Magoun, 1949). LC is considered a 'wakefulness-promoting' nucleus because increased LC activity is associated with behavioral and EEG signs of alertness (Berridge et al., 1993), while decreased LC activity always accompanies drowsiness (Aston-Jones & Bloom, 1981a). Fluctuations in LC activity, along with corresponding changes in brain-wide NE release, are thought to contribute to changes in overall arousal state, detectable in neural activity across

brain regions as well as in externally observable physiological changes like heart rate and pupil diameter. Previous studies have observed that variability in LC activity induces sleep-wake transitions (Carter et al., 2010) and correlates with pupil size both during quiet wakefulness (Breton-Provencher & Sur, 2019a; Joshi et al., 2016a; Reimer et al., 2016) and under some cognitive task conditions (Megemont et al., 2022; Varazzani et al., 2015; Yang et al., 2021). However, many questions remain about the extent to which pupil diameter is linked to LC activity. More work is necessary to understand whether the relationship between pupil diameter and LC activity is context-dependent and whether it persists across different timescales.

Collectively, previous work implies that the LC-NE system has an important role in coordinating information across many brain regions and is well posed to regulate cognitive function according to changes in arousal state. The most direct evidence for such LC-mediated changes in cognitive processes would come from experiments that simultaneously monitor LC activity, cortical activity, and external behavioral markers in awake animals preferably engaged in a cognitive task. To this date, only a few studies of this type have been done in rodents (Martins & Froemke, 2015; Yang et al., 2021) and just one such investigation was recently undertaken in primates (Joshi & Gold, 2022).

Our goal in this study was to examine how physiological, ongoing activity in the LC may relate to pupil diameter and changes in neural activity patterns in the dorsolateral prefrontal cortex (referred to as 'PFC' from now on) while monkeys engage in a demanding perceptual decision making task. We specifically chose to study PFC because this region has strong reciprocal connections with LC (Arnsten & Goldman-Rakic, 1984; Porrino & Goldman-Rakic, 1982b). Additionally, both PFC and LC have previously been linked to the same higher order-cognitive functions including goal-oriented behavioral responses and decision making (Clayton et al., 2004;

Funahashi et al., 1991; Kalwani et al., 2014; Kiani et al., 2014; Kim & Shadlen, 1999; Luo & Maunsell, 2018; Rainer et al., 1998; Seo et al., 2007; Tanji & Hoshi, 2008). These characteristics make PFC a suitable candidate area for investigating how fluctuations in LC activity may influence behaviorally relevant computations in cortical activity.

LC activity, just like cognition and the underlying neural activity across brain regions, fluctuates over multiple timescales. It has been suggested that the different timescales of LC activity may modulate different aspects of cognition-related neural activity and cognitive behavior (N. K. B. Totah et al., 2019b). Although there have been multiple reports of covariation between cognitive behavior and LC activity on different timescales, much remains unknown about the temporal and spatial scales of interaction between the LC-NE system and neurons in brain regions responsible for higher cognitive functions such as decision making. In a recent study from our lab, we uncovered a slow time scale variability ('slow drift') in both visual area 4 (V4) and PFC population activity that was strongly correlated with fluctuations in behavioral state metrics such as pupil diameter and reaction times, as well as with slow changes in behavioral performance on a perceptual task (Cowley et al., 2020). Because this slow drift signal was present in two cortical regions and correlated with pupil diameter which is an external marker of arousal, we hypothesized that the slow drift in V4 and PFC population activity could arise from slowly changing dynamics of norepinephrine release from long-distance projections of LC neurons to those and other brain regions.

In the current study, we were interested in assessing LC-PFC interactions on both slower (tens of minutes) and faster (seconds) timescales and investigating how activity in both of these regions relates to changes in pupil size. Additionally, we reasoned that relating LC activity to cortical population activity could be particularly informative because upon release in target areas,

NE can diffuse to modulate responses of many neurons at the same time (Callado & Stamford, 2000; Jacob et al., 2018). Therefore, we simultaneously recorded the activity of tens to hundreds of PFC neurons along with LC single unit activity. This experimental approach allowed us to assess how LC single unit activity may relate to responses of individual PFC neurons, as well as to PFC population activity patterns uncovered through dimensionality reduction methods.

4.2 Methods

4.2.1 Subjects and Surgical Preparation

Two adult rhesus macaques (Macaca Mulatta) were used for this study; these were the same monkeys as used for experiments described in Chapter 3 of this thesis. One of the monkeys was female (Monkey Do) and the other monkey was male (Monkey Wa). Experimental procedures were approved by the Carnegie Mellon University Institutional Animal Care and Use Committee and were in compliance with the United States Public Health Service Guide for the Care and Use of Laboratory Animals.

After initial training, each monkey was implanted with a recording chamber (Crist) that provided access to the Locus Coeruleus (LC). Detailed information on LC chamber placement, the procedure for mapping the location of LC neurons, and the specifics of electrophysiological recordings in LC is available in Chapter 3 of this thesis (section 3.2 of the Methods & section 3.3.1 of the Results). After locating LC, we implanted a 96-electrode “Utah” array (1mm electrode lengths; Blackrock Microsystems, Salt Lake City, UT) in the left hemisphere dorsolateral prefrontal cortex (dlPFC) of each monkey, using sterile surgical techniques under isoflurane

anesthesia. Previous anatomical tracing studies (Arnsten & Goldman-Rakic, 1984; Porrino & Goldman-Rakic, 1982b) have provided evidence for dense reciprocal connectivity between neurons throughout the LC and neurons throughout both ventral and dorsal banks of the principal sulcus which constitute the dorsolateral prefrontal cortex. Therefore, we implanted arrays in dlPFC in both monkeys. In Monkey Do, the array was implanted in the dorsal bank of the principal sulcus, while in Monkey Wa, the array was placed in the ventral bank of the principal sulcus. In both monkeys we aimed to position the arrays in pre-arcuate area 8Ar, a dlPFC region just anterior to the arcuate sulcus, that has both visual and motor related activity during visual tasks that require saccadic eye movements (Bullock et al., 2017; Stanton et al., 1993).

4.2.2 Data Collection

Within a data collection session, our procedure was as follows. First, a single tungsten electrode was lowered down to the approximate previously mapped location of LC. After establishing a stable signal from a putative LC neuron, we would begin a simultaneous recording of extracellular activity from the PFC array. Concurrently, we measured pupil diameter and eye position, using an infrared eye tracking system (EyeLink 1000; SR Research, Ottawa, Ontario). We collected this neurophysiological and eye data while monkeys performed a perceptual decision making task, the details of which are described in section 3.2.3 of Methods in Chapter 3 of this thesis (Figure 10A). In Chapter 3 we described results of analyses focused on relating LC activity and behavior, while here we assessed the relationships between LC, PFC, pupil diameter and behavior. The LC data set used in this chapter is identical to the LC data set described in Chapter 3.

During the experiments, stimuli were displayed on a 21" CRT monitor (resolution of 1024x768 pixels; refresh rate of 100 Hz), with a viewing distance of 36 cm. The visual stimuli were generated using custom software written in MATLAB (MathWorks, Natick, MA) and Psychophysics Toolbox extensions (Brainard, 1997, Kleiner et al., 2007, Pelli, 1997). Signals from the arrays and the single electrodes were band-pass filtered (0.3 – 7,500 Hz), digitized at 30 kHz, and amplified by a Grapevine system (Ripple, Salt Lake City, UT). Waveforms that crossed a threshold were recorded, saved and stored for offline classification. For array recordings, the threshold was set using a multiple of the root-mean-squared noise. We manually set the threshold for each LC neuron to allow recording of some noise and multi-unit activity in addition to the isolated single unit activity. We used custom spike-sorting software (written in MATLAB; The MathWorks, Natick, MA) to manually sort putative LC waveforms based on shape and inter-spike interval distributions (Kelly et al., 2007). PFC waveforms were first automatically sorted by an artificial neural network (Issar et al., 2020) and subsequently manually adjusted if needed based on shape and inter-spike interval distributions. It is likely that we recorded a combination of well-isolated single units and multiunit activity in both PFC and LC. We refer to both types of signals as 'neurons' and included both in our analyses. Our data set of simultaneous LC-PFC recordings was comprised of 23 separate sessions in Monkey Wa during task version 1 (Figure 10A), 20 separate sessions in Monkey Do during task version 1, and an additional 12 separate sessions in Monkey Wa during task version 2 (Figure 16A). The number of PFC neurons included for analyses ranged from 56-114 across sessions in Monkey Wa, and 14-69 neurons in Monkey Do.

4.2.3 Data Analysis

All data analysis was performed using custom code written in MATLAB (The MathWorks, Natick, MA). We removed PFC neurons with a firing rate of < 2 spikes/second. For LC-pupil and LC-PFC individual neuron analyses (results depicted in Figures 18-20) we included all 76 LC neurons recorded across the 55 sessions in two monkeys. For analyses of relationships between LC, PFC population activity and pupil diameter (results depicted in Figures 21-26) we removed 11 sessions (all in Monkey Wa) which were < 30 minutes in duration, as we were interested in relating these variables over a longer time course. We used data from a total of 44 sessions and 64 LC neurons across 2 monkeys for these analyses.

4.2.3.1 Time Windows

LC activity. For measurements referred to as 'initial fixation', or 'baseline', LC firing rate was computed in a 500ms window aligned on fixation point onset in each trial. For measurements referred to as 'first stimulus grating', LC firing rate was computed during a 350ms window aligned on the onset of the first stimulus grating shown in each trial. For measurements referred to as '30 second bins', we measured overall LC activity (including baseline spiking and phasic bursts) in a 30 second time window preceding each trial. For calculating spike count correlation (results depicted in Figure 20A,C), LC spike counts were measured during a 350ms window aligned on the onset of the first stimulus grating.

Pupil diameter. During experiments, pupil diameter was measured monocularly, in arbitrary units. We then z-scored raw pupil measurements across the entire session before allocating values into trials. We removed any outlier measurements (>3 SD), which would have included periods of eye closure or blinking. For measurements referred to as 'fixation', pupil

diameter was averaged in a 500ms window preceding the onset of the first stimulus grating. We avoided measuring pupil diameter in ~700ms following fixation onset in each trial, in order to avoid potential artifacts following a change in eye position. For measurements referred to as 'first stimulus grating', pupil diameter values were averaged in a time window of 500ms aligned on the onset of the first stimulus grating in each trial. We refer to fixation-based pupil diameter measurements as 'baseline'. Of note, the non-evoked pupil diameter measurements during the first stimulus grating were likely dominated by the baseline response, and these were used when relating pupil diameter to the PFC population activity on different timescales (same as in our previous work: Cowley et al., 2020). We also separately calculated pure visual stimulus-evoked pupil responses across trials. To calculate the evoked pupil response, we subtracted the mean pupil diameter during the initial fixation period of each trial from the 500ms-long pupil trace that followed visual stimulus onset on each trial.

PFC activity. For all described analyses, individual PFC neuron spike counts were taken during 350ms windows aligned on the onset of the first stimulus grating in each trial. The residual spike count response of each neuron was computed as the difference between the spike count during each repeat and the mean spike count across all repeats of the visual stimulus.

4.2.3.2 Estimating Changes in PFC Population Activity on Different Timescales

To estimate how co-variability of PFC population activity evolved over trials (Figure 21B), we first calculated the residual spike counts during all full (350ms), identical repeats of the first stimulus grating to standardize the responses. The residual spike count response of each neuron was computed as the difference between the spike count during each repeat and the mean spike count across all repeats of the visual stimulus. This yielded a matrix sized r trials by c neurons, to which we applied principal component analysis (PCA). We defined the c-sized vector of weights

of the 1st principal component as the trial-to-trial axis in population activity space. We then projected the residual spike counts onto the trial-to-trial axis. The resulting projection values were essentially linear combinations of the responses of the simultaneously recorded PFC neurons to each repeat of the first stimulus grating. These projection values were plotted across the time in session to visualize the change in covariance in the population activity across trials (i.e., Figures 21, 25, 26). The black line in Figures 21B depicts Gaussian-smoothed projection values, plotted for illustrative purposes (B: timescale of 4 seconds). To quantify the trial-to-trial relationship between LC and PFC activity in each session, we computed the Pearson correlation coefficient between trial-to-trial LC spike rates taken during the fixation period and the PFC response projections along the trial-to-trial axis. To quantify the trial-to-trial relationship between pupil diameter and PFC activity in each session, we computed the Pearson correlation coefficient between trial-to-trial measurements of mean pupil diameter (during the stimulus grating) and PFC response projections along the trial-to-trial axis.

To estimate the how the covariance of PFC population activity evolved on a slower timescale of tens of minutes (Figure 21C), we applied PCA to time binned averages of residual spike count responses; the same method was used in our previous work (Cowley et al., 2020). In this study, we averaged residual spike counts in moving time bins of 12-minutes in length, shifted every 3 minutes over the course of a session. In this case, we defined the vector of weights along the 1st principal component as the slow drift axis in population activity space. Projecting the trial-to-trial residual spike counts onto the slow drift axis uncovered a fluctuation in the co-variance of PFC population activity on a slow timescale; this signal was similar to the 'slow drift' we found in our previous work (Cowley et al., 2020). In Figure 21C, the black line depicts Gaussian-smoothed projection values, plotted for illustrative purposes (C: timescale of 9 minutes). In our

previous work, we found that the time course of the slow drift varied between 30 and 45 minutes across sessions, but using differently sized time windows for binning neural responses yielded similar results. Here, also, we found that using different binning windows (i.e. 6 minutes, 12 minutes, 20 minutes) yielded similar results. Here we chose to use shorter length 12 minute time bins because recording sessions in Monkey Wa were shorter. To quantify the slow timescale relationship between LC and PFC activity in each session, we computed the Pearson correlation coefficient between trial-to-trial LC spike rates taken during the fixation period and the PFC response projections along the slow drift axis. To quantify the slow timescale relationship between pupil diameter and PFC activity in each session, we computed the Pearson correlation coefficient between trial-to-trial measurements of mean pupil diameter (during the first stimulus grating) and the PFC response projections along the slow drift axis.

Aligning directions of trial-to-trial and slow drift axes across sessions. The weights along the principal components can be positive or negative in sign, but these signs are arbitrary (Jollife & Cadima, 2016) . Only the relative magnitudes of the weights, and the pattern of the signs in the vector matter. Therefore, we development an alignment procedure for ensuring that the correlation between over-time trends in the slow drift or the trial-to-trial axis and time courses of pupil diameter and LC was not arbitrary, but consistent across sessions. Our procedure was to align the orientation of the axis (the signs of the weights of the first principal component) such that the projections of mean spike counts of PFC neurons taken during the choice period yielded higher projection values than projections of mean responses during the fixation period. We chose these time windows for the alignment procedure because in all sessions in both monkeys the distributions of PFC responses in these trial periods were well separated.

4.2.3.3 Quantification and Statistics

Here, we provide a brief description of the correlation measures and statistical tests used to quantify relationships between PFC activity, LC activity and pupil diameter in this study.

The r_{sc} , also known as spike count correlation or noise correlation, captures the degree to which trial-to-trial fluctuations in responses are shared by two neurons. Quantifying the magnitude of the correlation in trial-to-trial response variability is achieved by computing the Pearson correlation coefficient of evoked spike counts of two cells to many presentations of an identical stimulus. For each session, we paired each LC neuron with the remaining simultaneously recorded PFC neurons. We then combined all the pairs from all of the recording sessions in each monkey, to assess the overall level of interaction between individual LC and PFC neurons across sessions. This resulted in 4,695 pairs for Monkey Wa and 1184 pairs for Monkey Do. For both regions, we measured neural spike counts during the first stimulus grating, which was identical across trials. For comparison with actual LC-PFC trial-to-trial response covariability, shuffled distributions of r_{sc} (gray in Figure 20) were computed after shuffling the LC responses across trials in each session.

All other relationships between PFC population activity, LC single neuron activity and pupil diameter were quantified via the Pearson correlation coefficient. For results depicted in Figures 22-24, we used the Wilcoxon signed rank test to test the null hypothesis that the distributions of Pearson correlation coefficients across sessions have a median of 0 (at $p = 0.05$).

4.3 Results

We simultaneously monitored LC activity, pupil diameter, and the responses of ~100 behaviorally relevant neurons in the PFC, all while monkeys performed a perceptually demanding task. We then assessed how these variables fluctuated with respect to each other on several different timescales within data collection sessions.

4.3.1 Relationship between Pupil Diameter and LC Spiking Activity Across Trials of a Perceptual Decision Making Task

We first examined how fluctuations in average trial-to-trial pupil diameter related to simultaneously recorded trial-to-trial LC firing rates while monkeys engaged in a perceptual decision making task. For this analysis, we measured pupil and LC responses in two different time windows within trials: the initial fixation period and the first stimulus grating (see Methods for details on time windows).

Over the whole population of recorded LC neurons in Monkey Do, the mean firing rate was 6.2 ± 3.3 sp/s during initial fixation, and 6.3 ± 3.9 sp/s during the first stimulus grating. LC neurons recorded in Monkey Wa had comparable responsivity, with a mean firing rate of 3.9 ± 2.8 sp/s during initial fixation, and 3.9 ± 3.3 sp/s during the first stimulus grating. Overall, we found statistically significant, positive correlations between trial-to-trial measurements of spike rates and both baseline and sensory-evoked pupil diameter for the majority of recorded LC neurons across both monkeys (Figures 18, 19). Thus, in agreement with previous findings (Joshi et al., 2016a; Yang et al., 2021), LC firing rates were higher on trials when the pupil was more dilated, while lower LC firing rates corresponded to trials during which the pupil was relatively constricted.

Importantly, in the results described below, we separately analyzed the relationship of LC activity to baseline vs sensory stimulus evoked pupil diameter.

We examined whether taking LC and pupil measurements in different time windows (initial fixation or stimulus grating 1) yielded different correlation strengths. In Monkey Do, when we measured baseline pupil diameter and baseline LC rate during the initial fixation, the median Pearson's correlation coefficient across all individual LC units was 0.12, significantly greater than 0 ($p = 1.77e-05$, Wilcoxon signed-rank test; 75.9% of neurons significantly positively correlated with pupil). In Monkey Wa, the median correlation coefficient for this time window was 0.146 ($p = 5.35e-08$, Wilcoxon signed-rank test; 72.3% of neurons significantly positively correlated with pupil). It is important to note that the start of the time window for measuring LC rate during initial fixation preceded the start of the time window used for measuring fixation pupil diameter by about 500ms (see Methods).

Next, we found that in both monkeys, LC baseline rates during fixation were strongly correlated with pupil diameter measurements during the first grating stimulus (Figure 18; Monkey Do: median Pearson's $r = 0.092$, $p = 2.6e-05$, Wilcoxon signed-rank test; Monkey Wa: median Pearson's $r = 0.166$, $p = 1.6e-08$, Wilcoxon signed-rank test). When we assessed the relationship between pupil diameter and LC rate across all first stimulus gratings in a session, the correlation was comparatively lower but still significantly greater than 0 in both monkeys (Figure 18; Monkey Do: median Pearson's $r = 0.048$, $p = 7.14e-04$, Wilcoxon signed-rank test; Monkey Wa: median Pearson's $r = 0.096$, $p = 3.57e-06$, Wilcoxon signed-rank test). We conclude that there was a reliable trial-to-trial relationship between changes in LC activity and pupil diameter in two different epochs of trials: during initial passive fixation and during visual stimulation. This

relationship was strongest when LC activity preceded a change in pupil diameter by approximately 500 ms.

In the above analysis, pupil measurements during the grating likely reflected visual stimulus evoked pupil responses superimposed over the baseline pupil diameter measured during the initial fixation. Therefore, we next considered how LC activity related to the pure visual stimulus-evoked pupil responses across trials. To calculate the evoked pupil response, we subtracted the mean baseline pupil diameter (measured during the initial fixation period of each trial) from the 500ms-pupil trace that followed visual stimulus onset on each trial. We found that in both monkeys, LC activity during the grating stimulus was positively correlated with the visually evoked pupil response (Figure 19; Monkey Do: median Pearson r = 0.077, p = 2.563e-06, Wilcoxon signed-rank test; Monkey Wa: median Pearson r = 0.08, p = 1.553e-06, Wilcoxon signed-rank test). LC baseline activity during fixation was significantly related to the subsequent visually-evoked pupil response in just one of the two monkeys (Figure 19; Monkey Do: median Pearson r = -0.04, p = 0.2, Wilcoxon signed-rank test; Monkey Wa: median Pearson r = 0.07, p = 6.224e-06, Wilcoxon signed-rank test).

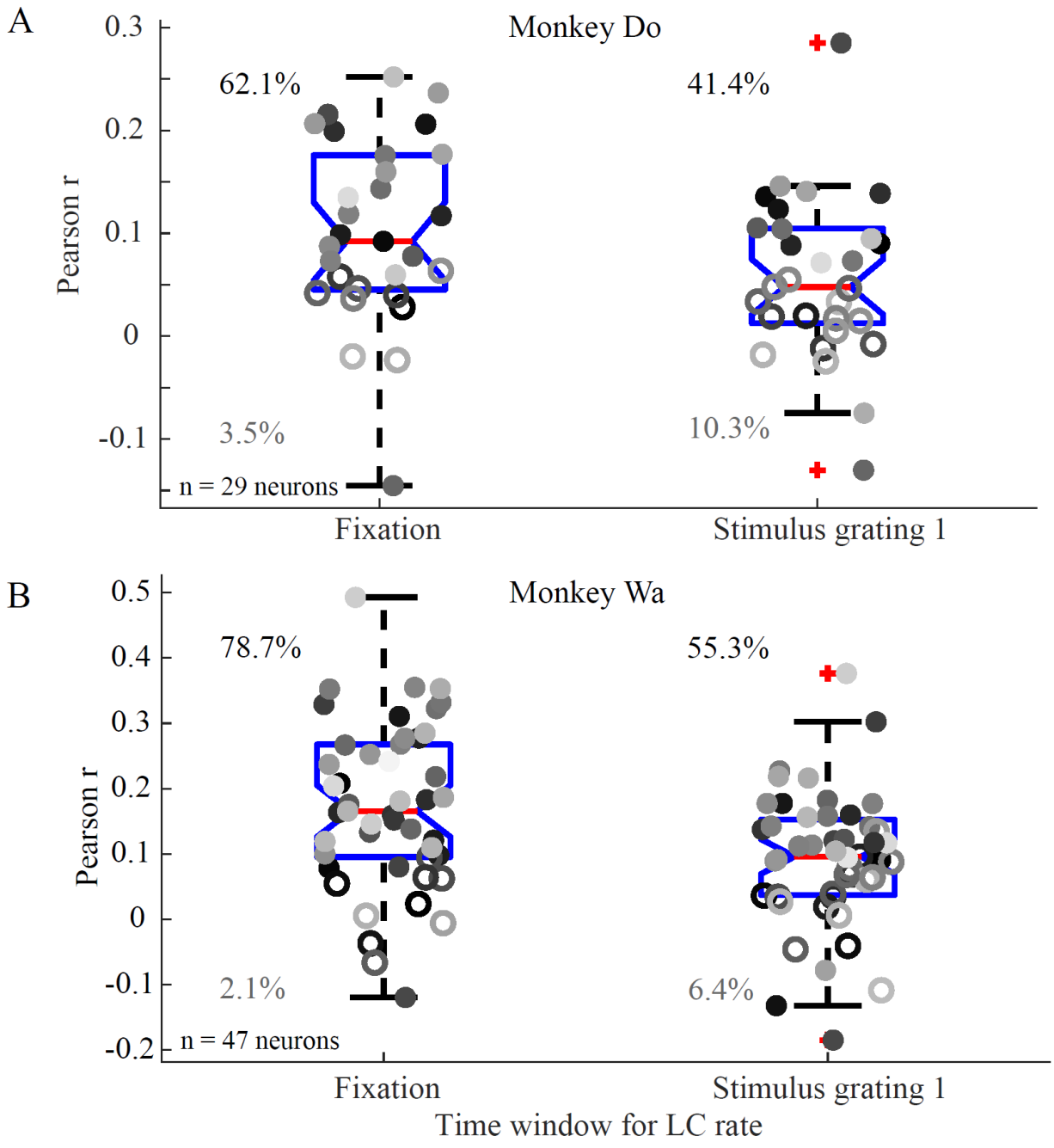

Figure 18. Trial-to-trial relationships between mean pupil diameter and LC spike rate in 2 monkeys. (A) Box plots and dots depict the medians (red lines) and distributions of Pearson correlations between *(left)* trial-to-trial LC firing rates and pupil diameter, both measured during initial fixation, and *(right)* trial-to-trial LC firing rates and pupil diameter, both measured during the first stimulus grating. Distributions are across 29 recorded LC neurons in Monkey Do. Filled/unfilled dots signify Pearson correlation coefficients significantly different/not from 0 ($p<0.05/p>0.05$). Percentages indicate proportion of all neurons that had significantly positive / negative correlations with pupil diameter. (B) same as (A), but for 47 LC neurons recorded in Monkey Wa.

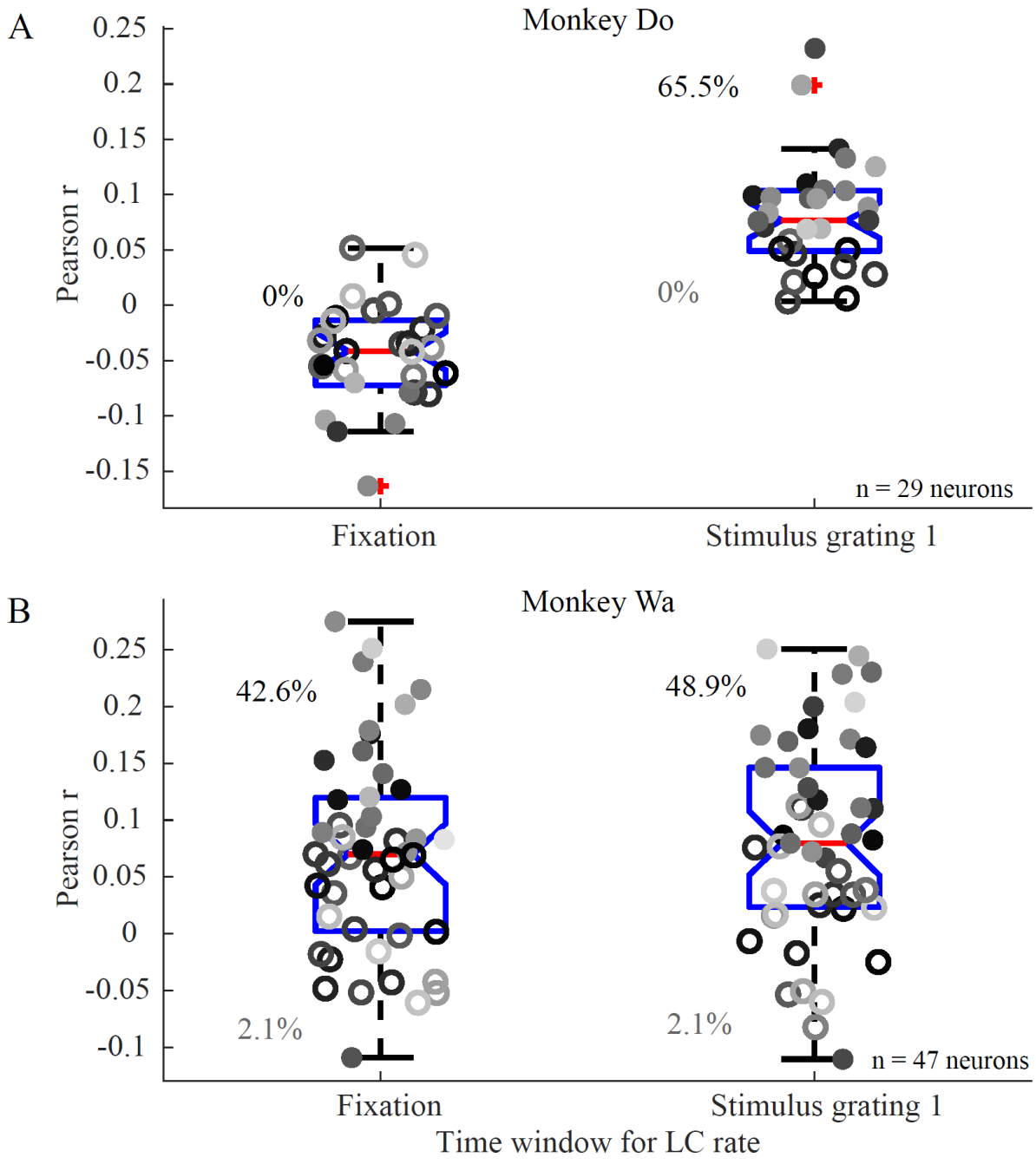

Figure 19. Trial-to-trial relationships between mean visual stimulus-evoked pupil diameter and LC spike rate in 2 monkeys.
(A) Box plots and dots depict the medians (red lines) and distributions of Pearson correlations between *(left)* trial-to-trial fixation LC firing rates and evoked pupil responses to the first stimulus grating , and *(right)* trial-to-trial LC firing rates during the first stimulus grating and evoked pupil responses. Distributions are across 29 recorded LC neurons in Monkey Do. Filled/unfilled dots signify Pearson correlation coefficients significantly different/not from 0 ($p<0.05$/$p>0.05$). Percentages indicate proportion of all neurons that had significantly positive / negative correlations with pupil diameter. (B) same as (A), but for 47 LC neurons recorded in Monkey Wa.

4.3.2 Relationship between Spiking Activity of Simultaneously Recorded Individual LC and PFC Neurons

In order to better understand how fluctuations in LC activity may relate to changes in PFC activity, we first examined how individual LC neuron responses related to the activity of each simultaneously recorded PFC neuron within the same session. In the following analyses, we first computed spike count correlations to quantify the relationship between LC and PFC responses to the first stimulus grating across trials. We then assessed the relationship between overall, ongoing LC activity in the 30 seconds preceding each trial and PFC responses to the first stimulus grating in each trial.

It is well known that both the spontaneous and evoked responses of individual neurons are variable even across repeated trials of identical visual stimulation conditions (Arieli et al., 1996; Shadlen & Newsome, 1998; Tolhurst et al., 1983). A small portion of the individual neuron response variability, or noise, is known to be shared between neighboring or cross-regionally interconnected neurons. The degree to which trial-to-trial fluctuations in responses are shared by two neurons can be quantified by computing the Pearson correlation of spike count responses to many presentations of the same stimulus (interchangeable terms include: spike count correlation, r_{sc}, or noise correlation). The strength and sign of spike count correlations can provide useful information about the level of communication between two neurons (Alonso & Martinez, 1998; Greschner et al., 2011). Changes in the strength of spike count correlation due to different stimulus or behavioral conditions have been shown to reflect changes in functional interactions and information processing in pairs of neurons (Acar et al., 2019; Cohen & Maunsell, 2009b; Kohn & Smith, 2005; Ni et al., 2018; Snyder et al., 2014).

We measured the correlated variability of neural responses to quantify the interactions in pairs of simultaneously recorded LC and PFC neurons. Figure 20A,C demonstrates that in both monkeys, r_{sc} values were distributed rather evenly around 0 (mean r_{sc} = -0.002 in Monkey Do; mean r_{sc} = -0.0076 in Monkey Wa). In Monkey Wa, 495/4695 (10.5%) pairs had spike count correlations that were significantly different from 0, while in Monkey Do 251/1184 (21.2%) pairs had significant correlations. These results indicate that the responses of some neurons in the two brain regions fluctuated up and down together across trials (positive r_{sc}), while other LC-PFC pairs had responses that fluctuated in opposing directions across trials (negative r_{sc}). Interestingly, when we estimated overall LC activity (including baseline spiking and phasic bursts) within a 30 second time window preceding each trial, more LC neurons were correlated or anticorrelated with individual PFC neuron responses in both monkeys (Figure 20B,D; Monkey Do, 378/1184 pairs (31.9%) with significant Pearson r, $p<0.05$; Monkey Wa, 1180/4695 pairs (25.1%) with significant Pearson r, $p<0.05$).

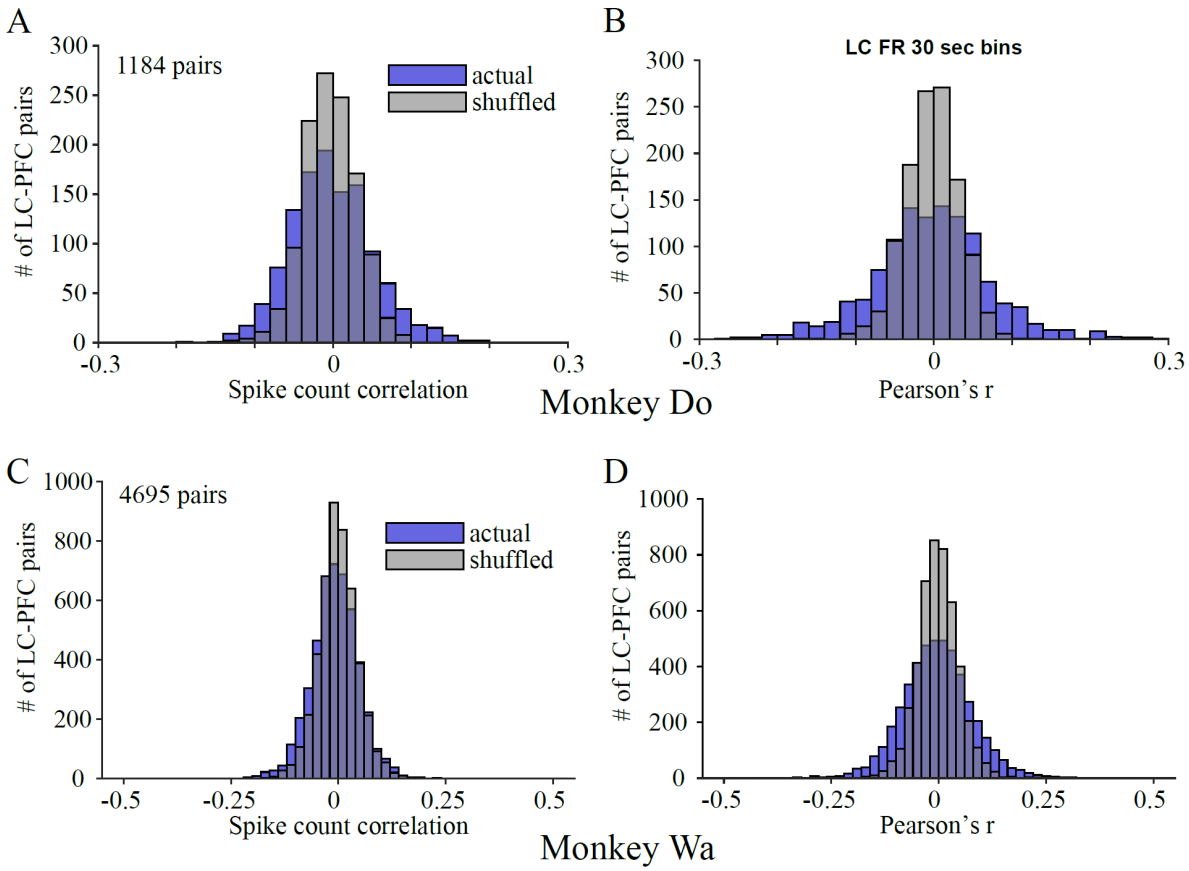

Figure 20. Trial-to-trial relationship between spiking activity of simultaneously recorded individual LC and PFC neurons.

(A, C) Shown are the distributions of spike count correlation (r_{sc}) computed across 1184 LC-PFC pairs of neurons in Monkey Do (A; blue; mean r_{sc} = -0.002; 251/1184 pairs had r_{sc} values significantly different from 0 ($p < 0.05$)) and 4695 LC-PFC pairs of neurons in Monkey Wa (C; blue; mean r_{sc} = -0.0076; 495/4695 pairs had r_{sc} values significantly different from 0 ($p < 0.05$)). Spike count correlation was computed for neuronal responses evoked by the trial-to-trial repeated identical presentations of the first stimulus grating in the orientation change detection task. Distributions in gray color depict spike count correlation values after trial-shuffling the LC neuron responses. (B, D) Relationship between PFC single unit responses during trial-to-trial first stimulus gratings and single unit LC activity within a 30 second time window preceding each trial (including baseline spiking and phasic bursts). (B) In Monkey Do, 378/1184 pairs (31.9%) had Pearson correlation coefficient values significantly different from 0 ($p<0.05$) (D) In Monkey Wa, 1180/4695 pairs (25.1%) had Pearson correlation coefficient values significantly different from 0 ($p<0.05$).

4.3.3 Relationships Between Pupil Diameter, LC Single Unit Activity, and PFC Population Activity Over Multiple Timescales

Collectively, past work clearly demonstrates that fluctuations in LC activity occur over a range of behaviorally relevant timescales, including fast sub-second phasic bursts and slower fluxes of ongoing activity on the order of minutes to hours (Totah et al., 2019b). However, it remains to be established if and how these diverse timescales of LC activity are reflected in cortical neural activity and behavioral measures. Here, we investigated whether PFC population activity and pupil diameter track changes in LC activity over faster (seconds) and slower (tens-of-minutes) timescales.

In most sessions, the recorded PFC population activity was comprised of individual neural responses that varied in magnitude over the course of time. As demonstrated by the 3 example neurons in Figure 21A, some neurons decreased in responsivity (Figure 21A, 'PFC neuron 7), while other neurons increased in responsivity (Figure 21A, 'PFC neuron 19'), or showed no obvious change in responsivity (Figure 21A, 'PFC neuron 24') throughout a session. We utilized principal component analysis (PCA) in order to capture how the activity of all the simultaneously recorded PFC neurons co-varied over the course of a session. To quantify this covariance on a faster trial-to-trial timescale, we applied PCA to the residual spike count responses during all first stimulus gratings (350ms) that occurred in each session (a matrix sized: r trials by c neurons). To reveal and quantify any existing slow fluctuation in PFC population activity, we used the same method as in our previous work (Cowley et al., 2020). We applied PCA to the bin averages of residual spike counts, where each time bin was 12-minutes in length and was shifted every 3 minutes over the course of a session (a matrix sized: r time bins by c neurons). Taking the mean of the PFC responses within these longer time bins allowed us to average out any trial-to-trial

variability of the neural responses and then use PCA to specifically capture the slower changes in the co-variability in the population activity across time.

By applying PCA, we reduced the high dimensional multi-neuron data set to a smaller number of linear combinations of the PFC neuronal responses. The weights along the first principal component (which explains the most variance in the data) represented an axis in the population activity space. Because we considered two different timescales for the evolution of the population activity throughout a session, we define two axes, a 'trial-to-trial axis' and a 'slow drift axis', to help differentiate between two timescales. Projecting the trial-to-trial vectors of all PFC responses onto the slow drift axis uncovered a slow timescale fluctuation in the population activity, similar to the 'slow drift' signal we found in our previous work (Figure 21C). Projecting the neural activity onto the trial-to-trial axis revealed how the responses of PFC neurons jointly varied throughout the session on a faster trial-to-trial timescale (Figure 21B). Figure 21B,C demonstrates that qualitatively, the slower and faster timescale axes in population activity space progressed comparably across time, trending from lower to higher values from the beginning to the end of the session. This was also the case across the whole data set of sessions. Below we describe how pupil diameter and LC activity related to the co-variability in PFC population activity on fast and slow timescales.

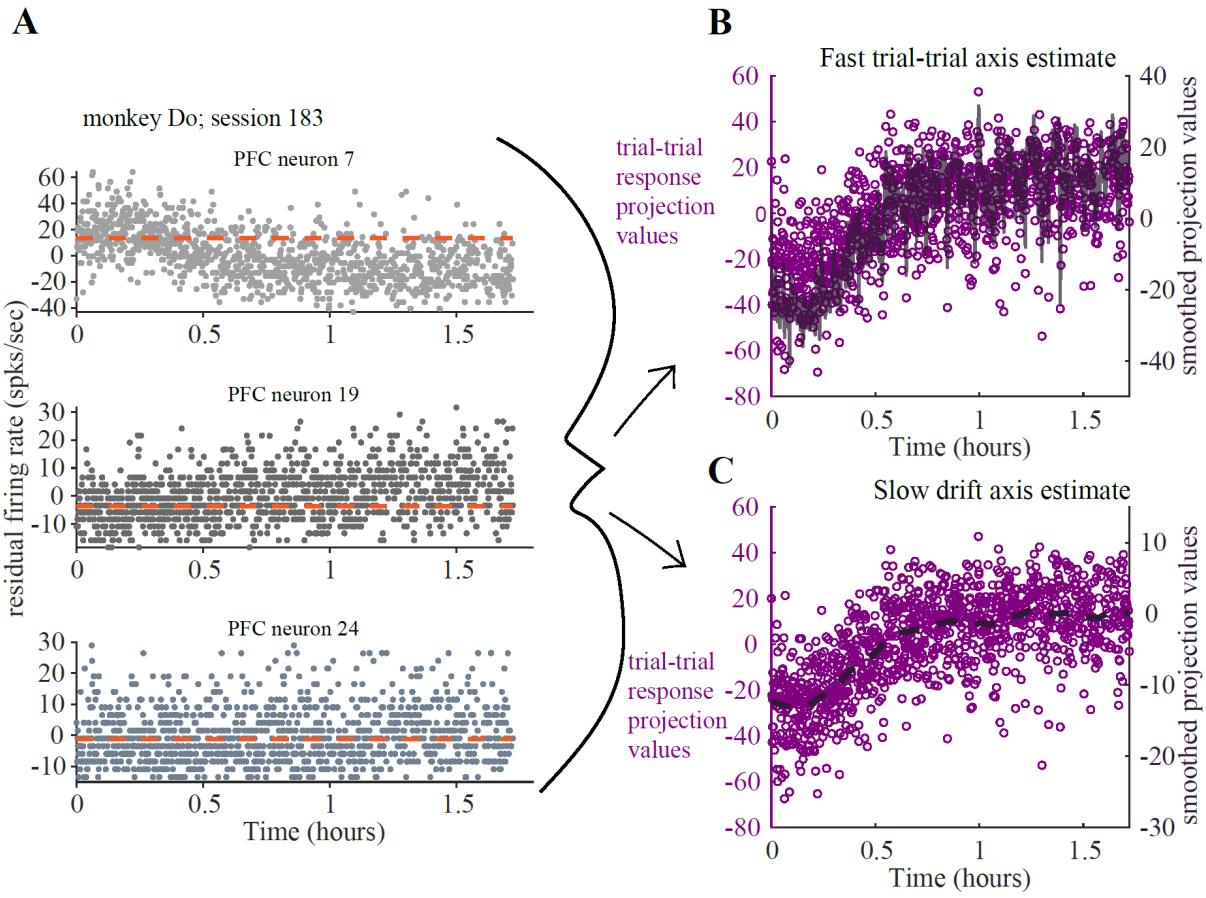

Figure 21. Drift in PFC population activity over the course of an example session.
(A) 3 example PFC neurons have different time courses of activity throughout an example session in Monkey Do. Each dot represents the residual firing rate of a PFC neuron during the first stimulus grating in each trial. The dashed orange lines represent the mean residual firing rate across all stimuli that occurred the first 20 minutes of the session. **(B)** Responses of PFC neurons jointly vary on a *trial-to-trial* timescale across a session. Each purple dot represents the linear combination of all simultaneously recorded PFC neuron responses to 1 instance of the first stimulus grating in a trial in the example session. Weights for linear combinations were identified by applying PCA to the residual spike count responses during all first stimulus gratings (350ms) that occurred in a session. Data is from the same session as in (A). The black line represents an estimate of the *trial-to-trial axis* in the population activity space, identified by Gaussian-smoothing the projections (linear combinations) of PFC population responses. **(C)** Responses of PFC neurons jointly vary on a *slower (tens of minutes)* timescale across a session. Each purple dot represents the linear combination of all simultaneously recorded PFC neuron responses to 1 instance of the first stimulus grating in a trial in the same session as (A,B). Method similar to (B) except to identify the *slow drift axis* (black dashed line), we applied PCA to the bin averages of residual spike counts, where each time bin was 12-minutes in length. This allowed us to capture the slower changes in co-variability in the PFC population activity across time.

4.3.3.1 Relationships Between Pupil Diameter, LC Single Unit Activity and PFC Population Activity over Fast, Trial-to-trial Timescale (seconds)

We found that trial-to-trial fluctuations in baseline LC activity (measured during the initial fixation period of each trial) were significantly and positively correlated with changes in PFC population activity along the trial-to-trial axis identified through PCA (Figure 22, data combined across 2 monkeys; median Pearson's correlation coefficient = 0.038, p = 4.695e-04, Wilcoxon signed-rank test for difference of median from 0). This relationship held true when examined within individual animals (Monkey Do: median Pearson's correlation coefficient = 0.03, p = 0.039, Wilcoxon signed-rank test; Monkey Wa: median Pearson's correlation coefficient = 0.05, p = 0.0037, Wilcoxon signed-rank test). Additionally, we considered how trial-to-trial changes in the combined baseline plus evoked pupil diameter (measured during the first grating stimulus) related to PFC and LC activity. We found a strongly positive correlation between trial-to-trial measurements of pupil diameter and fluctuations in PFC population activity along the trial-to-trial axis (Figure 22, data combined across 2 monkeys; median Pearson's correlation coefficient = 0.15, p = 4.03e-06, Wilcoxon signed-rank test). This trial-to-trial relationship between pupil diameter and PFC activity was also significantly positive in individual monkeys (Monkey Do: median Pearson's correlation coefficient = 0.2, p = 1.318e-04, Wilcoxon signed-rank test; Monkey Wa: median Pearson's correlation coefficient = 0.096, p = 0.0128, Wilcoxon signed-rank test). As reported above in section 4.3.2, we found that trial-to-trial baseline LC spike rates were strongly correlated with pupil diameter measurements during the first grating stimulus in both monkeys (Figure 22, data combined across 2 monkeys; median Pearson's correlation coefficient = 0.14, p = 5.61e-11, Wilcoxon signed-rank test).

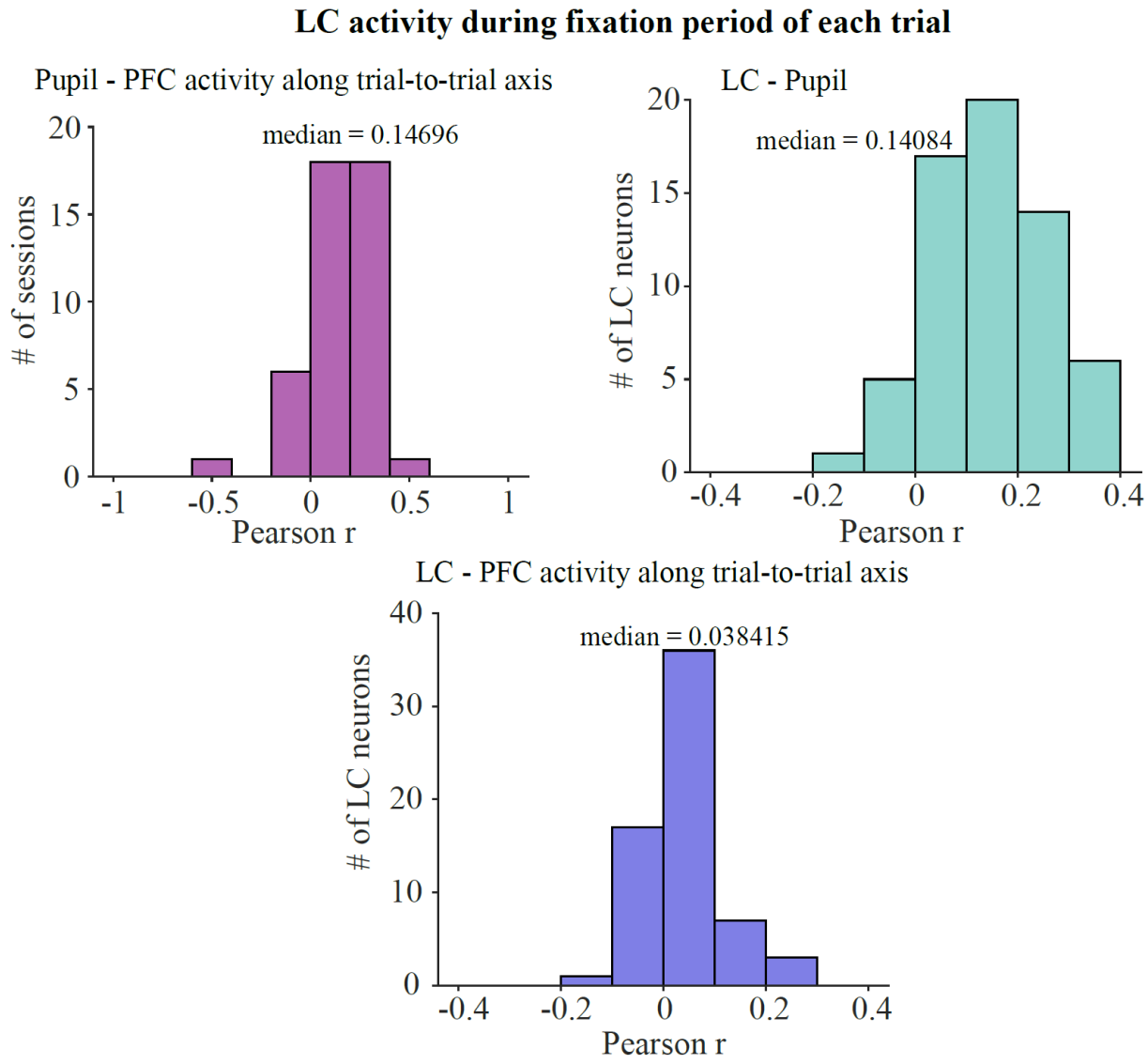

Figure 22. Relationship between *trial-to-trial fluctuations* in LC activity, pupil diameter and co-variability in PFC population activity.
(Purple) distribution shows that in most sessions, fluctuations in PFC population activity and pupil diameter were correlated over time. The median Pearson correlation coefficient (r) across sessions was 0.14696 (significantly different from 0, p = 4.03e-06, Wilcoxon signed-rank test; n = 44 sessions across 2 monkeys). ***(Green)*** distribution shows that in most sessions, trial-to-trial fluctuations in LC baseline activity and pupil diameter were correlated over time. The median Pearson correlation coefficient (r) across LC neurons was 0.14084 (p = 5.61e-11, Wilcoxon signed-rank test; n = 64 LC neurons across 2 monkeys). ***(Blue)*** distribution shows that in most sessions, trial-to-trial fluctuations in LC baseline activity were correlated with changes in PFC population activity along the trial-to-trial axis. The median Pearson r across LC neurons was 0.038 (p = 4.695e-04, Wilcoxon signed-rank test for difference of median from 0; n = 64 LC neurons across 2 monkeys).

We also examined whether overall ongoing LC activity in the 30 seconds preceding each trial was related to the trial-to-trial changes in pupil diameter and PFC population activity. We found that the 30-second-binned LC activity was not reliably related to changes in PFC population activity along the trial-to-trial axis in either of the monkeys (Figure 22, data combined across 2 monkeys, median Pearson's correlation coefficient = 0.03, $p = 0.136$, Wilcoxon signed-rank test). However, the 30-second-binned LC activity weakly, but reliably predicted corresponding trial-to-trial changes in pupil diameter in both monkeys (Figure 23, data combined across 2 monkeys, median Pearson's correlation coefficient = 0.09, $p = 0.04$; Monkey Do: median Pearson's correlation coefficient = 0.096, $p = 0.0238$; Monkey Wa: median Pearson's correlation coefficient = 0.069, $p = 0.0475$; Wilcoxon signed rank test in all 3 cases).

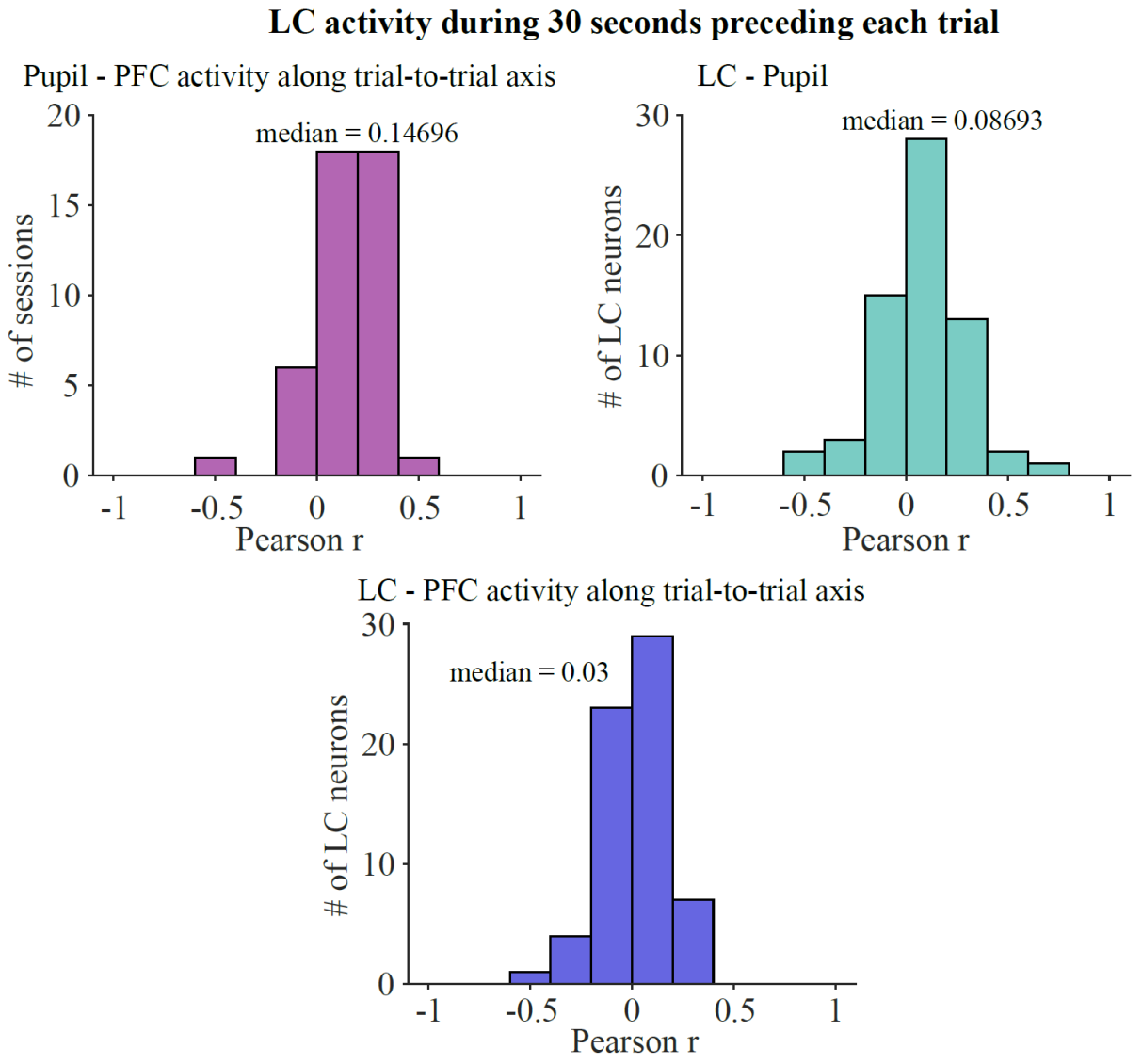

Figure 23. Relationship between trial-to-trial fluctuations in pupil diameter, changes in PFC population activity along trial-to-trial axis, and *30-second estimates of baseline LC activity*.
We considered whether overall ongoing LC activity in the 30 seconds preceding each trial was related to the trial-to-trial changes in pupil diameter and PFC population activity. ***(Purple)*** distribution (same as Figure 22) shows that trial-to-trial changes in pupil diameter were significantly positively correlated with trial-to-trial changes in PFC population activity. ***(Green)*** distribution shows that trial-to-trial fluctuations in pupil diameter were weakly correlated with 30-second-binned LC activity estimates. The median Pearson correlation coefficient (r) across LC neurons was 0.087 ($p = 0.04$, Wilcoxon signed-rank test; $n = 64$ LC neurons across 2 monkeys). ***(Blue)*** distribution shows that trial-to-trial changes in PFC population activity were not reliably related to 30-second-binned LC activity estimates. The median Pearson r across LC neurons was 0.03 ($p = 0.136$, Wilcoxon signed-rank test for difference of median from 0; $n = 64$ LC neurons across 2 monkeys).

4.3.3.2 Relationships Between Pupil Diameter, LC Single Unit Activity and PFC Population Activity over Slow Timescale (minutes)

Next, we examined whether fluctuations in single LC neuron responses and pupil diameter correspond to changes in PFC population activity along the slow drift axis. To estimate slow time scale changes, we computed running averages of LC firing rate and pupil diameter in time windows of 12 minutes, shifted every 3 minutes (the same time window as used for averaging residual spike counts of individual PFC neurons before applying PCA – see Methods). In agreement with our previous work, we found a strongly positive correlation between slow time scale fluctuations in pupil diameter and PFC population activity in both monkeys (Figure 24, data combined across 2 monkeys, median Pearson correlation coefficient = 0.7, $p = 5.28e-04$). However, we did not find a reliable relationship between LC activity and the slow drift in PFC population activity in either monkey (Figure 24, data combined across 2 monkeys; Monkey Do, median Pearson correlation coefficient = 0.3, $p = 0.56$, Wilcoxon signed rank test; Monkey Wa, median Pearson correlation coefficient = -0.21, $p = 0.81$, Wilcoxon signed rank test).

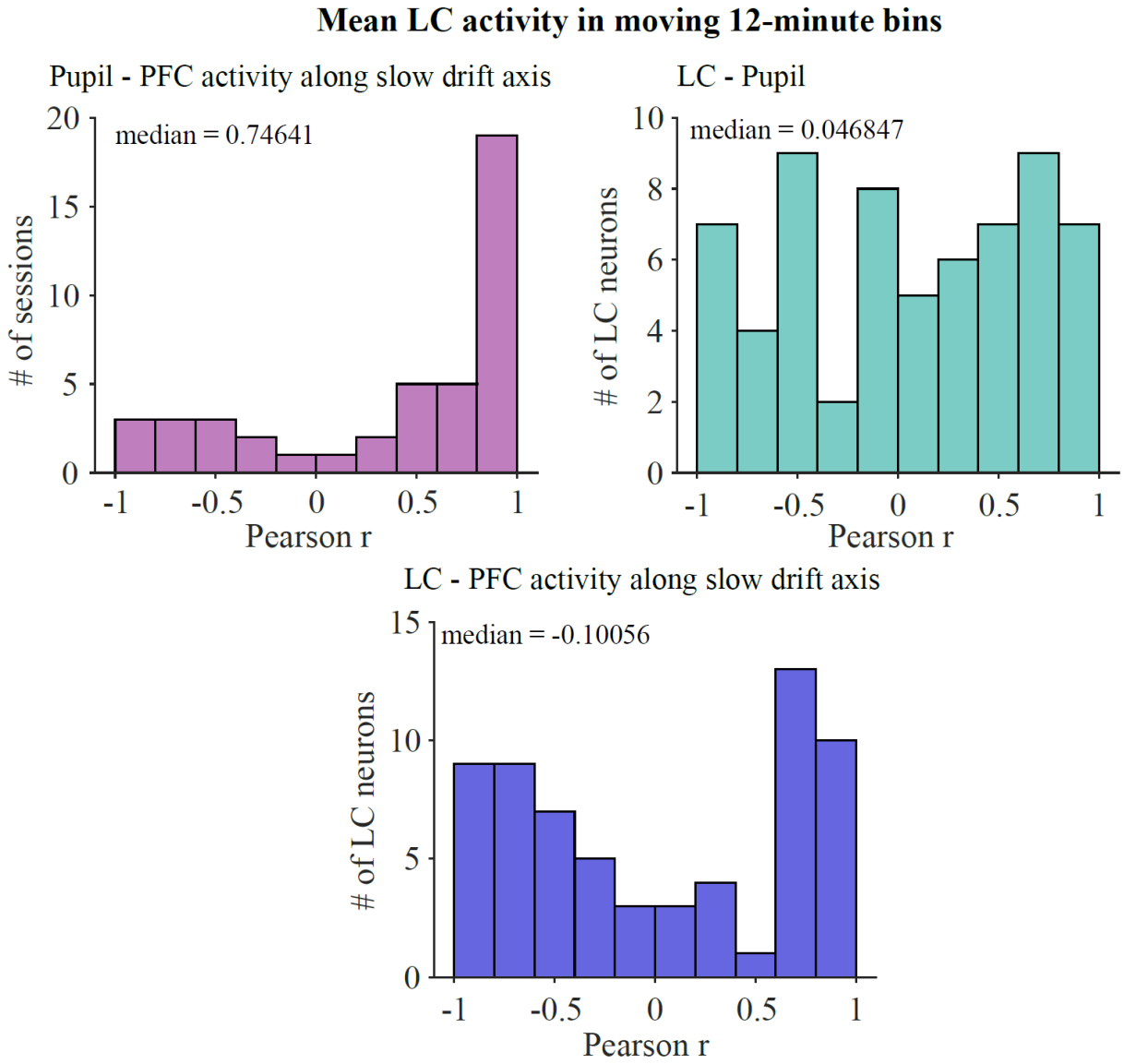

Figure 24. Relationships between *slow timescale fluctuations* in LC activity, pupil diameter and co-variability in PFC population activity.
(Purple) distribution shows that in most sessions, the slow drift in PFC population activity was strongly correlated with changes in pupil diameter over the course of time. The median Pearson correlation coefficient (r) across sessions was 0.746 (significantly different from 0, p = 5.28e-04, Wilcoxon signed-rank test; n = 44 sessions across 2 monkeys). ***(Green)*** distribution shows that slower timescale fluctuations in LC baseline activity and pupil diameter were not significantly correlated (mean LC rate and mean pupil diameter estimated in 12 minute bins shifting every 3 minutes over the course of session). The median Pearson correlation coefficient (r) across 64 LC neurons across both monkeys was 0.0468 (p > 0.05, not significantly different from 0 in either monkey, Wilcoxon signed-rank test). ***(Blue)*** distribution shows there was no reliable correlation between slow fluctuations in LC activity and the slow drift in PFC population activity when considering activity of all LC neurons across both monkeys. The median Pearson correlation coefficient (r) across 64 LC neurons was -0.1 (p > 0.05, not significantly different from 0 in either monkey, Wilcoxon signed-rank test).

4.4 Discussion

Our goal in this study was to characterize how natural, ongoing activity in the LC relates to changes in pupil diameter and prefrontal cortex activity while monkeys engaged in a demanding perceptual decision making task.

4.4.1 Relationship Between Pupil Diameter and LC Activity

Previous work provides considerable evidence that changes in LC activity can influence pupil diameter, although some details of the anatomical connectivity between LC and pupil control circuitry remain to be established (Joshi & Gold, 2020). One line of evidence comes from studies showing that electrical stimulation of LC leads to pupil dilation (Breton-Provencher & Sur, 2019b; Joshi et al., 2016b). Additionally, several studies have shown that fluctuations in the LC-NE system are correlated with simultaneously measured pupil diameter changes during passive fixation or quiet wakefulness (Aston-Jones & Cohen, 2005a; Joshi et al., 2016b; Joshi & Gold, 2022; Reimer et al., 2016). To this date, only a few studies across different species have examined LC activity in relation to sensory stimulus-evoked transient pupil responses (Joshi et al., 2016a; Joshi & Gold, 2022; Yang et al., 2021) or how pupil diameter relates to LC activity during performance of cognitive tasks (Aston-Jones & Cohen, 2005; Megemont et al., 2022; Murphy, O'Connell, et al., 2014; Varazzani et al., 2015; Yang et al., 2021).

In this study, we report an overall positive relationship between changes in LC firing rates and pupil diameter across trials in a perceptual decision making task. This result is consistent with recent findings of moment-to-moment co-fluctuations of LC and pupil responses in rodents engaged in a sensory stimulus detection task (Megemont et al., 2022; Yang et al., 2021). Our

results are also novel because we are among the first to report on the reliability and time course of the relationship between LC activity and pupil diameter across many experimental sessions in two monkeys in the context of a visual perceptual task (see Aston-Jones & Cohen, 2005a for a commonly cited single LC neuron example). We found that the strength of the correlation varied depending on the time windows used for LC firing rate estimates and pupil diameter measurements. We found that baseline LC activity measured during fixation was strongly correlated with subsequent changes in pupil diameter (about ~500 ms after). This result is in agreement with previous studies which have shown LC spike-triggered changes in pupil diameter at a time lag of about 305ms in monkeys (Joshi et al., 2016a; Joshi & Gold, 2022) and at a time lag of ~ 2 seconds in rodents (Yang et al., 2021). Additionally, we considered how an estimate of overall (baseline rate and phasic bursts) LC firing rate in a 30 second time bin would relate to an immediately subsequent measurement of pupil diameter. Although there was a significant positive relationship between LC activity and pupil diameter on this longer time course, it was comparatively weaker than the association between immediately adjacent LC and pupil measurements within the same trials. Finally, as far as we know, none of the previous studies have yet considered how LC spiking activity relates to visual stimulus-evoked pupil responses (isolated from any concurrent changes in baseline pupil diameter). Here, we report a strong positive trial-to-trial relationship between visual-stimulus evoked pupil responses and LC firing rates. Others have reported that evoked pupil responses following auditory tones (Joshi et al., 2016a; Joshi & Gold, 2022; Yang et al., 2021) and effortful actions (Varazzani et al., 2015) are related to LC spiking.

Many previous and current studies, especially in human subjects, tend to assume that changes in LC activity (and concurrent NE-mediated changes in behavioral state and cortical

activity) can be tracked noninvasively by measuring pupil diameter (de Gee et al., 2014; Ebitz & Platt, 2015; Gilzenrat et al., 2010; Murphy, Vandekerckhove, et al., 2014; Urai et al., 2017). However, we and others (Joshi & Gold, 2020; Megemont et al., 2022; Yang et al., 2021), have now consistently shown that the strength of this relationship is dependent on timescale, task-epoch, and behavioral context used for measurements of both variables. Future work should focus on more precisely establishing the conditions and timescales under which pupil diameter can be used as an accurate readout of changes in LC activity. For now, the most direct evidence for relating any fluctuations in the LC-NE system to pupil diameter, cortical activity and behavioral variability can only come from direct recordings of activity in LC or noradrenergic axons.

4.4.2 Relationships Between Simultaneous Changes in PFC Activity, LC Activity and Pupil Diameter

Taken together, correlative and causal evidence from previous studies indicates that variability in neuronal activity patterns on different spatial and temporal scales can result in variability in cognitive behavior (i.e., (Britten et al., 1996; Cohen & Maunsell, 2010; Cowley et al., 2020; Gutnisky et al., 2017; Hennig et al., 2021; Kaufman et al., 2015; Nienborg et al., 2012; Renart & Machens, 2014; Runyan et al., 2017). Recent work has also highlighted that at least part of the variability in neural and behavioral processes may be linked to noradrenergic neuromodulation arising from the brain-wide projections of the LC-NE system (Joshi & Gold, 2022; Martins & Froemke, 2015; Nienborg & Roelfsema, 2015; Reimer et al., 2016; N. K. B. Totah et al., 2019a; Yang et al., 2021). While a variety of studies have reported that LC activity and behavioral fluctuations correlate on diverse timescales ranging from seconds to hours,

comparatively much less is known about the relationship of physiological changes in LC activity to simultaneously monitored cortical activity in the context of cognitive behavior.

Ours is the first study to characterize the relationship between LC activation and prefrontal cortex (PFC) activity patterns on both slower (tens of minutes) and faster (seconds) timescales, and, additionally, relate the neural activity in these regions to changes in pupil diameter. Other studies have considered how LC activity and pupil diameter relate to simultaneously measured membrane potentials in the rodent somatosensory cortex (Yang et al., 2021), to coordinated activity in pairs of neurons in the primate anterior cingulate cortex (ACC) (Joshi & Gold, 2022), and to single unit responses in the primate superior colliculus, inferior colliculus and the cingulate cortex (Joshi et al., 2016a). A few rodent studies have reported functional interactions between PFC and LC, showing that PFC can have an inhibitory or excitatory influence on LC activity (Jodo et al., 1998; Sara & Hervé-Minvielle, 1995), and that LC activation occurs in phasic opposition with respect to slow oscillations in PFC single unit activity in anesthetized rodents (Lestienne et al., 1997; Sara & Bouret, 2012a; Sara & Hervé-Minvielle, 1995; Shinba et al., 2000).

Our results extend previous findings by showing that trial-to-trial baseline LC activity fluctuated together with the trial-to-trial variability in coordinated PFC population activity in two awake monkeys as they engaged in a perceptual task. We first considered the relationship between simultaneously measured single neuron responses in the two brain regions, but found that across trials, LC activity could be positively or negatively correlated with different PFC neuron responses. Perhaps this result is not particularly surprising, considering the existing evidence that the two regions are reciprocally interconnected (Arnsten & Goldman-Rakic, 1984; Porrino & Goldman-Rakic, 1982b). PFC neurons have been reported to project both to LC directly as well as to a group of neighboring interneurons that provide inhibitory inputs to LC (Arnsten & Goldman-Rakic,

1984; Aston-Jones et al., 2004; Breton-Provencher & Sur, 2019b), thereby supporting the result that the activity of some pairs of LC-PFC neurons in our data set was anticorrelated. Interestingly, a recent study found reduced noise correlations in pairs of neurons in the anterior cingulate cortex (ACC) following increases in baseline LC activity (Joshi & Gold, 2022). Similar to our findings, that study did not observe a consistent relationship between trial-to-trial responses of individual LC and ACC neurons. This may be because LC axon terminals can indiscriminately release NE in the vicinity of many neurons in targeted brain regions (via volume transmission, Callado & Stamford, 2000; Papadopoulos et al., 1989). Overall, our findings support the idea that physiological changes in LC activity may have more pronounced effects on activity patterns of neighboring cortical neurons, rather than individual neuron responses.

Recent work in primates has uncovered signals in cortical population activity that covaried with changes in concurrently measured pupil diameter and behavioral performance on cognitive tasks on slow (Cowley et al., 2020) and trial-to-trial (Hennig et al., 2021) timescales. Because pupil diameter is a commonly used indirect measure of behavioral state changes and activation in the LC-NE system (Aston-Jones & Cohen, 2005b; Ebitz & Platt, 2015; Eldar et al., 2013; McGinley et al., 2015; Urai et al., 2017), these studies hypothesized that the observed behaviorally relevant cortical activity fluctuations could arise from varied temporal dynamics of norepinephrine release from long-distance projections of LC neurons throughout the brain. Consistent with these previous findings, we found similar pupil-linked fluctuations in the covariability of PFC population activity across both trial-to-trial and slower tens of minutes timescales. We also extended the previous findings by showing that baseline activity of single LC neurons correlates with trial-to-trial fluctuations in PFC population activity and pupil diameter.

Interestingly, the analyses in our study revealed that baseline LC activity, PFC population activity and pupil diameter were related on a faster trial-to-trial timescale, but not on the slower tens of minutes timescale. Overall, our results support the hypothesis that activation of the LC-NE system may mediate previously identified (Cowley et al., 2020; Hennig et al., 2021) behaviorally important computations carried out by populations of PFC neurons. However, we remain cautious with respect to making any conclusions about the function or the temporal dynamics of the relationship between single LC neuron responses and PFC activity. One limitation of our study is that we quantified all relationships using the Pearson correlation coefficient, which offers a valid initial assessment of the reliability of a relationship between two variables but is by no means a complete evaluation. Future work should focus on more systematically evaluating how diverse temporal and spatial dynamics of LC activation could manifest in concurrently recorded PFC population activity patterns. For example, using the data set from this study, it is possible to use a method such as kernel regression to estimate the timescale of behaviorally linked changes in PFC population activity during cognitive task performance, and then assess whether LC activity co-fluctuates on a similar timescale.

Another limitation of our study is that we were only able to record from single LC neurons and had no way of precisely identifying the locations of recorded neurons within the nucleus. The strength of the relationship between LC and PFC activity could very well depend on the locations and numbers of concurrently recorded LC neurons. Recent work suggests that within LC, neurons are more heterogeneously organized than previously thought, with different groups of neurons throughout the nucleus providing more targeted neuromodulation to specific brain regions (Chandler et al., 2019; Schwarz & Luo, 2015; N. K. Totah et al., 2018; N. K. B. Totah et al., 2019a). This kind of organization suggests that LC neurons could operate in ensembles to exert

specific neuromodulatory effects on different timescales, in different parts of the brain. Uncovering such effects would require conducting population recordings in targeted brain regions along with recordings of multiple LC neurons simultaneously, which is now feasible in rodents (N. K. Totah et al., 2018). Additionally, a potentially illuminating result from our study was that pupil diameter was strongly correlated with both slower and faster timescale changes in PFC population activity patterns, but only with faster timescale changes in LC activity. Because pupil diameter can be influenced by both cholinergic and noradrenergic neuromodulation (Joshi & Gold, 2020), it is possible that the slow timescale correlation of pupil diameter and PFC population activity reflects the combined effect of multiple neuromodulatory systems (Reimer 2014). Anatomical tracing studies confirm that cholinergic neurons of the basal forebrain project to prefrontal cortex (Coppola & Disney, 2018; Rho et al., 2018). Simultaneous recordings from basal forebrain, LC and PFC neurons should be conducted in future studies, to address this possibility.

Previous work has shown that changes in LC activation correlate with cognitive processes on diverse timescales ranging from seconds to hours. Brief sub-second LC phasic activations may function to orient animals to important behavioral events (Bouret & Sara, 2004; Sara & Bouret, 2012a) while slower (minutes-hours) changes in the LC-NE system could promote behavioral strategy adjustments (Aston-Jones & Cohen, 2005a), perceptual changes (Martins & Froemke, 2015; Usher et al., 1999b), memory consolidation (Tronel et al., 2004), learning (Glennon et al., 2019b) along with shifts in arousal state (Carter et al., 2010). It is conceivable that different timescales of LC activation can produce different behavioral effects via distinct modulatory effects on targeted neurons. Different modes of LC activity have been shown to generate distinct (i.e., transient vs sustained) changes in cortical norepinephrine concentration (Berridge & Abercrombie, 1999). In turn, NE concentration, together with the adrenergic receptor subtypes expressed by

targeted neurons, determine the specific neuromodulatory effects that take place after LC activation and NE release (Arnsten, 1998; Robbins & Arnsten, 2009). In the current study, in both monkeys, we found many example sessions where slow timescale fluctuations in baseline LC activity closely tracked changes in PFC population activity, pupil diameter, perceptual decision making accuracy and overall engagement with the task at hand (see Figures 25 and 26 for examples). Future studies should focus on systematically relating simultaneously monitored LC and cortical activity to measures of cognitive task performance and arousal state, on different timescales. Such work will ultimately help us better understand the behavioral significance of the LC-mediated influences on cortical activity reported in this and other recent studies.

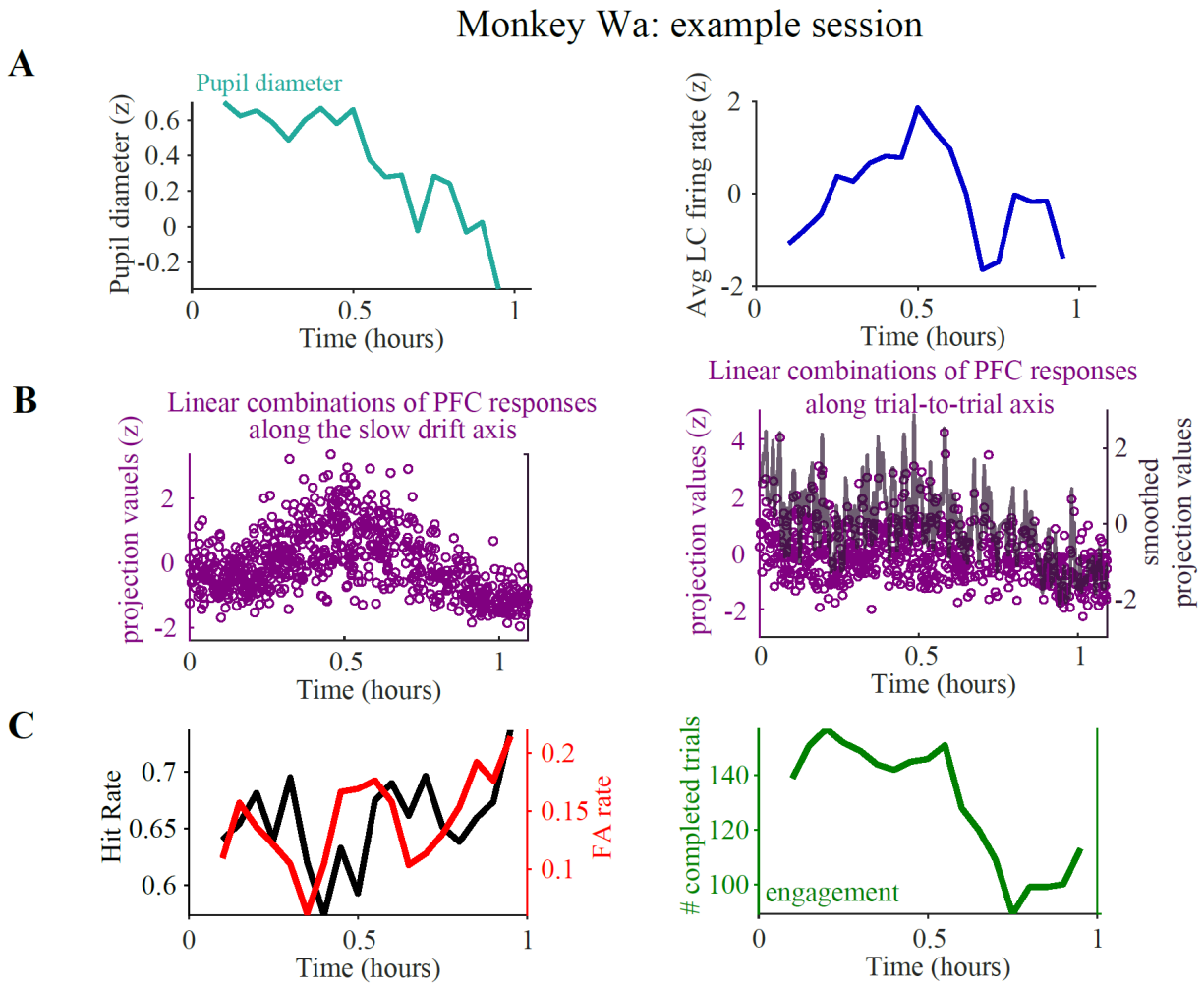

Figure 25. Fluctuations in simultaneously monitored pupil diameter, LC baseline activity, PFC population activity and behavioral performance over the course of time in an example experimental session from Monkey Wa.

(A) Shown are slow time scale changes in mean pupil diameter (left) and mean LC baseline rate (right) over time in the session. We computed moving average estimates of pupil diameter and LC baseline rate within 12 minute bins shifted every 3 minutes. (B) Shown are the slow (left) and fast, trial-to-trial (right) timescale changes in the co-variability of the responses of 65 simultaneously recorded PFC neurons. Each purple dot represents the linear combination of all simultaneously recorded PFC neuron responses to 1 instance of the first stimulus grating in a trial (see Methods and Figure 21 for details on quantifying different timescale changes in PFC population activity). (C) Shown are changes in behavioral performance (left) and task engagement (right) over the course of time in the session. Hit rate, false alarm rate, and engagement rate were computed across trials that occurred within the same sliding 12 minute bins as used for calculating changes in mean pupil diameter and LC rate in (A). Task engagement was computed as the number of completed trials (that ended in a choice) divided by the number of total trials that were attempted in each 12 minute time window. *Overall*, note 1) the matching timing of inflection points in the time courses of LC activity and slow drift in PFC population activity at 30 minutes 2) the matching timing of upward inflections in LC activity, pupil diameter and task engagement at ~45 minutes 3) an overall decreasing trend in time courses of pupil diameter, PFC population activity, LC activity and task engagement past the halfway time point in the session.

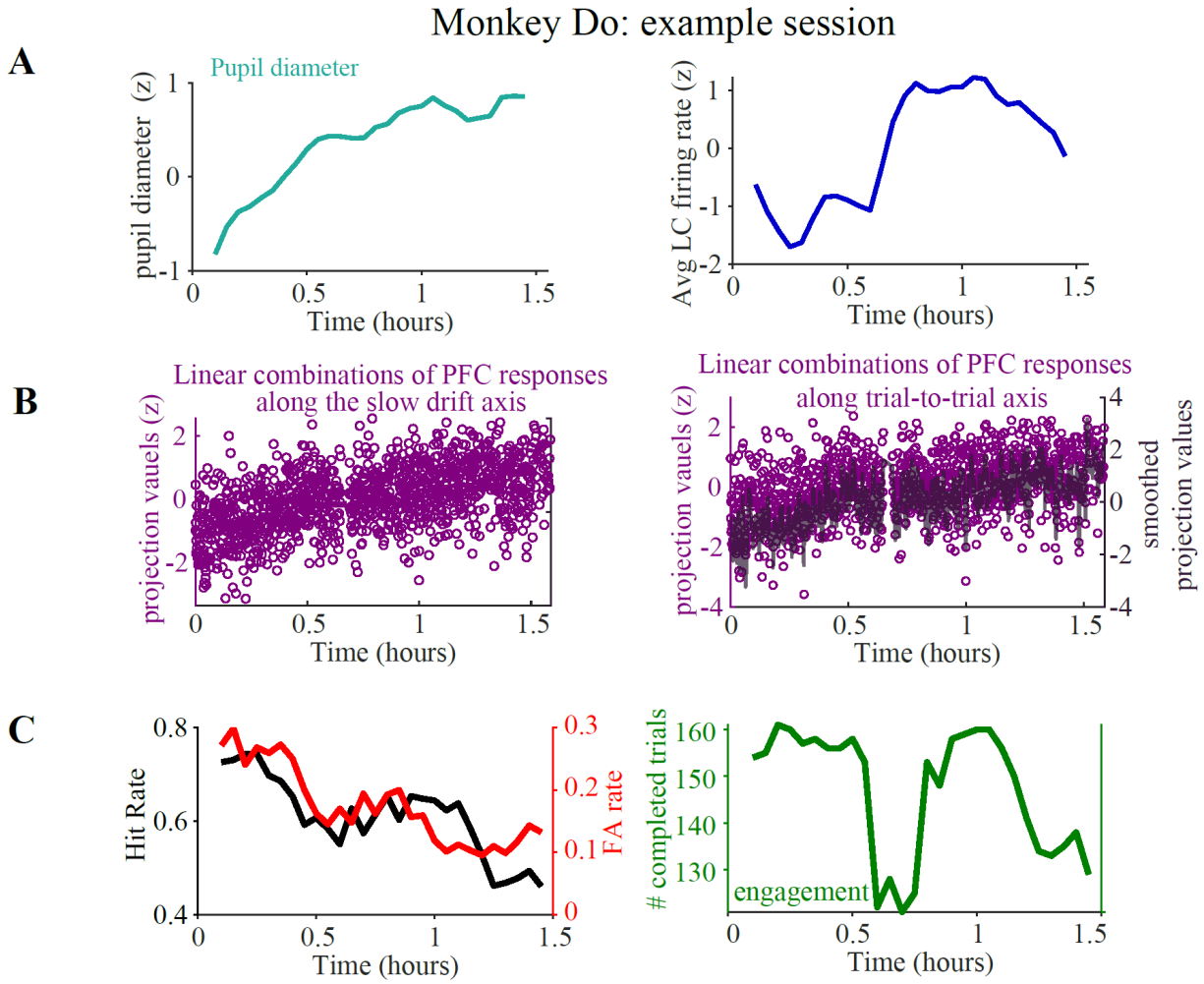

Figure 26. Fluctuations in simultaneously monitored pupil diameter, LC activity, PFC population activity and behavioral performance over the course of time in an example experimental session from Monkey Do.

(A) Shown are slow time scale changes in mean pupil diameter (left) and mean LC baseline rate (right) over 1.5 hours. We computed moving average estimates of pupil diameter and LC rate within 12 minute bins shifted every 3 minutes. (B) Shown are the slow (left) and fast, trial-to-trial (right) timescale changes in the co-variability of the responses of 51 simultaneously recorded PFC neurons. Each purple dot represents the linear combination of all simultaneously recorded PFC neuron responses to 1 instance of the first stimulus grating in a trial (see Methods and Figure 21 for details on quantifying different timescale changes in PFC population activity). (C) Shown are changes in behavioral performance (left) and task engagement (right) over the course of time in the session. Hit rate (black), false alarm rate (red), and engagement rate (green) were computed across trials that occurred within the same sliding 12 minute bins as used for calculating changes in mean pupil diameter and LC rate in (A). Task engagement was computed as the number of completed trials (that ended in a choice) divided by the total number of trials that were attempted in each 12 minute time window. *Overall*, *note* 1) the matching timing of inflection points in the time courses of LC activity, PFC population activity and task engagement at ~40 minutes into the session 2) an overall increasing trend for time courses of LC activity, pupil diameter, and PFC population activity that opposes an overall decreasing trend in hit rate and false alarm rate across the 1.5 hour session.

5.0 General Discussion

The purpose of the studies described in this dissertation was to investigate how specific developmental and neuromodulatory factors may contribute to variability in visual perception. In Chapter 2, we studied the effects of abnormal early visual experience on functional interactions in pairs of neurons in the primary visual cortex (V1) of adult macaque monkeys. In chapters 3 and 4, we investigated how activation of the Locus Coeruleus (LC), the primary source of noradrenergic (NE) neuromodulation in the central nervous system, relates to cortical population activity patterns and behavior on a perceptual decision making task. We provided a detailed discussion of the significance of each of our findings at the end of each previous chapter. Here, we offer some final thoughts on how our findings relate to past and current work in the field of visual perception.

5.1 Recent Advances in Understanding the Neural Basis of Visual Perception

Decades ago, researchers began studying the neural basis of visual perception by recording from single neurons in one brain region at a time. A neural correlate of visual perception was first established by studies that recorded the activity of single MT neurons while macaques reported their perceptual decisions in a visual motion direction discrimination task (Britten et al., 1992, 1996; Salzman & Newsome, 1994). This experimental approach allowed researchers to correlate variations in neural responses evoked by visual stimuli to fluctuations in perceptual choices based on the same information from the visual stimuli (Britten et al., 1996). This analysis, called choice probability, was then applied by many subsequent studies to show that individual neuron responses

in many different brain regions (e.g., LIP, somatosensory cortex, SC, FEF) are weakly predictive of animals' choices in perceptual tasks (reviewed by: Crapse & Basso, 2015; Cumming & Nienborg, 2016; Macke & Nienborg, 2019; Nienborg et al., 2012). Although single neuron responses undoubtedly carry some limited information about the animal's percepts, it is now known that choice probability values can be influenced by the structure of correlated variability in populations of neurons, and by cognitive signals from other brain regions (Cumming & Nienborg, 2016; Kohn et al., 2016; Macke & Nienborg, 2019; Nienborg et al., 2012). Similarly, early studies on the neural basis of amblyopia attributed the perceptual deficits to corresponding losses in responsivity of single neurons in V1 (Wiesel, 1982; WIESEL & HUBEL, 1963). However, it eventually became obvious that in monkeys with amblyopia, the degradation in single V1 neuron responsivity was not proportionate to the marked losses in visual sensitivity and resolution revealed by behavioral assessments (Bi et al., 2011; Kiorpes et al., 1998b; Shooner et al., 2015a). Thus, more recent studies, including the experiments described in this dissertation, have shifted to relating the coordinated activity of many simultaneously recorded neurons within and across brain regions to visual perception (reviewed in: Hanks & Summerfield, 2017; Kiorpes, 2016; Levi, 2013; Najafi & Churchland, 2018; O'Connell et al., 2018).

We now know that perceptual decisions require near-simultaneous, coordinated processing by multiple cortical and subcortical structures as animals receive sensory stimulus information, interpret it, and sometimes plan behavioral responses. Therefore, throughout the dissertation, one of our goals was to gain novel insight into the neural basis of perceptual variability by taking advantage of recent advancements in experimental data collection techniques and large-scale data analyses. In chapter 2 of this dissertation, we recorded simultaneously from populations of primary visual cortical (V1) neurons in macaques with amblyopia. Importantly, in contrast to previous

studies that focused on changes in visual processing by single neurons in visual cortex, the population recordings allowed us to test the novel hypothesis that part of the reduced visual capacity of amblyopes may be due to changes in the patterns of functional interaction among neurons in V1. We found changes in the strength and pattern of correlated variability between responses of pairs of neurons. Additionally, we showed how these changes in neuronal interactions could impair visual information representation by V1 populations driven by the amblyopic eye.

In chapter 4, we simultaneously recorded the activity of single LC neurons and the activity of a population of prefrontal cortex neurons. This experimental approach allowed us to examine the relationship between different timescales of fluctuations in the activation of the LC-NE neuromodulatory system, perception relevant processes in populations of PFC neurons and variability in visual perceptual behavior. Extensive work has been done on the organization of LC-NE system and the neuromodulatory effects of NE on individual sensory neurons, prompting some recent reviews to make bold statements such as "the effects of norepinephrine on target neurons are well established". Such conclusions are somewhat premature, considering that little has been done to understand how changing dynamics in the LC-NE system may manifest in coordinated activity of many simultaneously modulated targeted neurons during cognitive behavior, apart from the work presented here and another very recent study (Joshi & Gold, 2022). Here, we showed that trial-to-trial baseline LC activity fluctuated together with the trial-to-trial variability in coordinated PFC population activity and pupil diameter in two awake monkeys as they engaged in a perceptual task. Overall, our results support the recent hypothesis that activation of the LC-NE system mediates previously identified (Cowley et al., 2020; Hennig et al., 2021) behaviorally important computations carried out by populations of cortical neurons and can thus influence aspects of perceptual behavior. In the near future, we plan to systematically examine how the observed co-

variability in LC activity, PFC population activity and pupil diameter together relate to perceptual performance and task engagement. Such work will provide important insights into behavioral consequences of neuromodulation mediated by the LC-NE system.

5.2 How Well Do We Understand the Neural and Behavioral Effects of Neuromodulation by the LC-NE System?

A prevailing theory of LC-NE function has been that when released to target area, norepinephrine can affect a subject's ability to perceive a sensory stimulus by modulating responses of target neurons involved in computations underlying sensory perception (Berridge & Waterhouse, 2003; Devilbiss et al., 2006; Hurley et al., 2004; McBurney-Lin et al., 2019; Sara, 2009; Waterhouse & Navarra, 2019a). The most causal test of this theory would be a manipulation of LC activity while simultaneously recording from targeted neurons and measuring perceptual performance. To our knowledge only one such study has been done in rodents, and none in non-human primates. This study (Martins & Froemke, 2015), linked electrical stimulation of LC to simultaneous changes in response properties of primary auditory cortex neurons and improvements in auditory perception. It is possible that physiological vs artificially induced changes in the activation of the LC-NE system cause neural and behavioral effects of variable potency. To this point, in the study described in chapter 3 of this dissertation, we found no relationship between physiological LC phasic activation and a monkey's perceptual ability to detect stimulus changes of varied difficulty. Future studies should continue to examine the relationship between simultaneously monitored physiological LC activity, target neuron responses, and perceptual behavior in awake animals.

An important consideration for interpreting LC activity changes in relation to cortical activity and behavior, is the likely concomitant activation of other neuromodulatory systems. Because of the diffuse projections of the LC-NE system, there are several possible ways in which a change in LC activity could mediate modulation of other brain regions. A direct mechanism would be noradrenergic modulation after NE release from LC axon terminals. Another possibility is an indirect mechanism where NE-mediated activation of cholinergic neurons in the basal forebrain leads to the release of Acetylcholine in target brain regions (Samuels & Szabadi, 2008; Schwarz & Luo, 2015). Thus, to definitively relate the LC-NE system to changes in simultaneously recorded target neuron responses, it may be necessary to concurrently (pharmacologically) perturb noradrenergic signaling localized in the target brain region of interest. Such an experiment would also allow a test of how changes in LC activity without concurrent noradrenergic receptor activation in the target region of interest relate to behavior on a cognitive task. This would be a particularly illuminating, but challenging experiment. In primates, similar experiments have been done to assess cholinergic and dopaminergic modulation of cortical responses and behavior (Noudoost & Moore, 2011a, 2011b; Sun et al., 2017; Thiele et al., 2006, 2012).

Our results from chapters 3 and 4 highlight probable functional differences for different modes and timescales of LC activation, as has been suggested by more recent theories of LC function (N. K. B. Totah et al., 2019b). LC phasic responses have previously been reported to occur during a wide variety of contexts and behavioral paradigms, which has led to many theories and hypotheses about the behavioral or cognitive significance of the transient, sub-second long activations in the LC-NE system. Some researchers have theorized on a specific role of LC phasic activation in the decision making process (e.g., Clayton et al., 2004). In the study described in chapter 3 of this thesis, we set out to clarify what aspects of a perceptual decision making process

LC phasic activation could influence. Although we did not find any evidence for modulation of LC phasic responses based on differences in the animal's perceptual decision making ability (Figures 12-15), we observed consistent phasic activation as monkeys prepared to report their decisions (Figures 11,16,17). Thus, we are inclined to conclude that LC phasic activation is generally associated with any behavior that requires contextually-important sensorimotor processing, regardless of whether that behavior is instinctive or related to higher cognitive functions such as perceptual decision making.

It can be said that the understanding of the behavioral and neural consequences of LC phasic activation is more complete in comparison to what is known about the effects of slow timescale changes in activation of the LC-NE system. These long timescale fluctuations in LC activity and corresponding NE efflux may very well orchestrate shifts in perceptual ability and/or adaptive adjustments to behavioral strategies, depending on the needs of the animal (Aston-Jones & Cohen, 2005a). Future studies should address how slow timescale approximations of LC activity relate to slow fluctuations in performance on a perceptually demanding task similar to the one we used in chapters 3 and 4 of this thesis. Such experiments would allow for disambiguation of whether slower timescale, across trial changes in LC activity are more related to arousal-linked measures of behavioral performance (e.g., task engagement), to perceptual accuracy based measures of behavioral performance (e.g., perceptual sensitivity), or to both.

In conclusion, here we studied how 2 distinct factors: the noradrenergic neuromodulatory system and abnormal visual system development due to strabismic amblyopia, influence cortical population activity and visual perceptual behavior. Taken together, our findings provide novel insights into the neural basis of perceptual variability and emphasize how neural signals across multiple brain regions and temporal scales coordinate to influence visual perception.

Bibliography

Abbott, L. F., & Dayan, P. (1999). The effect of correlated variability on the accuracy of a population code. *Neural Computation*, *11*(1), 91–101. https://doi.org/10.1162/089976699300016827

Acar, K., Kiorpes, L., Movshon, J. A., & Smith, M. A. (2019). Altered functional interactions between neurons in primary visual cortex of macaque monkeys with experimental amblyopia. *Journal of Neurophysiology*, *122*(6), 2243–2258. https://doi.org/10.1152/JN.00232.2019/ASSET/IMAGES/LARGE/Z9K0111952680008.JPEG

Adams, D. L., Economides, J. R., & Horton, J. C. (2015). Contrasting effects of strabismic amblyopia on metabolic activity in superficial and deep layers of striate cortex. *Journal of Neurophysiology*, *113*(9), 3337–3344. https://doi.org/10.1152/jn.00159.2015

Allen, W. E., Chen, M. Z., Pichamoorthy, N., Tien, R. H., Pachitariu, M., Luo, L., & Deisseroth, K. (2019). Thirst regulates motivated behavior through modulation of brainwide neural population dynamics. *Science*, *364*(6437). https://doi.org/10.1126/science.aav3932

Alonso, J. M., & Martinez, L. M. (1998). Functional connectivity between simple cells and complex cells in cat striate cortex. *Nature Neuroscience*, *1*(5), 395–403. https://doi.org/10.1038/1609

Amsten, A. F. T., & Simon, F. (2000). Through the Looking Glass: Differential Noradenergic Modulation of Prefrontal Cortical Function. *Neural Plasticity*, *7*(1–2), 133. https://doi.org/10.1155/NP.2000.133

Arieli, A., Sterkin, A., Grinvald, A., & Aertsen, A. (1996). Dynamics of ongoing activity: explanation of the large variability in evoked cortical responses. *Science (New York, N.Y.)*, *273*(5283), 1868–1871. https://doi.org/10.1126/science.273.5283.1868

Arnsten, A. F. T. (1998). *Catecholamine modulation of prefrontal cortical cognitive function*. *6613*(November).

Arnsten, A. F. T., & Goldman-Rakic, P. S. (1984). Selective prefrontal cortical projections to the region of the locus coeruleus and raphe nuclei in the rhesus monkey. *Brain Research*, *306*(1), 9–18. https://doi.org/https://doi.org/10.1016/0006-8993(84)90351-2

Arnsten, A. F. T., Wang, M. J., & Paspalas, C. D. (2012). Neuromodulation of Thought: Flexibilities and Vulnerabilities in Prefrontal Cortical Network Synapses. *Neuron*, *76*(1), 223–239. https://doi.org/10.1016/J.NEURON.2012.08.038

Asper, L., Crewther, D., & Crewther, S. G. (2000). Strabismic amblyopia. Part 2. Neural processing. *Clinical & Experimental Optometry*, *83*(4), 200–211. https://doi.org/10.1111/j.1444-0938.2000.tb05003.x

Aston-Jones, G., & Bloom, F. E. (1981a). Activity of norepinephrine-containing locus coeruleus neurons in behaving rats anticipates fluctuations in the sleep-waking cycle. *Journal of Neuroscience*, *1*(8), 876–886. https://doi.org/10.1523/jneurosci.01-08-00876.1981

Aston-Jones, G., & Bloom, F. E. (1981b). Norepinephrine-containing locus coeruleus neurons in behaving rats exhibit pronounced responses to non-noxious environmental stimuli. *Journal of Neuroscience*, *1*(8), 887–900. https://doi.org/10.1523/jneurosci.01-08-00887.1981

Aston-Jones, G., & Cohen, J. D. (2005a). An integrative theory of locus coeruleus-norepinephrine function: Adaptive gain and optimal performance. *Annual Review of Neuroscience*, *28*, 403–450. https://doi.org/10.1146/annurev.neuro.28.061604.135709

Aston-Jones, G., & Cohen, J. D. (2005b). An integrative theory of locus coeruleus-norepinephrine function: Adaptive gain and optimal performance. *Annual Review of Neuroscience*, *28*, 403–450. https://doi.org/10.1146/annurev.neuro.28.061604.135709

Aston-Jones, G., Rajkowski, J., & Kubiak, P. (1997). Conditioned responses of monkey locus coeruleus neurons anticipate acquisition of discriminative behavior in a vigilance task. *Neuroscience*, *80*(3), 697–715. https://doi.org/10.1016/S0306-4522(97)00060-2

Aston-Jones, G., Rajkowski, J., Kubiak, P., & Alexinsky, T. (1994). Locus coeruleus neurons in monkey are selectively activated by attended cues in a vigilance task. *Journal of Neuroscience*, *14*(7), 4467–4480. https://doi.org/10.1523/jneurosci.14-07-04467.1994

Aston-Jones, G., & Waterhouse, B. (2016). Locus coeruleus: From global projection system to adaptive regulation of behavior. *Brain Research*, *1645*, 75–78. https://doi.org/10.1016/j.brainres.2016.03.001

Aston-Jones, G., Zhu, Y., & Card, J. P. (2004). Numerous GABAergic Afferents to Locus Ceruleus in the Pericerulear Dendritic Zone: Possible Interneuronal Pool. *Journal of Neuroscience*, *24*(9), 2313–2321. https://doi.org/10.1523/JNEUROSCI.5339-03.2004

Averbeck, B. B., Latham, P. E., & Pouget, A. (2006). Neural correlations, population coding and computation. *Nature Reviews. Neuroscience*, *7*(5), 358–366. https://doi.org/10.1038/nrn1888

Avery, M. C., Dutt, N., & Krichmar, J. L. (2013). A large-scale neural network model of the influence of neuromodulatory levels on working memory and behavior. *Frontiers in Computational Neuroscience*, *7*(OCT), 1–14. https://doi.org/10.3389/fncom.2013.00133

Baker, D. H., Meese, T. S., & Hess, R. F. (2008). Contrast masking in strabismic amblyopia: attenuation, noise, interocular suppression and binocular summation. *Vision Research*, *48*(15), 1625–1640. https://doi.org/10.1016/j.visres.2008.04.017

Baker, F. H., Grigg, P., & von Noorden, G. K. (1974). Effects of visual deprivation and strabismus on the response of neurons in the visual cortex of the monkey, including studies on the striate and prestriate cortex in the normal animal. *Brain Research*, *66*(2), 185–208. https://doi.org/https://doi.org/10.1016/0006-8993(74)90140-1

Basso, M. A., Bickford, M. E., & Cang, J. (2021). Unraveling circuits of visual perception and cognition through the superior colliculus. *Neuron*, *109*(6), 918–937. https://doi.org/10.1016/J.NEURON.2021.01.013

Beaman, C. B., Eagleman, S. L., & Dragoi, V. (2017). Sensory coding accuracy and perceptual performance are improved during the desynchronized cortical state. *Nature Communications*, *8*(1), 1308. https://doi.org/10.1038/s41467-017-01030-4

Berridge, C. W., & Abercrombie, E. D. (1999). Relationship between locus coeruleus discharge rates and rates of norepinephrine release within neocortex as assessed by in vivo microdialysis. *Neuroscience*, *93*(4), 1263–1270. https://doi.org/10.1016/S0306-4522(99)00276-6

Berridge, C. W., Page, M. E., Valentino, R. J., & Foote, S. L. (1993). Effects of locus coeruleus inactivation on electroencephalographic activity in neocortex and hippocampus. *Neuroscience*, *55*(2), 381–393. https://doi.org/10.1016/0306-4522(93)90507-C

Berridge, C. W., & Spencer, R. C. (2016). Differential cognitive actions of norepinephrine a2 and a1 receptor signaling in the prefrontal cortex. *Brain Research*, *1641*, 189–196. https://doi.org/10.1016/j.brainres.2015.11.024

Berridge, C. W., & Waterhouse, B. D. (2003). The locus coeruleus-noradrenergic system: Modulation of behavioral state and state-dependent cognitive processes. *Brain Research Reviews*, *42*(1), 33–84. https://doi.org/10.1016/S0165-0173(03)00143-7

Bi, H., Zhang, B., Tao, X., Harwerth, R. S., Smith, E. L., & Chino, Y. M. (2011). Neuronal responses in visual area V2 (V2) of macaque monkeys with strabismic amblyopia. *Cerebral Cortex*, *21*(9), 2033–2045. https://doi.org/10.1093/cercor/bhq272

Bisley, J. W., & Goldberg, M. E. (2003). Neuronat activity in the lateral intraparietal area and spatial attention. *Science*, *299*(5603), 81–86. https://doi.org/10.1126/SCIENCE.1077395/SUPPL_FILE/BISLEY.SOM.PDF

Blakemore, C., & Vital-Durand, F. (1986). Effects of visual deprivation on the development of the monkey's lateral geniculate nucleus. *The Journal of Physiology*, *380*, 493–511. https://doi.org/10.1113/jphysiol.1986.sp016298

Bornert, P., & Bouret, S. (2021). Locus coeruleus neurons encode the subjective difficulty of triggering and executing actions. *PLOS Biology*, *19*(12), e3001487. https://doi.org/10.1371/JOURNAL.PBIO.3001487

Bouret, S., & Richmond, B. J. (2009). Relation of locus coeruleus neurons in monkeys to Pavlovian and operant behaviors. *Journal of Neurophysiology*, *101*(2), 898–911. https://doi.org/10.1152/jn.91048.2008

Bouret, S., & Richmond, B. J. (2015). Sensitivity of Locus Ceruleus Neurons to Reward Value for Goal-Directed Actions. *The Journal of Neuroscience : The Official Journal of the Society for Neuroscience*, *35*(9), 4005–4014. https://doi.org/10.1523/JNEUROSCI.4553-14.2015

Bouret, S., & Sara, S. J. (2004). Reward expectation, orientation of attention and locus coeruleus-medial frontal cortex interplay during learning. *European Journal of Neuroscience*, *20*(3), 791–802. https://doi.org/10.1111/j.1460-9568.2004.03526.x

Bouret, S., & Sara, S. J. (2005). Network reset: A simplified overarching theory of locus coeruleus noradrenaline function. *Trends in Neurosciences*, *28*(11), 574–582. https://doi.org/10.1016/j.tins.2005.09.002

Bradley, A., & Freeman, R. D. (1981). Contrast sensitivity in anisometropic amblyopia. *Investigative Ophthalmology & Visual Science*, *21*(3), 467–476.

Breton-Provencher, V., & Sur, M. (2019a). Active control of arousal by a locus coeruleus GABAergic circuit. *Nature Neuroscience*, *22*(2), 218–228. https://doi.org/10.1038/s41593-018-0305-z

Breton-Provencher, V., & Sur, M. (2019b). Active control of arousal by a locus coeruleus GABAergic circuit. *Nature Neuroscience*, *22*(2), 218–228. https://doi.org/10.1038/s41593-018-0305-z

Britten, K. H., Newsome, W. T., Shadlen, M. N., Celebrini, S., & Movshon, J. A. (1996). A relationship between behavioral choice and the visual responses of neurons in macaque MT. *Visual Neuroscience*, *13*(1), 87–100. https://doi.org/10.1017/S095252380000715X

Britten, K. H., Shadlen, M. N., Newsome, W. T., & Movshon, J. A. (1992). The analysis of visual motion: a comparison of neuronal and psychophysical performance. *Journal of Neuroscience*, *12*(12), 4745–4765. https://doi.org/10.1523/JNEUROSCI.12-12-04745.1992

Brown, R. M., Crane, A. M., & Goldman, P. S. (1979). Regional distribution of monoamines in the cerebral cortex and subcortical structures of the rhesus monkey: concentrations and in vivo synthesis rates. *Brain Research*, *168*(1), 133–150. https://doi.org/10.1016/0006-8993(79)90132-X

Bruce, C. J., & Goldberg, M. E. (1985). Primate frontal eye fields. I. Single neurons discharging before saccades. *Https://Doi.Org/10.1152/Jn.1985.53.3.603*, *53*(3), 603–635. https://doi.org/10.1152/JN.1985.53.3.603

Bullock, K. R., Pieper, F., Sachs, A. J., & Martinez-Trujillo, J. C. (2017). *Visual and presaccadic activity in area 8Ar of the macaque monkey lateral prefrontal cortex*. https://doi.org/10.1152/jn.00278.2016.-Common

Callado, L. F., & Stamford, J. A. (2000). Spatiotemporal interaction of α2 autoreceptors and noradrenaline transporters in the rat locus coeruleus: Implications for volume transmission. *Journal of Neurochemistry*, *74*(6), 2350–2358. https://doi.org/10.1046/J.1471-4159.2000.0742350.X

Campbell, M. J., Lewis, D. A., Foote, S. L., & Morrison, J. H. (1987). Distribution of choline acetyltransferase-, serotonin-, dopamine-β-hydroxylase-, tyrosine hydroxylase-immunoreactive fibers in monkey primary auditory cortex. *Journal of Comparative Neurology*, *261*(2), 209–220. https://doi.org/10.1002/CNE.902610204

Carter, M. E., Yizhar, O., Chikahisa, S., Nguyen, H., Adamantidis, A., Nishino, S., Deisseroth, K., & de Lecea, L. (2010). Tuning arousal with optogenetic modulation of locus coeruleus neurons. *Nature Neuroscience*, *13*(12), 1526–1535. https://doi.org/10.1038/nn.2682

Chandler, D. J. (2016). Evidence for a specialized role of the locus coeruleus noradrenergic system in cortical circuitries and behavioral operations. *Brain Research*, *1641*, 197–206. https://doi.org/10.1016/j.brainres.2015.11.022

Chandler, D. J., Gao, W., & Waterhouse, B. D. (2014). *Heterogeneous organization of the locus coeruleus projections to prefrontal and motor cortices*. *111*(18). https://doi.org/10.1073/pnas.1320827111

Chandler, D. J., Jensen, P., McCall, J. G., Pickering, A. E., Schwarz, L. A., & Totah, N. K. (2019). Redefining Noradrenergic Neuromodulation of Behavior: Impacts of a Modular Locus Coeruleus Architecture. *The Journal of Neuroscience : The Official Journal of the Society for Neuroscience*, *39*(42), 8239–8249. https://doi.org/10.1523/JNEUROSCI.1164-19.2019

Chino, Y. M., Shansky, M. S., Jankowski, W. L., & Banser, F. A. (1983). Effects of rearing kittens with convergent strabismus on development of receptive-field properties in striate cortex neurons. *Journal of Neurophysiology*, *50*(1), 265–286. https://doi.org/10.1152/jn.1983.50.1.265

Churchland, M. M., Yu, B. M., Cunningham, J. P., Sugrue, L. P., Cohen, M. R., Corrado, G. S., Newsome, W. T., Clark, A. M., Hosseini, P., Scott, B. B., Bradley, D. C., Smith, M. A., Kohn, A., Movshon, J. A., Armstrong, K. M., Moore, T., Chang, S. W., Snyder, L. H., Lisberger, S. G., … Shenoy, K. v. (2010). Stimulus onset quenches neural variability: a widespread cortical phenomenon. *Nature Neuroscience*, *13*(3), 369–378. https://doi.org/10.1038/nn.2501

Clark, K., Squire, R. F., Merrikhi, Y., & Noudoost, B. (2015). Visual attention: Linking prefrontal sources to neuronal and behavioral correlates. *Progress in Neurobiology*, *132*, 59–80. https://doi.org/10.1016/j.pneurobio.2015.06.006

Clayton, E. C., Rajkowski, J., Cohen, J. D., & Aston-Jones, G. (2004). Phasic activation of monkey locus ceruleus neurons by simple decisions in a forced-choice task. *Journal of Neuroscience*, *24*(44), 9914–9920. https://doi.org/10.1523/JNEUROSCI.2446-04.2004

Cohen, M. R., & Kohn, A. (2011a). Measuring and interpreting neuronal correlations. *Nature Neuroscience*, *14*(7), 811–819. https://doi.org/10.1038/nn.2842

Cohen, M. R., & Kohn, A. (2011b). Measuring and interpreting neuronal correlations. *Nature Neuroscience*, *14*(7), 811. https://doi.org/10.1038/NN.2842

Cohen, M. R., & Maunsell, J. H. R. (2009a). Attention improves performance primarily by reducing interneuronal correlations. *Nature Neuroscience*, *12*(12), 1594–1600. https://doi.org/10.1038/nn.2439

Cohen, M. R., & Maunsell, J. H. R. (2009b). Attention improves performance primarily by reducing interneuronal correlations. *Nature Neuroscience*, *12*(12), 1594–1600. https://doi.org/10.1038/nn.2439

Cohen, M. R., & Maunsell, J. H. R. (2010). A neuronal population measure of attention predicts behavioral performance on individual trials. *Journal of Neuroscience*, *30*(45), 15241–15253. https://doi.org/10.1523/JNEUROSCI.2171-10.2010

Cohen, M. R., & Maunsell, J. H. R. (2011). When attention wanders: How uncontrolled fluctuations in attention affect performance. *Journal of Neuroscience*, *31*(44), 15802–15806. https://doi.org/10.1523/JNEUROSCI.3063-11.2011

Cohen, M. R., & Newsome, W. T. (2008). Context-Dependent Changes in Functional Circuitry in Visual Area MT. *Neuron*, *60*(1), 162–173. https://doi.org/10.1016/j.neuron.2008.08.007

Colby, C. L., Duhamel, J. R., & Goldberg, M. E. (1996). Visual, presaccadic, and cognitive activation of single neurons in monkey lateral intraparietal area. *Journal of Neurophysiology*, *76*(5), 2841–2852. https://doi.org/10.1152/JN.1996.76.5.2841

Coppola, J. J., & Disney, A. A. (2018). *Is There a Canonical Cortical Circuit for the Cholinergic System ? Anatomical Differences Across Common Model Systems*. *12*(January), 1–13. https://doi.org/10.3389/fncir.2018.00008

Cowley, B. R., Snyder, A. C., Acar, K., Williamson, R. C., Yu, B. M., & Smith, M. A. (2020). Slow Drift of Neural Activity as a Signature of Impulsivity in Macaque Visual and Prefrontal Cortex. *Neuron*, 1–17. https://doi.org/10.1016/j.neuron.2020.07.021

Crapse, T. B., & Basso, M. A. (2015). Insights into decision making using choice probability. *Journal of Neurophysiology*, *114*(6), 3039–3049. https://doi.org/10.1152/jn.00335.2015

Crapse, T. B., Lau, H., & Basso, M. A. (2018). A Role for the Superior Colliculus in Decision Criteria. *Neuron*, *97*(1), 181-194.e6. https://doi.org/10.1016/J.NEURON.2017.12.006

Crawford, M. L., de Faber, J. T., Harwerth, R. S., Smith, E. L. 3rd, & von Noorden, G. K. (1989). The effects of reverse monocular deprivation in monkeys. II. Electrophysiological and anatomical studies. *Experimental Brain Research*, *74*(2), 338–347. https://doi.org/10.1007/BF00248867

Crawford, M. L. J., & Harwerth, R. S. (2004). Ocular dominance column width and contrast sensitivity in monkeys reared with strabismus or anisometropia. *Investigative Ophthalmology & Visual Science*, *45*(9), 3036–3042. https://doi.org/10.1167/iovs.04-0029

Crawford, M. L., & von Noorden, G. K. (1979). Concomitant strabismus and cortical eye dominance in young rhesus monkeys. *Transactions of the Ophthalmological Societies of the United Kingdom*, *99*(3), 369–374.

Crewther, D. P., & Crewther, S. G. (1990). Neural site of strabismic amblyopia in cats: spatial frequency deficit in primary cortical neurons. *Experimental Brain Research*, *79*(3), 615–622. https://doi.org/10.1007/BF00229329

Cumming, B. G., & Nienborg, H. (2016). Feedforward and feedback sources of choice probability in neural population responses. *Current Opinion in Neurobiology*, *37*, 126–132. https://doi.org/10.1016/j.conb.2016.01.009

Cunningham, J. P., & Yu, B. M. (2014). Dimensionality reduction for large-scale neural recordings. *Nature Neuroscience*, *17*(11), 1500–1509. https://doi.org/10.1038/nn.3776

Dalley, J. W., McGaughy, J., O'Connell, M. T., Cardinal, R. N., Levita, L., & Robbins, T. W. (2001). Distinct changes in cortical acetylcholine and noradrenaline efflux during contingent and noncontingent performance of a visual attentional task. *Journal of Neuroscience*, *21*(13), 4908–4914. https://doi.org/10.1523/jneurosci.21-13-04908.2001

Dayan, P. (2012). Review Twenty-Five Lessons from Computational Neuromodulation. *Neuron*, *76*(1), 240–256. https://doi.org/10.1016/j.neuron.2012.09.027

de Gee, J. W., Knapen, T., & Donner, T. H. (2014). Decision-related pupil dilation reflects upcoming choice and individual bias. *Proceedings of the National Academy of Sciences of the United States of America*, *111*(5), 1–8. https://doi.org/10.1073/pnas.1317557111

Desimone, R., & Schein, S. J. (1987). Visual properties of neurons in area V4 of the macaque: Sensitivity to stimulus form. *Journal of Neurophysiology*, *57*(3), 835–868. https://doi.org/10.1152/jn.1987.57.3.835

Devilbiss, D. M. (2019). Consequences of tuning network function by tonic and phasic locus coeruleus output and stress: Regulating detection and discrimination of peripheral stimuli. *Brain Research*, *1709*, 16–27. https://doi.org/10.1016/j.brainres.2018.06.015

Devilbiss, D. M., Page, M. E., & Waterhouse, B. D. (2006). *Locus Ceruleus Regulates Sensory Encoding by Neurons and Networks in Waking Animals*. *26*(39), 9860–9872. https://doi.org/10.1523/JNEUROSCI.1776-06.2006

Ding, L., & Gold, J. I. (2012). Neural correlates of perceptual decision making before, during, and after decision commitment in monkey frontal eye field. *Cerebral Cortex*, *22*(5), 1052–1067. https://doi.org/10.1093/cercor/bhr178

Doiron, B., Litwin-Kumar, A., Rosenbaum, R., Ocker, G. K., & Josić, K. (2016). The mechanics of state-dependent neural correlations. *Nature Neuroscience*, *19*(3), 383–393. https://doi.org/10.1038/nn.4242

Ebitz, R. B., & Platt, M. L. (2015). Neuronal activity in primate dorsal anterior cingulate cortex signals task conflict and predicts adjustments in pupil-linked arousal. *Neuron*, *85*(3), 628–640. https://doi.org/10.1016/j.neuron.2014.12.053

Ecker, A. S., Berens, P., Tolias, A. S., & Bethge, M. (2011). The effect of noise correlations in populations of diversely tuned neurons. *The Journal of Neuroscience : The Official Journal of the Society for Neuroscience*, *31*(40), 14272–14283. https://doi.org/10.1523/JNEUROSCI.2539-11.2011

Eldar, E., Cohen, J. D., & Niv, Y. (2013). The effects of neural gain on attention and learning. *Nature Neuroscience*, *16*(8), 1146. https://doi.org/10.1038/NN.3428

El-Shamayleh, Y., Kiorpes, L., Kohn, A., & Movshon, J. A. (2010). Visual motion processing by neurons in area MT of macaque monkeys with experimental amblyopia. *The Journal of Neuroscience : The Official Journal of the Society for Neuroscience*, *30*(36), 12198–12209. https://doi.org/10.1523/JNEUROSCI.3055-10.2010

Engbert, R., & Kliegl, R. (2003). Microsaccades uncover the orientation of covert attention. *Vision Research*, *43*(9), 1035–1045. https://doi.org/10.1016/S0042-6989(03)00084-1

Engbert, R., & Kliegl, R. (2004). Microsaccades keep the eyes' balance during fixation. *Psychological Science*, *15*(6), 431–436. https://doi.org/10.1111/j.0956-7976.2004.00697.x

Engel, T. A., & Steinmetz, N. A. (2019). New perspectives on dimensionality and variability from large-scale cortical dynamics. *Current Opinion in Neurobiology*, *58*, 181–190. https://doi.org/10.1016/j.conb.2019.09.003

Ennis, M., & Aston-Jones, G. (1989). Potent inhibitory input to locus coeruleus from the nucleus prepositus hypoglossi. *Brain Research Bulletin*, *22*(5), 793–803. https://doi.org/10.1016/0361-9230(89)90022-1

Everitt, B. J., & Robbins, T. W. (2003). CENTRAL CHOLINERGIC SYSTEMS AND COGNITION. *Http://Dx.Doi.Org/10.1146/Annurev.Psych.48.1.649*, *48*, 649–684. https://doi.org/10.1146/ANNUREV.PSYCH.48.1.649

Farzin, F., & Norcia, A. M. (2011). Impaired visual decision-making in individuals with amblyopia. *Journal of Vision*, *11*(14). https://doi.org/10.1167/11.14.6

Felleman, D. J., & van Essen, D. C. (1991). Distributed hierarchical processing in the primate cerebral cortex. *Cerebral Cortex (New York, N.Y. : 1991)*, *1*(1), 1. https://doi.org/10.1093/CERCOR/1.1.1-A

Fenstemaker, S. B., Kiorpes, L., & Movshon, J. A. (2001). Effects of experimental strabismus on the architecture of macaque monkey striate cortex. *The Journal of Comparative Neurology*, *438*(3), 300–317. https://doi.org/10.1002/cne.1317

Finlayson, P. G., & Marshall, K. C. (1988). Synchronous bursting of locus coeruleus neurons in tissue culture. *Neuroscience*, *24*(1), 217–225. https://doi.org/10.1016/0306-4522(88)90325-9

Florin-Lechner, S. M., Druhan, J. P., Aston-Jones, G., & Valentino, R. J. (1996). Enhanced norepinephrine release in prefrontal cortex with burst stimulation of the locus coeruleus. *Brain Research*, *742*(1), 89–97. https://doi.org/https://doi.org/10.1016/S0006-8993(96)00967-5

Foote, S. L., Aston-Jones, G., & Bloom, F. E. (1980). Impulse activity of locus coeruleus neurons in awake rats and monkeys is a function of sensory stimulation and arousal. *Proceedings of the National Academy of Sciences of the United States of America*, *77*(5 I), 3033–3037. https://doi.org/10.1073/pnas.77.5.3033

Foote, S. L., & Berridge, C. W. (2019). New developments and future directions in understanding locus coeruleus – Norepinephrine (LC-NE) function. *Brain Research*, *1709*(September 2018), 81–84. https://doi.org/10.1016/j.brainres.2018.09.033

Foote, S. L., Freedman, R., & Oliver, A. P. (1975). Effects of putative neurotransmitters on neuronal activity in monkey auditory cortex. *Brain Research*, *86*(2), 229–242. https://doi.org/10.1016/0006-8993(75)90699-x

Foster, K. H., Gaska, J. P., Nagler, M., & Pollen, D. A. (1985). Spatial and temporal frequency selectivity of neurones in visual cortical areas V1 and V2 of the macaque monkey. *The Journal of Physiology*, *365*, 331–363. https://doi.org/10.1113/jphysiol.1985.sp015776

Funahashi, S. (2014). Saccade-related activity in the prefrontal cortex: Its role in eye movement control and cognitive functions. *Frontiers in Integrative Neuroscience*, *8*(JUNE), 54. https://doi.org/10.3389/FNINT.2014.00054/BIBTEX

Funahashi, S., Bruce, C. J., & Goldman-Rakic, P. S. (1991). Neuronal activity related to saccadic eye movements in the monkey's dorsolateral prefrontal cortex. *Https://Doi.Org/10.1152/Jn.1991.65.6.1464*, *65*(6), 1464–1483. https://doi.org/10.1152/JN.1991.65.6.1464

Gattass, R., Galkin, T. W., Desimone, R., & Ungerleider, L. G. (2014). Subcortical connections of area V4 in the macaque. *Journal of Comparative Neurology*, *522*(8), 1941–1965. https://doi.org/10.1002/CNE.23513

Gelbard-Sagiv, H., Magidov, E., Sharon, H., Hendler, T., & Nir, Y. (2018). Noradrenaline Modulates Visual Perception and Late Visually Evoked Activity. *Current Biology*, *28*(14), 2239-2249.e6. https://doi.org/10.1016/j.cub.2018.05.051

Gilzenrat, M. S., Nieuwenhuis, S., Jepma, M., & Cohen, J. D. (2010). Pupil diameter tracks changes in control state predicted by the adaptive gain theory of locus coeruleus function. *Cognitive, Affective & Behavioral Neuroscience*, *10*(2), 252–269. https://doi.org/10.3758/CABN.10.2.252

Glennon, E., Carcea, I., Martins, A. R. O., Multani, J., Shehu, I., Svirsky, M. A., & Froemke, R. C. (2019a). Locus coeruleus activation accelerates perceptual learning. *Brain Research*, *1709*, 39–49. https://doi.org/10.1016/j.brainres.2018.05.048

Glennon, E., Carcea, I., Martins, A. R. O., Multani, J., Shehu, I., Svirsky, M. A., & Froemke, R. C. (2019b). Locus coeruleus activation accelerates perceptual learning. *Brain Research*, *1709*, 39–49. https://doi.org/10.1016/j.brainres.2018.05.048

Gold, J. I., & Shadlen, M. N. (2003). The influence of behavioral context on the representation of a perceptual decision in developing oculomotor commands. *Journal of Neuroscience*, *23*(2), 632–651. https://doi.org/10.1523/jneurosci.23-02-00632.2003

Gold, J. I., & Shadlen, M. N. (2007). The neural basis of decision making. *Annual Review of Neuroscience*, *30*, 535–574. https://doi.org/10.1146/annurev.neuro.29.051605.113038

Grant, S. J., Aston-Jones, G., & Redmond, D. E. (1988). Responses of primate locus coeruleus neurons to simple and complex sensory stimuli. *Brain Research Bulletin*, *21*(3), 401–410. https://doi.org/10.1016/0361-9230(88)90152-9

Greschner, M., Shlens, J., Bakolitsa, C., Field, G. D., Gauthier, J. L., Jepson, L. H., Sher, A., Litke, A. M., & Chichilnisky, E. J. (2011). Correlated firing among major ganglion cell types in primate retina. *The Journal of Physiology*, *589*(Pt 1), 75–86. https://doi.org/10.1113/jphysiol.2010.193888

Gu, Y., Liu, S., Fetsch, C. R., Yang, Y., Fok, S., Sunkara, A., DeAngelis, G. C., & Angelaki, D. E. (2011). Perceptual learning reduces interneuronal correlations in macaque visual cortex. *Neuron*, *71*(4), 750–761. https://doi.org/10.1016/j.neuron.2011.06.015

Guedj, C., Reynaud, A., Monfardini, E., Salemme, R., Farnè, A., Meunier, M., & Hadj-Bouziane, F. (2019). Atomoxetine modulates the relationship between perceptual abilities and response bias. *Psychopharmacology*, *236*(12), 3641–3653. https://doi.org/10.1007/s00213-019-05336-7

Gutnisky, D. A., Beaman, C., Lew, S. E., & Dragoi, V. (2017). Cortical response states for enhanced sensory discrimination. *ELife*, *6*, 1–23. https://doi.org/10.7554/eLife.29226

Gutnisky, D. A., & Dragoi, V. (2008). Adaptive coding of visual information in neural populations. *Nature*, *452*(7184), 220–224. https://doi.org/10.1038/nature06563

Hafed, Z. M., & Clark, J. J. (2002). Microsaccades as an overt measure of covert attention shifts. *Vision Research*, *42*(22), 2533–2545. https://doi.org/10.1016/S0042-6989(02)00263-8

Hafed, Z. M., Goffart, L., & Krauzlis, R. J. (2009). A Neural Mechanism for Microsaccade Generation in the Primate Superior Colliculus. *Science*, *323*(5916), 940–943. https://doi.org/10.1126/science.1166112

Hallum, L. E., Shooner, C., Kumbhani, R. D., Kelly, J. G., García-Marín, V., Majaj, N. J., Movshon, J. A., & Kiorpes, L. (2017). Altered Balance of Receptive Field Excitation and Suppression in Visual Cortex of Amblyopic Macaque Monkeys. *The Journal of Neuroscience : The Official Journal of the Society for Neuroscience*, *37*(34), 8216–8226. https://doi.org/10.1523/JNEUROSCI.0449-17.2017

Hamm, L. M., Black, J., Dai, S., & Thompson, B. (2014). Global processing in amblyopia: a review. *Frontiers in Psychology*, *5*, 583. https://doi.org/10.3389/fpsyg.2014.00583

Hanks, T. D., & Summerfield, C. (2017). Perceptual Decision Making in Rodents, Monkeys, and Humans. *Neuron*, *93*(1), 15–31. https://doi.org/10.1016/j.neuron.2016.12.003

Hansen, B. J., Chelaru, M. I., & Dragoi, V. (2012). Correlated variability in laminar cortical circuits. *Neuron*, *76*(3), 590–602. https://doi.org/10.1016/j.neuron.2012.08.029

Harris, K. D., & Thiele, A. (2011). Cortical state and attention. *Nature Reviews Neuroscience 2011 12:9*, *12*(9), 509–523. https://doi.org/10.1038/nrn3084

Hendrickson, A. E., Movshon, J. A., Eggers, H. M., Gizzi, M. S., Boothe, R. G., & Kiorpes, L. (1987). Effects of early unilateral blur on the macaque's visual system. II. Anatomical observations. *The Journal of Neuroscience : The Official Journal of the Society for Neuroscience*, *7*(5), 1327–1339. https://doi.org/10.1523/JNEUROSCI.07-05-01327.1987

Hennig, J. A., Oby, E. R., Golub, M. D., Bahureksa, L. A., Sadtler, P. T., Quick, K. M., Ryu, S. I., Tyler-Kabara, E. C., Batista, A. P., Chase, S. M., & Yu, B. M. (2021). Learning is shaped by abrupt changes in neural engagement. *Nature Neuroscience 2021 24:5*, *24*(5), 727–736. https://doi.org/10.1038/s41593-021-00822-8

Hess, R. F., & Howell, E. R. (1977). The threshold contrast sensitivity function in strabismic amblyopia: evidence for a two type classification. *Vision Research*, *17*(9), 1049–1055. https://doi.org/10.1016/0042-6989(77)90009-8

Hirschberg, S., Li, Y., Randall, A., Kremer, E. J., & Pickering, A. E. (2017). Functional dichotomy in spinal-vs prefrontal-projecting locus coeruleus modules splits descending noradrenergic analgesia from ascending aversion and anxiety in rats. *ELife*, *6*. https://doi.org/10.7554/ELIFE.29808.001

Hobson, J. A., Mccarley, R. W., & Wyzinski, P. W. (1975). Sleep Cycle Oscillation: Reciprocal Discharge by Two Brainstem Neuronal Groups. *Science*, *189*(4196), 55–58. https://doi.org/10.1126/SCIENCE.1094539

Horton, J. C., Hocking, D. R., & Kiorpes, L. (1997). Pattern of ocular dominance columns and cytochrome oxidase activity in a macaque monkey with naturally occurring anisometropic amblyopia. *Visual Neuroscience*, *14*(4), 681–689. https://doi.org/10.1017/s0952523800012645

Hou, C., Kim, Y.-J., Lai, X. J., & Verghese, P. (2016). Degraded attentional modulation of cortical neural populations in strabismic amblyopia. *Journal of Vision*, *16*(3), 16. https://doi.org/10.1167/16.3.16

Hubel, D. H., & Wiesel, T. N. (1959). Receptive fields of single neurones in the cat's striate cortex. *The Journal of Physiology*, *148*(3), 574. https://doi.org/10.1113/JPHYSIOL.1959.SP006308

Hubel, D. H., & Wiesel, T. N. (1962). Receptive fields, binocular interaction and functional architecture in the cat's visual cortex. *The Journal of Physiology*, *160*(1), 106. https://doi.org/10.1113/JPHYSIOL.1962.SP006837

HUBEL, D. H., & WIESEL, T. N. (1965). RECEPTIVE FIELDS AND FUNCTIONAL ARCHITECTURE IN TWO NONSTRIATE VISUAL AREAS (18 AND 19) OF THE CAT. *Https://Doi.Org/10.1152/Jn.1965.28.2.229*, *28*, 229–289. https://doi.org/10.1152/JN.1965.28.2.229

Hubel, D. H., & Wiesel, T. N. (1965). Binocular interaction in striate cortex of kittens reared with artificial squint. *Journal of Neurophysiology*, *28*(6), 1041–1059. https://doi.org/10.1152/jn.1965.28.6.1041

Hubel, D. H., & Wiesel, T. N. (1977). Ferrier lecture - Functional architecture of macaque monkey visual cortex. *Proceedings of the Royal Society of London. Series B. Biological Sciences*, *190*(1130), 1–59. https://doi.org/10.1098/RSPB.1977.0085

Huk, A. C., Katz, L. N., & Yates, J. L. (2017). The Role of the Lateral Intraparietal Area in (the Study of) Decision Making. *Https://Doi.Org/10.1146/Annurev-Neuro-072116-031508*, *40*, 349–372. https://doi.org/10.1146/ANNUREV-NEURO-072116-031508

Hurley, L. M., Devilbiss, D. M., & Waterhouse, B. D. (2004). A matter of focus: Monoaminergic modulation of stimulus coding in mammalian sensory networks. In *Current Opinion in Neurobiology* (Vol. 14, Issue 4, pp. 488–495). https://doi.org/10.1016/j.conb.2004.06.007

Issar, D., Williamson, R. C., Khanna, S. B., & Smith, M. A. (2020). A neural network for online spike classification that improves decoding accuracy. *Journal of Neurophysiology*, *123*(4), 1472–1485. https://doi.org/10.1152/JN.00641.2019/ASSET/IMAGES/LARGE/Z9K0042054150006.JPEG

Jacob, S. N., Nienborg, H., Sara, S. J., & Jacob, S. N. (2018). *Monoaminergic Neuromodulation of Sensory Processing*. *12*(July), 1–17. https://doi.org/10.3389/fncir.2018.00051

Jahn, C. I., Varazzani, C., Sallet, J., Walton, M. E., & Bouret, S. (2020). Noradrenergic But Not Dopaminergic Neurons Signal Task State Changes and Predict Reengagement After a Failure. *Cerebral Cortex (New York, N.Y. : 1991)*, *30*(9), 4979–4994. https://doi.org/10.1093/cercor/bhaa089

Jeanne, J. M., Sharpee, T. O., & Gentner, T. Q. (2013). Associative learning enhances population coding by inverting interneuronal correlation patterns. *Neuron*, *78*(2), 352–363. https://doi.org/10.1016/j.neuron.2013.02.023

Jiang, M., Griff, E. R., Ennis, M., Zimmer, L. A., & Shipley, M. T. (1996). Activation of locus coeruleus enhances the responses of olfactory bulb mitral cells to weak olfactory nerve input. *The Journal of Neuroscience : The Official Journal of the Society for Neuroscience*, *16*(19), 6319–6329. https://doi.org/10.1523/JNEUROSCI.16-19-06319.1996

Jodo, E., Chiang, C., & Aston-Jones, G. (1998). Potent excitatory influence of prefrontal cortex activity on noradrenergic locus coeruleus neurons. *Neuroscience*, *83*(1), 63–79. https://doi.org/10.1016/S0306-4522(97)00372-2

Jollife, I. T., & Cadima, J. (2016). Principal component analysis: a review and recent developments. *Philosophical Transactions of the Royal Society A: Mathematical, Physical and Engineering Sciences*, *374*(2065). https://doi.org/10.1098/RSTA.2015.0202

Joshi, S., & Gold, J. I. (2020). Pupil Size as a Window on Neural Substrates of Cognition. *Trends in Cognitive Sciences*, *24*(6), 466–480. https://doi.org/10.1016/j.tics.2020.03.005

Joshi, S., & Gold, J. I. (2022). Context-dependent relationships between locus coeruleus firing patterns and coordinated neural activity in the anterior cingulate cortex. *ELife*, *11*. https://doi.org/10.7554/eLife.63490

Joshi, S., Li, Y., Kalwani, R., & Gold, J. (2016a). Relationships between Pupil Diameter and Neuronal Activity in the Locus Coeruleus, Colliculi, and Cingulate Cortex. *Neuron*, *89*(1), 221–234. https://doi.org/10.1016/j.physbeh.2017.03.040

Joshi, S., Li, Y., Kalwani, R. M., & Gold, J. I. (2016b). Relationships between Pupil Diameter and Neuronal Activity in the Locus Coeruleus, Colliculi, and Cingulate Cortex. *Neuron*, *89*(1), 221–234. https://doi.org/10.1016/j.neuron.2015.11.028

Jun, E. J., Bautista, A. R., Nunez, M. D., Allen, D. C., Tak, J. H., Alvarez, E., & Basso, M. A. (2021). Causal role for the primate superior colliculus in the computation of evidence for perceptual decisions Elizabeth. *Nat Neurosci*, *24*(8), 1121–1131. https://doi.org/10.1038/s41593-021-00878-6.Causal

Kalwani, R. M., Joshi, S., & Gold, J. I. (2014). Phasic Activation of Individual Neurons in the Locus Ceruleus/Subceruleus Complex of Monkeys Reflects Rewarded Decisions to Go But Not Stop. *Journal of Neuroscience*, *34*(41), 13656–13669. https://doi.org/10.1523/JNEUROSCI.2566-14.2014

Kanitscheider, I., Coen-Cagli, R., & Pouget, A. (2015). Origin of information-limiting noise correlations. *Proceedings of the National Academy of Sciences of the United States of America*, *112*(50), E6973-82. https://doi.org/10.1073/pnas.1508738112

Kaufman, M. T., Churchland, M. M., Ryu, S. I., & Shenoy, K. v. (2015). Vacillation, indecision and hesitation in moment-by-moment decoding of monkey motor cortex. *ELife*, *4*(MAY). https://doi.org/10.7554/ELIFE.04677

Kebschull, J. M., Garcia da Silva, P., Reid, A. P., Peikon, I. D., Albeanu, D. F., & Zador, A. M. (2016). High-Throughput Mapping of Single-Neuron Projections by Sequencing of Barcoded RNA. *Neuron*, *91*(5), 975–987. https://doi.org/10.1016/J.NEURON.2016.07.036

Kelly, R. C., Smith, M. A., Samonds, J. M., Kohn, A., Bonds, A. B., Movshon, J. A., & Lee, T. S. (2007). Comparison of recordings from microelectrode arrays and single electrodes in the visual cortex. *The Journal of Neuroscience : The Official Journal of the Society for Neuroscience*, *27*(2), 261–264. https://doi.org/10.1523/JNEUROSCI.4906-06.2007

Kiani, R., Cueva, C. J., Reppas, J. B., & Newsome, W. T. (2014). Indicate Changes of Mind on Single Trials. *Current Biology*, *24*(13), 1542–1547. https://doi.org/10.1016/j.cub.2014.05.049.Dynamics

Kim, J. N., & Shadlen, M. N. (1999). Neural correlates of a decision in the dorsolateral prefrontal cortex of the macaque. *Nature Neuroscience*, *2*(2), 176–185. https://doi.org/10.1038/5739

Kiorpes, L. (2006). Visual processing in amblyopia: Animal studies. *Strabismus*, *14*(1), 3–10. https://doi.org/10.1080/09273970500536193

Kiorpes, L. (2016). The Puzzle of Visual Development: Behavior and Neural Limits. *The Journal of Neuroscience : The Official Journal of the Society for Neuroscience*, *36*(45), 11384–11393. https://doi.org/10.1523/JNEUROSCI.2937-16.2016

Kiorpes, L., & Daw, N. (2018). Cortical correlates of amblyopia. *Visual Neuroscience*, *35*, E016. https://doi.org/10.1017/S0952523817000232

Kiorpes, L., Kiper, D. C., O'Keefe, L. P., Cavanaugh, J. R., & Movshon, J. A. (1998a). Neuronal correlates of amblyopia in the visual cortex of macaque monkeys with experimental

strabismus and anisometropia. *Journal of Neuroscience*, *18*(16), 6411–6424. https://doi.org/10.1523/jneurosci.18-16-06411.1998

Kiorpes, L., Kiper, D. C., O'Keefe, L. P., Cavanaugh, J. R., & Movshon, J. A. (1998b). Neuronal correlates of amblyopia in the visual cortex of macaque monkeys with experimental strabismus and anisometropia. *The Journal of Neuroscience : The Official Journal of the Society for Neuroscience*, *18*(16), 6411–6424. https://doi.org/10.1523/JNEUROSCI.18-16-06411.1998

Kiorpes, L., Tang, C., & Movshon, J. A. (2006). Sensitivity to visual motion in amblyopic macaque monkeys. *Visual Neuroscience*, *23*(2), 247–256. https://doi.org/10.1017/S0952523806232097

Kohn, A., Coen-Cagli, R., Kanitscheider, I., & Pouget, A. (2016). Correlations and Neuronal Population Information. *Annual Review of Neuroscience*, *39*, 237–256. https://doi.org/10.1146/annurev-neuro-070815-013851

Kohn, A., & Smith, M. A. (2005). Stimulus dependence of neuronal correlation in primary visual cortex of the macaque. *The Journal of Neuroscience : The Official Journal of the Society for Neuroscience*, *25*(14), 3661–3673. https://doi.org/10.1523/JNEUROSCI.5106-04.2005

Kozma, P., & Kiorpes, L. (2003). Contour integration in amblyopic monkeys. *Visual Neuroscience*, *20*(5), 577–588. https://doi.org/10.1017/s0952523803205113

Krauzlis, R. J., Lovejoy, L. P., & Zénon, A. (2013). Superior colliculus and visual spatial attention. *Annual Review of Neuroscience*, *36*, 165–182. https://doi.org/10.1146/annurev-neuro-062012-170249

Lee, S. H., & Dan, Y. (2012). Neuromodulation of Brain States. *Neuron*, *76*(1), 209–222. https://doi.org/10.1016/J.NEURON.2012.09.012

Lestienne, R., Hervé-Minvielle, A., Robinson, D., Briois, L., & Sara, S. J. (1997). Slow oscillations as a probe of the dynamics of the locus coeruleus-frontal cortex interaction in anesthetized rats. *Journal of Physiology-Paris*, *91*(6), 273–284. https://doi.org/https://doi.org/10.1016/S0928-4257(97)82407-2

LeVay, S., Wiesel, T. N., & Hubel, D. H. (1980). The development of ocular dominance columns in normal and visually deprived monkeys. *The Journal of Comparative Neurology*, *191*(1), 1–51. https://doi.org/10.1002/cne.901910102

Levi, D. M. (2013). Linking assumptions in amblyopia. *Visual Neuroscience*, *30*(5–6), 277–287. https://doi.org/10.1017/S0952523813000023

Levi, D. M., & Harwerth, R. S. (1977). Spatio-temporal interactions in anisometropic and strabismic amblyopia. *Investigative Ophthalmology & Visual Science*, *16*(1), 90–95.

Levi, D. M., Klein, S. A., & Chen, I. (2008). What limits performance in the amblyopic visual system: seeing signals in noise with an amblyopic brain. *Journal of Vision*, *8*(4), 1.1-23. https://doi.org/10.1167/8.4.1

Levi, D. M., Yu, C., Kuai, S. G., & Rislove, E. (2007). Global contour processing in amblyopia. *Vision Research*, *47*(4), 512–524. https://doi.org/10.1016/j.visres.2006.10.014

Levitt, P., Rakic, P., & Goldman-Rakic, P. (1984). Region-specific distribution of catecholamine afferents in primate cerebral cortex: A fluorescence histochemical analysis. *Journal of Comparative Neurology*, *227*(1), 23–36. https://doi.org/10.1002/cne.902270105

Lewis, D. A., & Morrison, J. H. (1989). Noradrenergic innervation of monkey prefrontal cortex: A dopamine-β-hydroxylase immunohistochemical study. *Journal of Comparative Neurology*, *282*(3), 317–330. https://doi.org/10.1002/cne.902820302

Loughlin, S. E., Foote, S. L., & Grzanna, R. (1986). Efferent projections of nucleus locus coeruleus: Morphologic subpopulations have different efferent targets. *Neuroscience*, *18*(2), 307–319. https://doi.org/10.1016/0306-4522(86)90156-9

Löwel, S. (1994). Ocular dominance column development: strabismus changes the spacing of adjacent columns in cat visual cortex. *The Journal of Neuroscience : The Official Journal of the Society for Neuroscience*, *14*(12), 7451–7468. https://doi.org/10.1523/JNEUROSCI.14-12-07451.1994

Löwel, S., & Singer, W. (1992). Selection of intrinsic horizontal connections in the visual cortex by correlated neuronal activity. *Science (New York, N.Y.)*, *255*(5041), 209–212. https://doi.org/10.1126/science.1372754

Luo, T. Z., & Maunsell, J. H. R. (2015). Neuronal Modulations in Visual Cortex Are Associated with Only One of Multiple Components of Attention. *Neuron*, *86*(5), 1182–1188. https://doi.org/10.1016/j.neuron.2015.05.007

Luo, T. Z., & Maunsell, J. H. R. (2018). Attentional Changes in Either Criterion or Sensitivity Are Associated with Robust Modulations in Lateral Prefrontal Cortex. *Neuron*, *97*(6), 1382-1393.e7. https://doi.org/10.1016/J.NEURON.2018.02.007/ATTACHMENT/75620817-2BE0-4D60-B429-21F9830E7170/MMC1.PDF

Luppi, P. H., Aston-Jones, G., Akaoka, H., Chouvet, G., & Jouvet, M. (1995). Afferent projections to the rat locus coeruleus demonstrated by retrograde and anterograde tracing with cholera-toxin B subunit and Phaseolus vulgaris leucoagglutinin. *Neuroscience*, *65*(1), 119–160. https://doi.org/10.1016/0306-4522(94)00481-J

Macke, J. H., & Nienborg, H. (2019). Choice (-history) correlations in sensory cortex: cause or consequence? *Current Opinion in Neurobiology*, *58*, 148–154. https://doi.org/10.1016/j.conb.2019.09.005

Macko, K. A., Jarvis, C. D., Kennedy, C., Miyaoka, M., Shinohara, M., Sokoloff, L., & Mishkin, M. (1982). Mapping the primate visual system with [2-14C]deoxyglucose. *Science*, *218*(4570), 394–397. https://doi.org/10.1126/science.7123241

Macmillan, N., & Creelman, C. (2004). *Detection Theory: A User's Guide*. Psychology Press.

Manella, L. C., Petersen, N., & Linster, C. (2017). Stimulation of the Locus Ceruleus Modulates Signal-to-Noise Ratio in the Olfactory Bulb. *The Journal of Neuroscience*, *37*(48), 11605. https://doi.org/10.1523/JNEUROSCI.2026-17.2017

Manger, P. R., & Eschenko, O. (2021). The Mammalian Locus Coeruleus Complex—Consistencies and Variances in Nuclear Organization. *Brain Sciences 2021, Vol. 11, Page 1486*, *11*(11), 1486. https://doi.org/10.3390/BRAINSCI11111486

Mao, Z. M., Arnsten, A. F. T., & Li, B. M. (1999). Local infusion of an α-1 adrenergic agonist into the prefrontal cortex impairs spatial working memory performance in monkeys. *Biological Psychiatry*, *46*(9), 1259–1265. https://doi.org/10.1016/S0006-3223(99)00139-0

Martinez-Conde, S., Otero-Millan, J., & MacKnik, S. L. (2013). The impact of microsaccades on vision: Towards a unified theory of saccadic function. *Nature Reviews Neuroscience*, *14*(2), 83–96. https://doi.org/10.1038/nrn3405

Martins, A. R. O., & Froemke, R. C. (2015). Coordinated forms of noradrenergic plasticity in the locus coeruleus and primary auditory cortex. *Nature Neuroscience*, *18*(10), 1483–1492. https://doi.org/10.1038/nn.4090

McBurney-Lin, J., Lu, J., Zuo, Y., & Yang, H. (2019). Locus coeruleus-norepinephrine modulation of sensory processing and perception: A focused review. *Neuroscience & Biobehavioral Reviews*, *105*, 190–199. https://doi.org/10.1016/J.NEUBIOREV.2019.06.009

McCamy, M. B., Otero-Millan, J., Macknik, S. L., Yang, Y., Troncoso, X. G., Baer, S. M., Crook, S. M., & Martinez-Conde, S. (2012). Microsaccadic Efficacy and Contribution to Foveal and Peripheral Vision. *Journal of Neuroscience*, *32*(27), 9194–9204. https://doi.org/10.1523/JNEUROSCI.0515-12.2012

McCormick, D. A., Pape, H. C., & Williamson, A. (1991). Actions of norepinephrine in the cerebral cortex and thalamus: implications for function of the central noradrenergic system. *Progress in Brain Research*, *88*(C), 293–305. https://doi.org/10.1016/S0079-6123(08)63817-0

McGinley, M. J., Vinck, M., Reimer, J., Batista-Brito, R., Zagha, E., Cadwell, C. R., Tolias, A. S., Cardin, J. A., & McCormick, D. A. (2015). Waking State: Rapid Variations Modulate Neural and Behavioral Responses. *Neuron*, *87*(6), 1143–1161. https://doi.org/10.1016/j.neuron.2015.09.012

McKee, S. P., Levi, D. M., & Movshon, J. A. (2003). The pattern of visual deficits in amblyopia. *Journal of Vision*, *3*(5), 380–405. https://doi.org/10.1167/3.5.5

McLean, J., & Waterhouse, B. D. (1994). Noradrenergic modulation of cat area 17 neuronal responses to moving visual stimuli. *Brain Research*, *667*(1), 83–97. https://doi.org/10.1016/0006-8993(94)91716-7

Megemont, M., McBurney-Lin, J., & Yang, H. (2022). Pupil diameter is not an accurate realtime readout of locus coeruleus activity. *ELife*, *11*, 1–17. https://doi.org/10.7554/ELIFE.70510

Meier, K., & Giaschi, D. (2017). Unilateral Amblyopia Affects Two Eyes: Fellow Eye Deficits in Amblyopia. *Investigative Ophthalmology & Visual Science*, *58*(3), 1779–1800. https://doi.org/10.1167/iovs.16-20964

Meier, K., Sum, B., & Giaschi, D. (2016). Global motion perception in children with amblyopia as a function of spatial and temporal stimulus parameters. *Vision Research*, *127*, 18–27. https://doi.org/10.1016/j.visres.2016.06.011

Mello-Carpes, P. B., & Izquierdo, I. (2013). The Nucleus of the Solitary Tract → Nucleus Paragigantocellularis → Locus Coeruleus → CA1 region of dorsal hippocampus pathway is important for consolidation of object recognition memory. *Neurobiology of Learning and Memory*, *100*, 56–63. https://doi.org/10.1016/J.NLM.2012.12.002

Mitchell, J. F., Sundberg, K. A., & Reynolds, J. H. (2009). Spatial attention decorrelates intrinsic activity fluctuations in macaque area V4. *Neuron*, *63*(6), 879–888. https://doi.org/10.1016/j.neuron.2009.09.013

Mohler, C. W., & Wurtz, R. H. (1977). Role of striate cortex and superior colliculus in visual guidance of saccadic eye movements in monkeys. *Https://Doi.Org/10.1152/Jn.1977.40.1.74*, *40*(1), 74–94. https://doi.org/10.1152/JN.1977.40.1.74

Moore, R. Y., & Bloom, F. E. (2003). Central Catecholamine Neuron Systems: Anatomy and Physiology of the Norepinephrine and Epinephrine Systems. *Https://Doi.Org/10.1146/Annurev.Ne.02.030179.000553*, *2*, 113–168. https://doi.org/10.1146/ANNUREV.NE.02.030179.000553

Moore, T. (2001). Control of eye movements and spatial attention. *Proceedings of the National Academy of Sciences*, *98*(3), 1273–1276. https://doi.org/10.1073/pnas.021549498

Moore, T. (2006). The neurobiology of visual attention: finding sources. *Current Opinion in Neurobiology*, *16*(2), 159–165. https://doi.org/10.1016/j.conb.2006.03.009

Moore, T., & Armstrong, K. M. (2003). Selective gating of visual signals by microstimulation of frontal cortex. *Nature*, *421*(6921), 370–373. https://doi.org/10.1038/nature01341

Morrison, J. H., & Foote, S. L. (1986). Noradrenergic and serotoninergic innervation of cortical, thalamic, and tectal visual structures in old and new world monkeys. *Journal of Comparative Neurology*, *243*(1), 117–138. https://doi.org/10.1002/cne.902430110

Moruzzi, G., & Magoun, H. W. (1949). Brain stem reticular formation and activation of the EEG. *Electroencephalography and Clinical Neurophysiology*, *1*(1–4), 455–473. https://doi.org/10.1016/0013-4694(49)90219-9

Movshon, J. A., Eggers, H. M., Gizzi, M. S., Hendrickson, A. E., Kiorpes, L., & Boothe, R. G. (1987). Effects of early unilateral blur on the macaque's visual system. III. Physiological observations. *The Journal of Neuroscience : The Official Journal of the Society for Neuroscience*, *7*(5), 1340–1351. https://doi.org/10.1523/JNEUROSCI.07-05-01340.1987

Munoz, D. P., & Wurtz, R. H. (1993). Fixation cells in monkey superior colliculus. I. Characteristics of cell discharge. *Https://Doi.Org/10.1152/Jn.1993.70.2.559*, *70*(2), 559–575. https://doi.org/10.1152/JN.1993.70.2.559

Murphy, P. R., O'Connell, R. G., O'Sullivan, M., Robertson, I. H., & Balsters, J. H. (2014). Pupil diameter covaries with BOLD activity in human locus coeruleus. *Human Brain Mapping*, *35*(8), 4140–4154. https://doi.org/10.1002/hbm.22466

Murphy, P. R., Vandekerckhove, J., & Nieuwenhuis, S. (2014). Pupil-Linked Arousal Determines Variability in Perceptual Decision Making. *PLoS Computational Biology*, *10*(9). https://doi.org/10.1371/journal.pcbi.1003854

Najafi, F., & Churchland, A. K. (2018). Perceptual Decision-Making: A Field in the Midst of a Transformation. *Neuron*, *100*(2), 453–462. https://doi.org/10.1016/j.neuron.2018.10.017

Ni, A. M., Ruff, D. A., Alberts, J. J., Symmonds, J., & Cohen, M. R. (2018). Learning and attention reveal a general relationship between population activity and behavior. *Science (New York, N.Y.)*, *359*(6374), 463–465. https://doi.org/10.1126/science.aao0284

Nienborg, H., Cohen, M. R., & Cumming, B. G. (2012). Decision-Related Activity in Sensory Neurons: Correlations Among Neurons and with Behavior. *Http://Dx.Doi.Org/10.1146/Annurev-Neuro-062111-150403*, *35*, 463–483. https://doi.org/10.1146/ANNUREV-NEURO-062111-150403

Nienborg, H., & Roelfsema, P. R. (2015). Belief states as a framework to explain extra-retinal influences in visual cortex. *Current Opinion in Neurobiology*, *32*, 45–52. https://doi.org/10.1016/j.conb.2014.10.013

Noudoost, B., Clark, K. L., & Moore, T. (2014). A distinct contribution of the frontal eye field to the visual representation of saccadic targets. *Journal of Neuroscience*, *34*(10), 3687–3698. https://doi.org/10.1523/JNEUROSCI.3824-13.2014

Noudoost, B., & Moore, T. (2011a). A reliable microinjectrode system for use in behaving monkeys. *Journal of Neuroscience Methods*, *194*(2), 218–223. https://doi.org/10.1016/J.JNEUMETH.2010.10.009

Noudoost, B., & Moore, T. (2011b). CONTROL OF VISUAL CORTICAL SIGNALS BY PREFRONTAL DOPAMINE. *Nature*, *474*(7351), 372. https://doi.org/10.1038/NATURE09995

O'Connell, R. G., Shadlen, M. N., Wong-Lin, K. F., & Kelly, S. P. (2018). Bridging Neural and Computational Viewpoints on Perceptual Decision-Making. *Trends in Neurosciences*, *41*(11), 838–852. https://doi.org/10.1016/j.tins.2018.06.005

Papadopoulos, G. C., Parnavelas, J. G., & Buijs, R. M. (1989). Light and electron microscopic immunocytochemical analysis of the noradrenaline innervation of the rat visual cortex. *Journal of Neurocytology 1989 18:1*, *18*(1), 1–10. https://doi.org/10.1007/BF01188418

Pham, A., Carrasco, M., & Kiorpes, L. (2018). Endogenous attention improves perception in amblyopic macaques. *Journal of Vision*, *18*(3), 11. https://doi.org/10.1167/18.3.11

Poe, G. R., Foote, S., Eschenko, O., Johansen, J. P., Bouret, S., Aston-Jones, G., Harley, C. W., Manahan-Vaughan, D., Weinshenker, D., Valentino, R., Berridge, C., Chandler, D. J., Waterhouse, B., & Sara, S. J. (2020). Locus coeruleus: a new look at the blue spot. *Nature Reviews Neuroscience*, *21*(11), 644–659. https://doi.org/10.1038/s41583-020-0360-9

Porrino, L. J., & Goldman-Rakic, P. S. (1982a). Brainstem innervation of prefrontal and anterior cingulate cortex in the rhesus monkey revealed by retrograde transport of HRP. *Journal of Comparative Neurology*, *205*(1), 63–76. https://doi.org/10.1002/cne.902050107

Porrino, L. J., & Goldman-Rakic, P. S. (1982b). Brainstem innervation of prefrontal and anterior cingulate cortex in the rhesus monkey revealed by retrograde transport of HRP. *Journal of Comparative Neurology*, *205*(1), 63–76. https://doi.org/10.1002/CNE.902050107

Rainer, G., Asaad, W. F., & Miller, E. K. (1998). Selective representation of relevant information by neurons in the primate prefrontal cortex. *Nature*, *393*(6685), 577–579. https://doi.org/10.1038/31235

Rajkowski, J., Majczynski, H., Clayton, E., & Aston-Jones, G. (2004). Activation of monkey locus coeruleus neurons varies with difficulty and performance in a target detection task. *Journal of Neurophysiology*, *92*(1), 361–371. https://doi.org/10.1152/jn.00673.2003

Ramos, B. P., & Arnsten, A. F. T. (2007). Adrenergic Pharmacology and Cognition: Focus on the Prefrontal Cortex. *Pharmacology & Therapeutics*, *113*(3), 523. https://doi.org/10.1016/J.PHARMTHERA.2006.11.006

Reich, D. S., Mechler, F., & Victor, J. D. (2001). Independent and redundant information in nearby cortical neurons. *Science (New York, N.Y.)*, *294*(5551), 2566–2568. https://doi.org/10.1126/science.1065839

Reid, R. C., & Alonso, J. M. (1995). Specificity of monosynaptic connections from thalamus to visual cortex. *Nature*, *378*(6554), 281–284. https://doi.org/10.1038/378281a0

Reimer, J., Froudarakis, E., Cadwell, C. R., Yatsenko, D., Denfield, G. H., & Tolias, A. S. (2014). Pupil Fluctuations Track Fast Switching of Cortical States during Quiet Wakefulness. *Neuron*, *84*(2), 355–362. https://doi.org/10.1016/j.neuron.2014.09.033

Reimer, J., McGinley, M. J., Liu, Y., Rodenkirch, C., Wang, Q., McCormick, D. A., & Tolias, A. S. (2016). Pupil fluctuations track rapid changes in adrenergic and cholinergic activity in cortex. *Nature Communications*, *7*(May), 1–7. https://doi.org/10.1038/ncomms13289

Renart, A., & Machens, C. K. (2014). Variability in neural activity and behavior. *Current Opinion in Neurobiology*, *25*, 211–220. https://doi.org/10.1016/J.CONB.2014.02.013

Rho, H. J., Kim, J. H., & Lee, S. H. (2018). Function of selective neuromodulatory projections in the mammalian cerebral cortex: Comparison between cholinergic and noradrenergic systems. *Frontiers in Neural Circuits*, *12*(June), 1–13. https://doi.org/10.3389/fncir.2018.00047

Rislove, E. M., Hall, E. C., Stavros, K. A., & Kiorpes, L. (2010). Scale-dependent loss of global form perception in strabismic amblyopia. *Journal of Vision*, *10*(12), 25. https://doi.org/10.1167/10.12.25

Robbins, T. W., & Arnsten, A. F. T. (2009). The neuropsychopharmacology of fronto-executive function: Monoaminergic modulation. *Annual Review of Neuroscience*, *32*, 267–287. https://doi.org/10.1146/annurev.neuro.051508.135535

Robinson, D. A. (1972). Eye movements evoked by collicular stimulation in the alert monkey. *Vision Research*, *12*(11), 1795–1808. https://doi.org/10.1016/0042-6989(72)90070-3

Roe, AW, Chelazzi, L, Connor CE, Conway, BR, Fijita, IR, Gallant, J, Lu, H, and V. W. (2016). *Toward a Unified Theory of Visual Area V4*. *74*(1), 12–29. https://doi.org/10.1016/j.neuron.2012.03.011.Toward

Roelfsema, P. R., König, P., Engel, A. K., Sireteanu, R., & Singer, W. (1994). Reduced synchronization in the visual cortex of cats with strabismic amblyopia. *The European Journal of Neuroscience*, *6*(11), 1645–1655. https://doi.org/10.1111/j.1460-9568.1994.tb00556.x

Rousche, P. J., & Normann, R. A. (1992). A method for pneumatically inserting an array of penetrating electrodes into cortical tissue. *Annals of Biomedical Engineering*, *20*(4), 413–422. https://doi.org/10.1007/BF02368133

Roussel, B., Buguet, A., Bobillier, P., & Jouvet, M. (1967). [Locus ceruleus, paradoxal sleep, and cerebral noradrenaline]. *Comptes rendus des seances de la Societe de biologie et de ses filiales*, *161*(12), 2537–2541.

Ruff, D. A., & Cohen, M. R. (2016). Stimulus Dependence of Correlated Variability across Cortical Areas. *The Journal of Neuroscience : The Official Journal of the Society for Neuroscience*, *36*(28), 7546–7556. https://doi.org/10.1523/JNEUROSCI.0504-16.2016

Runyan, C. A., Piasini, E., Panzeri, S., & Harvey, C. D. (2017). Distinct timescales of population coding across cortex. *Nature*, *548*(7665), 92. https://doi.org/10.1038/NATURE23020

Safaai, H., Neves, R., Eschenko, O., Logothetis, N. K., & Panzeri, S. (2015). Modeling the effect of locus coeruleus firing on cortical state dynamics and single-trial sensory processing. *Proceedings of the National Academy of Sciences of the United States of America*, *112*(41), 12834–12839. https://doi.org/10.1073/pnas.1516539112

Salzman, C. D., & Newsome, W. T. (1994). Neural mechanisms for forming a perceptual decision. *Science*, *264*(5156), 231–237. https://doi.org/10.1126/science.8146653

Samuels, E., & Szabadi, E. (2008). Functional Neuroanatomy of the Noradrenergic Locus Coeruleus: Its Roles in the Regulation of Arousal and Autonomic Function Part I: Principles of Functional Organisation. *Current Neuropharmacology*, *6*(3), 235–253. https://doi.org/10.2174/157015908785777229

Sara, S. J. (2009). The locus coeruleus and noradrenergic modulation of cognition. *Nature Reviews Neuroscience*, *10*(3), 211–223. https://doi.org/10.1038/nrn2573

Sara, S. J., & Bouret, S. (2012a). Orienting and Reorienting: The Locus Coeruleus Mediates Cognition through Arousal. *Neuron*, *76*(1), 130–141. https://doi.org/10.1016/j.neuron.2012.09.011

Sara, S. J., & Bouret, S. (2012b). Orienting and Reorienting: The Locus Coeruleus Mediates Cognition through Arousal. *Neuron*, *76*(1), 130–141. https://doi.org/10.1016/j.neuron.2012.09.011

Sara, S. J., & Hervé-Minvielle, A. (1995). Inhibitory influence of frontal cortex on locus coeruleus neurons. *Proceedings of the National Academy of Sciences of the United States of America*, *92*(13), 6032–6036. https://doi.org/10.1073/pnas.92.13.6032

Sawaguchi, T. (1998). Attenuation of delay-period activity of monkey prefrontal neurons by an α2-adrenergic antagonist during an oculomotor delayed-response task. *Journal of Neurophysiology*, *80*(4), 2200–2205. https://doi.org/10.1152/jn.1998.80.4.2200

Schall, J. D. (2015). Visuomotor Functions in the Frontal Lobe. In *Annual Review of Vision Science* (Vol. 1, Issue 1). https://doi.org/10.1146/annurev-vision-082114-035317

Schall, J. D., Morel, A., King, D. J., & Bullier, J. (1995). Topography of visual cortex connections with frontal eye field in macaque: convergence and segregation of processing streams. *Journal of Neuroscience*, *15*(6), 4464–4487. https://doi.org/10.1523/JNEUROSCI.15-06-04464.1995

Schiller, P. H., & Koerner, F. (1971). Discharge characteristics of single units in superior colliculus of the alert rhesus monkey. *Journal of Neurophysiology*, *34*(5), 920–936. https://doi.org/10.1152/JN.1971.34.5.920

Schiller, P. H., & Stryker, M. (1972). Single-unit recording and stimulation in superior colliculus of the alert rhesus monkey. *Journal of Neurophysiology*, *35*(6), 915–924. https://doi.org/10.1152/JN.1972.35.6.915

Schiller, P. H., & Tehovnik, E. J. (2005). Neural mechanisms underlying target selection with saccadic eye movements. *Progress in Brain Research*, *149*, 157–171. https://doi.org/10.1016/S0079-6123(05)49012-3

Schmolesky, M. T., Wang, Y., Hanes, D. P., Thompson, K. G., Leutgeb, S., Schall, J. D., & Leventhal, A. G. (1998). Signal timing access the macaque visual system. *Journal of Neurophysiology*, *79*(6), 3272–3278. https://doi.org/10.1152/jn.1998.79.6.3272

Schröder, J. H., Fries, P., Roelfsema, P. R., Singer, W., & Engel, A. K. (2002). Ocular dominance in extrastriate cortex of strabismic amblyopic cats. *Vision Research*, *42*(1), 29–39. https://doi.org/10.1016/S0042-6989(01)00263-2

Schwarz, L. A., & Luo, L. (2015). Organization of the locus coeruleus-norepinephrine system. *Current Biology*, *25*(21), R1051–R1056. https://doi.org/10.1016/j.cub.2015.09.039

Schwarz, L. A., Miyamichi, K., Gao, X. J., Beier, K. T., Weissbourd, B., Deloach, K. E., Ren, J., Ibanes, S., Malenka, R. C., Kremer, E. J., & Luo, L. (2015). Viral-genetic tracing of the input-output organization of a central noradrenaline circuit. *Nature*, *524*(7563), 88–92. https://doi.org/10.1038/nature14600

Seo, H., Barraclough, D. J., & Lee, D. (2007). Dynamic signals related to choices and outcomes in the dorsolateral prefrontal cortex. *Cerebral Cortex (New York, N.Y. : 1991)*, *17 Suppl 1*(SUPPL. 1). https://doi.org/10.1093/CERCOR/BHM064

Servan-Schreiber, D., Printz, H., & Cohen, J. D. (1990). A network model of catecholamine effects: gain, signal-to-noise ratio, and behavior. *Science*, *249*(4971), 892 LP – 895. https://doi.org/10.1126/science.2392679

Shadlen, M. N., & Kiani, R. (2013). Decision making as a window on cognition. *Neuron*, *80*(3), 791–806. https://doi.org/10.1016/j.neuron.2013.10.047

Shadlen, M. N., & Newsome, W. T. (1998). The variable discharge of cortical neurons: implications for connectivity, computation, and information coding. *The Journal of*

Neuroscience : The Official Journal of the Society for Neuroscience, *18*(10), 3870–3896. https://doi.org/10.1523/JNEUROSCI.18-10-03870.1998

Sharma, Y., Xu, T., Graf, W. M., Fobbs, A., Sherwood, C. C., Hof, P. R., Allman, J. M., & Manaye, K. F. (2010). Comparative Anatomy of the Locus Coeruleus in Humans and Non-Human Primates. *The Journal of Comparative Neurology*, *518*(7), 963. https://doi.org/10.1002/CNE.22249

Shima, K., & Tanji, J. (1998). Role for Cingulate Motor Area Cells in Voluntary Movement Selection Based on Reward. *Science*, *282*(5392), 1335–1338. https://doi.org/10.1126/SCIENCE.282.5392.1335

Shinba, T., Briois, L., & Sara, S. J. (2000). Spontaneous and auditory-evoked activity of medial agranular cortex as a function of arousal state in the freely moving rat: interaction with locus coeruleus activity. *Brain Research*, *887*(2), 293–300. https://doi.org/https://doi.org/10.1016/S0006-8993(00)03009-2

Shoham, S., Fellows, M. R., & Normann, R. A. (2003). Robust, automatic spike sorting using mixtures of multivariate t-distributions. *Journal of Neuroscience Methods*, *127*(2), 111–122. https://doi.org/10.1016/s0165-0270(03)00120-1

Shooner, C., Hallum, L. E., Kumbhani, R. D., García-Marín, V., Kelly, J. G., Majaj, N. J., Movshon, J. A., & Kiorpes, L. (2017). Asymmetric Dichoptic Masking in Visual Cortex of Amblyopic Macaque Monkeys. *The Journal of Neuroscience : The Official Journal of the Society for Neuroscience*, *37*(36), 8734–8741. https://doi.org/10.1523/JNEUROSCI.1760-17.2017

Shooner, C., Hallum, L. E., Kumbhani, R. D., Ziemba, C. M., Garcia-Marin, V., Kelly, J. G., Majaj, N. J., Movshon, J. A., & Kiorpes, L. (2015a). Population representation of visual information in areas V1 and V2 of amblyopic macaques. *Vision Research*, *114*, 56–67. https://doi.org/10.1016/j.visres.2015.01.012

Shooner, C., Hallum, L. E., Kumbhani, R. D., Ziemba, C. M., Garcia-Marin, V., Kelly, J. G., Majaj, N. J., Movshon, J. A., & Kiorpes, L. (2015b). Population representation of visual information in areas V1 and V2 of amblyopic macaques. *Vision Research*, *114*, 56–67. https://doi.org/10.1016/j.visres.2015.01.012

Smith, E. L. 3rd, Chino, Y. M., Ni, J., Cheng, H., Crawford, M. L., & Harwerth, R. S. (1997). Residual binocular interactions in the striate cortex of monkeys reared with abnormal binocular vision. *Journal of Neurophysiology*, *78*(3), 1353–1362. https://doi.org/10.1152/jn.1997.78.3.1353

Smith, M. A., Bair, W., & Movshon, J. A. (2002). Signals in macaque striate cortical neurons that support the perception of glass patterns. *The Journal of Neuroscience : The Official Journal of the Society for Neuroscience*, *22*(18), 8334–8345. https://doi.org/10.1523/JNEUROSCI.22-18-08334.2002

Smith, M. A., & Kohn, A. (2008). Spatial and temporal scales of neuronal correlation in primary visual cortex. *The Journal of Neuroscience : The Official Journal of the Society for Neuroscience*, *28*(48), 12591–12603. https://doi.org/10.1523/JNEUROSCI.2929-08.2008

Smith, M. A., & Sommer, M. A. (2013). Spatial and temporal scales of neuronal correlation in visual area V4. *The Journal of Neuroscience : The Official Journal of the Society for Neuroscience*, *33*(12), 5422–5432. https://doi.org/10.1523/JNEUROSCI.4782-12.2013

Snyder, A. C., Morais, M. J., Kohn, A., & Smith, M. A. (2014). Correlations in V1 are reduced by stimulation outside the receptive field. *The Journal of Neuroscience : The Official Journal of the Society for Neuroscience*, *34*(34), 11222–11227. https://doi.org/10.1523/JNEUROSCI.0762-14.2014

Snyder, A. C., Morais, M. J., & Smith, M. A. (2016). Dynamics of excitatory and inhibitory networks are differentially altered by selective attention. *Journal of Neurophysiology*, *116*(4), 1807–1820. https://doi.org/10.1152/jn.00343.2016

Sparks, D. L. (1978). Functional properties of neurons in the monkey superior colliculus: Coupling of neuronal activity and saccade onset. *Brain Research*, *156*(1), 1–16. https://doi.org/10.1016/0006-8993(78)90075-6

Sparks, D. L. (1986). Translation of sensory signals into commands for control of saccadic eye movements: role of primate superior colliculus. *Https://Doi.Org/10.1152/Physrev.1986.66.1.118*, *66*(1), 118–171. https://doi.org/10.1152/PHYSREV.1986.66.1.118

Stanton, G. B., Bruce, C. J., & Goldberg, M. E. (1993). Topography of projections to the frontal lobe from the macaque frontal eye fields. *Journal of Comparative Neurology*, *330*(2), 286–301. https://doi.org/10.1002/CNE.903300209

Stringer, C., Pachitariu, M., Steinmetz, N., Reddy, C. B., Carandini, M., Harris, K. D., Resources, K. D. H., & Funding, K. D. H. (2019). Spontaneous Behaviors Drive Multidimensional, Brain-wide Activity Europe PMC Funders Group. *Science*, *364*(6437), 255. https://doi.org/10.1126/science.aav7893

Sun, Y., Yang, Y., Galvin, V. C., Yang, S., Arnsten, A. F., & Wang, M. (2017). *Nicotinic 42 Cholinergic Receptor Influences on Dorsolateral Prefrontal Cortical Neuronal Firing during a Working Memory Task*. https://doi.org/10.1523/JNEUROSCI.0364-17.2017

Tanji, J., & Hoshi, E. (2008). Role of the lateral prefrontal cortex in executive behavioral control. *Physiological Reviews*, *88*(1), 37–57. https://doi.org/10.1152/PHYSREV.00014.2007/ASSET/IMAGES/LARGE/Z9J0010824590003.JPEG

Tao, X., Zhang, B., Shen, G., Wensveen, J., Smith, E. L. 3rd, Nishimoto, S., Ohzawa, I., & Chino, Y. M. (2014). Early monocular defocus disrupts the normal development of receptive-field structure in V2 neurons of macaque monkeys. *The Journal of Neuroscience : The Official Journal of the Society for Neuroscience*, *34*(41), 13840–13854. https://doi.org/10.1523/JNEUROSCI.1992-14.2014

Thiele, A., & Bellgrove, M. A. (2018). Neuromodulation of Attention. *Neuron*, *97*(4), 769–785. https://doi.org/10.1016/J.NEURON.2018.01.008

Thiele, A., Delicato, L. S., Roberts, M. J., & Gieselmann, M. A. (2006). A novel electrode–pipette design for simultaneous recording of extracellular spikes and iontophoretic drug application in awake behaving monkeys. *Journal of Neuroscience Methods*, *158*(2–4), 207. https://doi.org/10.1016/J.JNEUMETH.2006.05.032

Thiele, A., Herrero, J. L., Distler, C., & Hoffmann, K. P. (2012). Contribution of Cholinergic and GABAergic Mechanisms to Direction Tuning, Discriminability, Response Reliability, and Neuronal Rate Correlations in Macaque Middle Temporal Area. *The Journal of Neuroscience*, *32*(47), 16602. https://doi.org/10.1523/JNEUROSCI.0554-12.2012

Tolhurst, D. J., Movshon, J. A., & Dean, A. F. (1983). The statistical reliability of signals in single neurons in cat and monkey visual cortex. *Vision Research*, *23*(8), 775–785. https://doi.org/10.1016/0042-6989(83)90200-6

Totah, N. K. B., Logothetis, N. K., & Eschenko, O. (2019a). Noradrenergic ensemble-based modulation of cognition over multiple timescales. *Brain Research*, *1709*(September 2017), 50–66. https://doi.org/10.1016/j.brainres.2018.12.031

Totah, N. K. B., Logothetis, N. K., & Eschenko, O. (2019b). Noradrenergic ensemble-based modulation of cognition over multiple timescales. *Brain Research*, *1709*(September 2017), 50–66. https://doi.org/10.1016/j.brainres.2018.12.031

Totah, N. K., Neves, R. M., Panzeri, S., Logothetis, N. K., & Eschenko, O. (2018). The Locus Coeruleus Is a Complex and Differentiated Neuromodulatory System. *Neuron*, *99*(5), 1055-1068.e6. https://doi.org/10.1016/j.neuron.2018.07.037

Trachtenberg, J. T., & Stryker, M. P. (2001). Rapid anatomical plasticity of horizontal connections in the developing visual cortex. *The Journal of Neuroscience : The Official Journal of the Society for Neuroscience*, *21*(10), 3476–3482. https://doi.org/10.1523/JNEUROSCI.21-10-03476.2001

Tronel, S., Feenstra, M. G. P., & Sara, S. J. (2004). Noradrenergic Action in Prefrontal Cortex in the Late Stage of Memory Consolidation. *Learning & Memory*, *11*(4), 453–458. https://doi.org/10.1101/LM.74504

Tychsen, L., & Burkhalter, A. (1992). Naturally-strabismic primate lacks intrinsic horizontal connections for binocular vision in striate cortex. *Soc Neurosci Abstr*, *18*, 1455.

Tychsen, L., & Burkhalter, A. (1997). Nasotemporal asymmetries in V1: ocular dominance columns of infant, adult, and strabismic macaque monkeys. *The Journal of Comparative Neurology*, *388*(1), 32–46. https://doi.org/10.1002/(sici)1096-9861(19971110)388:1<32::aid-cne3>3.0.co;2-p

Tychsen, L., Wong, A. M.-F., & Burkhalter, A. (2004). Paucity of horizontal connections for binocular vision in V1 of naturally strabismic macaques: Cytochrome oxidase compartment specificity. *The Journal of Comparative Neurology*, *474*(2), 261–275. https://doi.org/10.1002/cne.20113

Uematsu, A., Tan, B. Z., Ycu, E. A., Cuevas, J. S., Koivumaa, J., Junyent, F., Kremer, E. J., Witten, I. B., Deisseroth, K., & Johansen, J. P. (2017). Modular organization of the brainstem noradrenaline system coordinates opposing learning states. *Nature Neuroscience 2017 20:11*, *20*(11), 1602–1611. https://doi.org/10.1038/nn.4642

Urai, A. E., Braun, A., & Donner, T. H. (2017). Pupil-linked arousal is driven by decision uncertainty and alters serial choice bias. *Nature Communications*, *8*. https://doi.org/10.1038/ncomms14637

Usher, M., Cohen, J. D., Servan-Schreiber, D., Rajkowski, J., & Aston-Jones, G. (1999a). The role of locus coeruleus in the regulation of cognitive performance. *Science*, *283*(5401), 549–554. https://doi.org/10.1126/science.283.5401.549

Usher, M., Cohen, J. D., Servan-Schreiber, D., Rajkowski, J., & Aston-Jones, G. (1999b). The role of locus coeruleus in the regulation of cognitive performance. *Science*, *283*(5401), 549–554. https://doi.org/10.1126/science.283.5401.549

van Bockstaele, E. J., Akaoka, H., & Aston-Jones, G. (1993). Brainstem afferents to the rostral (juxtafacial) nucleus paragigantocellularis: integration of exteroceptive and interoceptive sensory inputs in the ventral tegmentum. *Brain Research*, *603*(1), 1–18. https://doi.org/10.1016/0006-8993(93)91293-2

van Essen, D. C. (2003). Visual Areas of the Mammalian Cerebral Cortex. *Http://Dx.Doi.Org/10.1146/Annurev.Ne.02.030179.001303*, *2*, 227–263. https://doi.org/10.1146/ANNUREV.NE.02.030179.001303

Varazzani, C., San-Galli, A., Gilardeau, S., & Bouret, S. (2015). Noradrenaline and dopamine neurons in the reward/effort trade-off: A direct electrophysiological comparison in behaving monkeys. *Journal of Neuroscience*, *35*(20), 7866–7877. https://doi.org/10.1523/JNEUROSCI.0454-15.2015

Wang, H., Crewther, S. G., Liang, M., Laycock, R., Yu, T., Alexander, B., Crewther, D. P., Wang, J., & Yin, Z. (2017). Impaired activation of visual attention network for motion salience is accompanied by reduced functional connectivity between frontal eye fields and visual cortex in strabismic amblyopia. *Frontiers in Human Neuroscience*, *11*(April), 1–13. https://doi.org/10.3389/fnhum.2017.00195

Wang, X., Piñol, R. A., Byrne, P., & Mendelowitz, D. (2014). Optogenetic stimulation of locus ceruleus neurons augments inhibitory transmission to parasympathetic cardiac vagal neurons via activation of brainstem α1 and β1 receptors. *Journal of Neuroscience*, *34*(18), 6182–6189. https://doi.org/10.1523/JNEUROSCI.5093-13.2014

Wang, Y., Zhang, B., Tao, X., Wensveen, J. M., Smith, E. L. R., & Chino, Y. M. (2017). Noisy Spiking in Visual Area V2 of Amblyopic Monkeys. *The Journal of Neuroscience : The Official Journal of the Society for Neuroscience*, *37*(4), 922–935. https://doi.org/10.1523/JNEUROSCI.3178-16.2016

Waschke, L., Kloosterman, N. A., Obleser, J., & Garrett, D. D. (2021). Behavior needs neural variability. *Neuron*, *109*(5), 751–766. https://doi.org/10.1016/J.NEURON.2021.01.023

Waterhouse, B. D., & Chandler, D. (2012). Evidence for broad versus segregated projections from cholinergic and noradrenergic nuclei to functionally and anatomically discrete subregions of prefrontal cortex. *Frontiers in Behavioral Neuroscience*, *6*(MAY). https://doi.org/10.3389/FNBEH.2012.00020

Waterhouse, B. D., Moises, H. C., & Woodward, D. J. (1998). Phasic activation of the locus coeruleus enhances responses of primary sensory cortical neurons to peripheral receptive field stimulation. *Brain Research*, *790*(1–2), 33–44. https://doi.org/10.1016/S0006-8993(98)00117-6

Waterhouse, B. D., & Navarra, R. L. (2019a). The locus coeruleus-norepinephrine system and sensory signal processing: A historical review and current perspectives. *Brain Research*, *1709*(September 2018), 1–15. https://doi.org/10.1016/j.brainres.2018.08.032

Waterhouse, B. D., & Navarra, R. L. (2019b). The locus coeruleus-norepinephrine system and sensory signal processing: A historical review and current perspectives. *Brain Research*, *1709*(September 2018), 1–15. https://doi.org/10.1016/j.brainres.2018.08.032

Wiesel, T. N. (1982). Postnatal development of the visual cortex and the influence of environment. *Nature*, *299*(5884), 583–591. https://doi.org/10.1038/299583a0

WIESEL, T. N., & HUBEL, D. H. (1963). SINGLE-CELL RESPONSES IN STRIATE CORTEX OF KITTENS DEPRIVED OF VISION IN ONE EYE. *Journal of Neurophysiology*, *26*, 1003–1017. https://doi.org/10.1152/jn.1963.26.6.1003

Williamson, R. C., Doiron, B., Smith, M. A., & Yu, B. M. (2019). Bridging large-scale neuronal recordings and large-scale network models using dimensionality reduction. *Current Opinion in Neurobiology*, *55*, 40. https://doi.org/10.1016/J.CONB.2018.12.009

Wilson, M. E., Cragg, B. G., & Cerebral, M. R. C. (1967). Projections from the lateral geniculate nucleus in the cat and monkey. *Journal of Anatomy*, *101*(Pt 4), 677. https://www.ncbi.nlm.nih.gov/pmc/articles/PMC1270902/

Wurtz, R. H., Sommer, M. A., Paré, M., & Ferraina, S. (2001). Signal transformations from cerebral cortex to superior colliculus for the generation of saccades. *Vision Research*, *41*(25–26), 3399–3412. https://doi.org/10.1016/S0042-6989(01)00066-9

Yang, H., Bari, B. A., Cohen, J. Y., & Connor, D. H. O. (2021). *Locus coeruleus spiking differently correlates with S1 cortex activity and pupil diameter in a tactile detection task*. 1–14.

Yu, G., Herman, J. P., Katz, L. N., & Krauzlis, R. J. (2022). Microsaccades as a marker not a cause for attention-related modulation. *ELife*, *11*, 1–14. https://doi.org/10.7554/eLife.74168

Zeki, S. M. (1974). Functional organization of a visual area in the posterior bank of the superior temporal sulcus of the rhesus monkey. *The Journal of Physiology*, *236*(3), 549–573. https://doi.org/10.1113/JPHYSIOL.1974.SP010452

Zohary, E., Shadlen, M. N., & Newsome, W. T. (1994). Correlated neuronal discharge rate and its implications for psychophysical performance. *Nature*, *370*(6485), 140–143. https://doi.org/10.1038/370140a0